Università degli Studi di Ferrara

DOCTORAL COURSE IN
"MOLECULAR MEDICINE AND PHARMACOLOGY"

CYCLE XXXIII

DIRECTOR Prof. Francesco Di Virgilio

# Pathophysiology of the P2X7 receptor in the skeleton

Scientific/Disciplinary Sector (SDS) BIO/10

**Candidate**
Dott. Scussel Bergamin Leticia

**Supervisor**
Prof. Piva Roberta

Years 2017/2020

# TABLE OF CONTENTS

**ABBREVIATIONS** ..... **4**

**1. INTRODUCTION** ..... **7**

1.1 SKELETAL SYSTEM ..... 7

1.1.1 Bone tissue ..... 7

1.1.2 Articular cartilage ..... 10

1.2 INNOVATIVE METHODS FOR STUDYING SKELETAL DISEASES ..... 11

1.3 PURINERGIC SYSTEM ..... 12

1.3.1 Extracellular ATP, ectonucleotidases enzymes and purinergic receptors ..... 13

1.3.2 P2X7 receptor (P2X7R) ..... 15

1.4 RELATION BETWEEN P2X7R AND SKELETAL SYSTEM: BONE CELLS AND INTERVERTEBRAL DISC CELLS ..... 19

1.4.1 Bone tissue ..... 20

1.4.2 IVD cells ..... 22

**2. AIMS OF THE STUDY** ..... **24**

**3. P2X7R IN BONE BIOLOGY** ..... **25**

3.1 EXPERIMENTAL MODELS ..... 25

3.2 METHODOLOGY ..... 25

3.2.1 Isolation and culture of human osteblasts (hOBs) ..... 25

3.2.2 Isolation procedure and culture of Wharton's jelly mesenchymal stromal cells (hWJ-MSCs) 26

3.2.3 Flow cytometric analysis ..... 27

3.2.4 Controlled culture conditions ..... 27

3.2.5 Immunocytochemistry ..... 28

3.2.6 Cell viability ..... 28

3.2.7 Osteogenic induction ..... 29

3.2.8 Mineralization assay ..... 29

3.2.9 Western blot ..... 30

3.2.10 Cytosolic free calcium concentration measurements ..... 30

3.2.11 Luciferase reporter assay ..... 31

3.2.12 Chromatin immunoprecipitation assay (ChIP) ..... 31

3.2.13 Statistical analysis ..... 32

3.3 RESULTS ..... 32
3.3.1 Characterization of human Wharton's jelly mesenchymal stromal cells and osteoblasts ..... 32
3.3.2 P2X7R expression ..... 34
3.3.3 Effect of P2X7R antagonist ..... 35
3.3.4 Characterization and activity of *P2RX7* gene promoter ..... 38
3.4 DISCUSSION ..... 44
**4. P2X7R IN INTERVERTEBRAL DISC ..... 48**
4.1 EXPERIMENTAL MODELS ..... 48
4.2 EXPERIMENTAL PLANNING ..... 51
4.3 METHODOLOGY ..... 52
4.3.1 Isolation of human IVD cells ..... 52
4.3.2 Histochemical analysis ..... 52
4.3.3 RNA Extraction and Quantitative Real-Time (qRT)-PCR ..... 53
4.3.4 Immunocytochemistry ..... 53
4.3.5 Immunofluorescence ..... 54
4.3.6 Cytosolic free calcium concentration measurements ..... 54
4.3.7 Ethidium bromide uptake ..... 54
4.3.8 Cytokines release ..... 55
4.3.9 Proliferation assay ..... 55
4.3.10 Statistical analysis ..... 55
4.4 RESULTS ..... 56
4.4.1 The expression level of P2X7R and NLRP3 in lumbar degenerated IVD tissue ..... 56
4.4.2 Characterization of P2X7R espression and functionality in IVD cells ..... 57
4.4.3 IL-1β release by IVD cells ..... 60
4.4.4 Growth kinetics in IVD cells in presence of P2X7R antagonist and agonists ..... 61
4.5 DISCUSSION ..... 63
**5. REFERENCES ..... 66**
**6. LIST OF PUBLICATIONS ..... 86**

# ABBREVIATIONS

**ABC**- ATP binding cassette transporters

**ACAN-** aggrecan

**ADAMTS-** disintegrin and metalloproteinase with thrombospondin motifs

**ADO-** adenosine

**ADP-** adenosine diphosphate

**AF-** annulus fibrosus

**ALP-** ectoalkaline/alkaline phosphatases

**AMP-** adenosine monophosphate

**ARS-** alizarin Red S staining

**ASC-** C-terminal caspase recruitment domain

**AP1**- activator protein 1

**ATP-** adenosine triphosphate

**BMPs-** bone morphogenetic proteins

**BSP-** bone sialoprotein

**BzATP-** 2', 3'-(4-benzoil)-ATP

**C/EBPs-** CCAAT/enhancer binding proteins

**CALMH-** calcium homeostasis modulator channel

**CREB**- c-AMP-responsive element-binding proteins

**CCL3-** CC-chemokine ligand 3

**CEP-** cartilaginous endplates

**ChIP-** chromatin immunoprecipitation

**Col1A-** type I collagen

**CXCL2-** CXC chemokine ligand 2

**DAMPs-** damage-associated molecular patterns

**Dlx5-** distal-less homeobox 5

**ECM-** extracellular matrix

**E-NPP-** ectonucleotide pyrophosphatase phosphodiesterases

**E-NTPDase-** ectonucleoside triphosphate diphosphohydrolases

**ES-** early stage of differentiation

**FCS-** fetal calf serum

**Fura-2/AM**- fura-2-acetoxymethyl ester

**GSK3β-** glycogen synthase kinase 3 beta

**HIF-1**- hypoxia-inducible factor 1

**hOBs-** human osteoblasts

**HSP-** heat shock protein

**hWJ-MSCs-** human Wharton' jelly mesenchymal stromal cells from

**IGF-** insulin-like growth factor

**IL-** interleukin

**IVD-** intervertebral disc

**IVDD-** intervertebral disc degeneration

**LPS-** lipopolysaccharide

**LS-** late stage of differentiation

**MCP-1/CCL2-** monocyte chemoattractant protein 1

**MMP-** matrix metalloproteinases

**MS-** middle stage of differentiation

**MSC-** mesenchymal stromal cells

**MV-** microvesicles

**NELL-1**- neural epidermal growth factor 1

**NFAT-** nuclear factor of activated T-cells

**NF-kB-** nuclear factor kappa B

**NLRP3-** NOD-, LRR- and pyrin domain-containing protein 3

**NP-** nucleus pulposus

**OA**- osteoarthritis

**OBs-** osteoblasts

**OCs-** osteoclasts

**OI**- osteogenesis imperfecta

**OPG-** osteoprotegerin

**OPN-** osteopontin

**Osx-** osterix/Sp7

**OXPHOS**- oxidative phosphorylation

**PAMPs-** pathogen-associated molecular patterns

**PBS-** phosphate buffered solution

**PGE2-** prostaglandin E2

**Pi-** phosphate

**PF-** Pfirrmann grade

**PI3K/AKT-** phosphoinositide 3-kinases/serine/threonine-protein kinase

**PLD-** phospholipase D

**PMA-** phorbol 12-myristate 13-acetate

**$pO_2$-** partial pressures of oxygen

**PPARγ -** peroxisome proliferator activated receptor gamma

**PPi-** pyrophosphate

**RA**- rheumatoid arthritis

**RT-** room temperature

**Runx2-** runt-related transcription factor 2

**SMAD-** SMAD family member

**SNP**- single nucleotide polymorphisms

**SOX9-** SRY-box 9

**Sp1**- specificity protein 1

**STAT-** signal transducers and activators of transcription

**TBS-** tris-buffered saline

**TCF/LEF1-** T-cell factor/lymphoid enhancer factor

**TFs**- transcription factors

**TGF-β-** transforming growth factor beta

**TIMP-1**- tissue inhibitor of metalloproteinase -1

**TLR-** toll like receptor

**TNF-α-** tumor necrosis factor alpha

**TRPS1-** tricho-rhino-phalangeal syndrome type I

**TSS**- transcription start site

**VEGF-** vascular endothelial growth factor

# 1. INTRODUCTION

## 1.1 SKELETAL SYSTEM

The skeletal system is composed of bones and cartilage connected by ligaments to form a dynamic framework for the body tissues. The skeletal system has several key functions, including: mechanical support and movement, protection for the soft tissue, mineral homeostasis, and hematopoiesis [Clarke, 2008; Florencio-Silva et al., 2015; Findlay and Kuliwaba, 2016]. Numerous diseases (osteoporosis, osteopetrosis, osteoarthritis, cancers), trauma and physiological aging cause skeletal frailty which at different levels may compromise the quality of life together with important socioeconomic impact [Clarke, 2008; Florencio-Silva et al., 2015; Findlay and Kuliwaba, 2016; Roberts et al., 2016]. Both in the pharmacological, in the surgical and tissue engineering areas, much progress has been made to develop strategies to repair skeletal defects and slow down the progression of bone tissue and cartilage degeneration [Johnstone et al., 2013; Amini et al., 2012; Liu et al., 2017]. However, many questions still remain open. The contribution that basic research can give in this scenario is particularly important, especially as regards the discovery of new molecular targets against which new effective therapeutics may be designed.

### 1.1.1 Bone tissue

#### 1.1.1.1 Bone formation and composition

The main components of bone, like all connective tissues, are cells and matrix. Bone cells represent a small amount of the bone volume and are crucial to the function of bones. There are four types of cells within bone tissue: osteoblasts, osteocytes, osteogenic cells, and osteoclasts [Raggatt et al., 2010; Toosi and Behravan, 2020; Clarke, 2008; Florencio Silva et al., 2015].

The process of bone formation is called osteogenesis or ossification. There are two types of ossification that occur in mesenchymal stromal cells (MSCs): in the intramembranous ossification (flat bones-cranium and medial clavicles), MSCs proliferate and differentiate directly into preosteoblasts and then into osteoblasts (OBs). Here, osteoblasts synthesize and secrete a collagen-proteoglycan matrix that will be calcified and mineralized [Cashman and Ginty, 2003; Mackie et al., 2011]. In the endochondral ossification (long bones-appendicular and facial bones, vertebrae and lateral clavicles), MSCs proliferate and differentiate into prochondroblasts and then into chondroblasts that synthesize and secrete cartilaginous matrix. Afterwards the chondroblasts are progressively embedded within their own matrix becoming hypertrophic chondrocytes [Cashman and Ginty, 2003; Mackie et al., 2008; Mackie et al., 2011]. In the last phases, cartilage is invaded by blood vessels and the chondrocytes undergo apoptosis, while surrounding cells differentiate into

osteoblasts, which start to produce bone extracellular matrix (ECM) over the degrading cartilage matrix [Cashman and Ginty, 2003; Mackie et al., 2008; Mackie et al., 2011]. In both processes, bone mature osteoblasts remain entrapped into the mineralized ECM and become osteocytes [Teitelbaum, 2007; Florencio-Silva et al., 2015; Katsimbri, 2017]. These cells act as endocrine organ [Katsimbri, 2017; Teitelbaum, 2007; Florencio-Silva et al., 2015] and also as mechanosensors, thanks to an intricate canalicular network, converting the mechanical pressures in biological molecules (e.g. ATP, nitric oxide, calcium and prostaglandins) [Teitelbaum, 2007; Florencio-Silva et al, 2015; Katsimbri, 2017].

The osteoclasts (OCs) are large multinucleated cells derived from mononuclear precursors of the monocyte-macrophage lineage and are the bone resorbing cells [Clarke, 2008; Florencio-Silva et al., 2015].

The osteoblasts (OBs) are the bone forming cells and are involved in bone remodeling and bone repair being designated to deposit mineral matrix [Raggatt et al., 2010; Toosi and Behravan, 2020]. The OBs are derived from MSCs through a multi-phase differentiation process, called osteogenesis and different maturation stages are recognized (mesenchymal progenitors, preosteoblasts and osteoblasts) [Infante and Rodriguez, 2018]. The differentiation of MSCs into OBs is a very complex multi-step process where a key role is played by specific transcription factors (TFs) only in part known. TFs action is guided in different stages of osteodifferentiation by specific soluble factors such as bone morphogenetic proteins (BMPs), insulin-like growth factors (IGF), neural epidermal growth factor 1 (NELL-1), and Wnt ligands [Wang et al, 2014; Capulli et al., 2014; Rico-Llanos et al., 2017; Hutchings et al., 2020; Pakvasa et al., 2017]. The role of many of cytokines in this process is fundamental, for example, the induction of the Wnt/βcatenin signal promotes bone formation by activating osteogenic factors, including runt-related transcription factor 2 (Runx2), distal-less homeobox 5 (Dlx5) and Osterix/Sp7 (Osx), and repressing the expression of peroxisome proliferator activated receptor gamma (PPARγ), the main adipogenic inducer [Baron et al., 2013]. Runx2, also known as Cbfa1, Osf2 and AML3, is the master regulator of osteogenesis able to promote the upregulation of osteoblast-related genes such type I collagen (Col1A) and alkaline phosphatase (ALP). The transition from immature to mature osteoblasts is accompanied by a morphological change and an increased in the expression of Osx, osteocalcin, Col1A and bone sialoprotein (BSP) [Fakhry et al., 2013; Capulli et al., 2014; Arboleya and Castañeda, 2013; Florencio-Silva et al, 2015; Hutchings et al., 2020]. Others TFs including hypoxia-inducible factor 1 (HIF-1α), SMAD family member (SMAD2/SMAD3), JunB, ETS2, signal transducers and activators of transcription (STAT1), nuclear factor of activated T-cells (NFATc1), FosB, JunD, Bapx1, Msx2, p53 [Song et al., 2009; Wang et al., 2017; Raouf and Seth, 2000; Kirkham and Cartmell, 2007] are involved in the

osteogenesis. Thanks to the employment of more sophisticated investigations and adequate experimental models the role of these transcription factors is becoming clear, even if in some cases contradictory evidence remains.

The balance between osteoblast and osteoclast activity governs bone turnover and ensures that bone is neither overproduced nor overdegraded. Bone remodeling begins before birth and continues through life until death, in order to respond to biomechanical and body changes, to remove micro damaged tissue and to preserve bone strength and functions [Clarke, 2008; Katsimbri, 2017]. When, for different reasons, bone remodeling is altered, pathological conditions or failure in the repair or regeneration processes occur.

Understanding those factors and molecular mechanisms that govern maturation and function of bone cells in the bone microenvironment is crucial, not only from biological point of view, but also for many implications in diverse areas of human health, from skeletal diseases to regenerative medicine. Although bone tissue has a regenerative capacity of healing, this process can fail, leading to delayed healing or development of non-union fractures. Acceleration of the fracture healing process would bring some benefits, such as the reduction of medical costs and enhancement of quality of life for the patients.

#### 1.1.1.2 Mineral matrix deposition

Biological mineralization is an orchestrated and finely regulated process that takes place in the bone tissue. Despite the plethora of studies investigating physiological mineralization in skeletal tissues, the process governing the production of the calcified extracellular matrix remains only partially understood.

Several mechanisms have been proposed as: i) cell-independent process, where noncollagenous proteins associating with collagen mediate mineral nucleation from ions in solution [Glimcher, 1984; Boonrungsiman et al., 2012]; ii) a cell-controlled mechanism by which vesicles from the plasma membrane accumulate ions extracellularly, mediate calcium phosphate precipitation, and subsequently pour their contents into the ECM [Anderson, 1995; Boonrungsiman et al., 2012]; iii) the transient formation of amorphous calcium phosphate [Boonrungsiman et al., 2012]. Many evidences suggest that the initial event of mineral matrix formation is the extracellular release of small membrane-bound microvesicles (MV) containing calcium and phosphate ions before associating with the collagenous components of ECM. Alternatively, amorphous calcium phosphate and ionic calcium stored in mitochondria are transported via vesicles to the ECM before converting to more crystalline apatite and propagating from dense foci [Boonrungsiman et al., 2012].

The elucidation of mineralization process is very important for the clinic implication in the field of bone and joint diseases. Furthermore, in view of potential therapeutic application, the dysregulation of mineral matrix deposition associated with aging, and to the onset of diseases such as ectopic ossification, joint calcification, atherosclerosis associated vascular calcification needs further mechanistic insights [Demer and Tintut, 2014].

The extracellular matrix of calcified bone is composed by organic matrix (20%), inorganic mineral (60%) and water (20%). Collagen is the main structural component of bone matrix and the majority is type I collagen (90%) with smaller amounts of types III, V, X, and XII collagens [Buckwalter et al., 1996; Fuchs et al., 2019]. The organic matrix also contains noncollagenous proteins, e.g. osteopontin, bone sialoprotein, osteocalcin and proteoglycans (hyaluronic acid, aggrecan, decorin, biglycan and versican). Although the noncollagenous proteins and proteoglycans little contribute to the total mass of the organic matrix, they have several important functions during osteoblast differentiation, tissue mineralization, cell adhesion, and bone remodeling [Fuchs et al., 2019]. The inorganic matrix serves as an ion reservoir storing approximately 99% of total body calcium, approximately 85% of phosphorus, and between 40% and 60% of the body's sodium and magnesium [Buckwalter et al., 1996; Fuchs et al., 2019]. Therefore, the bone quality depends from proteic composition, collagen crosslinks, microarchitecture and the correct mineralization. All these factors could vary with age, ethnicity, gender, presence of disease and/or drug therapies affecting the tissue quality.

### 1.1.2 Articular cartilage

#### 1.1.2.1 Cartilage composition

Articular cartilage is the highly specialized connective tissue of the joints. It is characterized by the lack of blood, lymphatic vessels and nerves and is subject to a complex biomechanical environment. For these reasons articular cartilage has a limited capacity for intrinsic healing/repair. Therefore, the preservation and health of joint cartilage are crucial for joint health [Archer and Francis-West, 2003]. Chondrocytes are metabolically active cells that synthesize and secrete the components of the cartilage extracellular matrix: collagens, glycoproteins, and proteoglycans [Archer and Francis-West, 2003]. As the osteoblasts, chondrocytes are derived from MSCs in a very well-regulated process called chondrogenesis [Camarero-Espinosa et al., 2016; Armiento et al., 2019].

#### 1.1.2.2 Intervertebral disc (IVD)

Articular cartilage with unique properties is that of the intervertebral disc (IVD). IVD is the fibrocartilaginous part of a 'three-joint complex' that governs motion, flexibility and weight-bearing

in the spine [Berg et al., 2018; Huang et al., 2018; Waxenbaum and Bennet, 2018]. The IVD is composed of different tissues, including a central highly hydrated nucleus pulposus (NP), the surrounding elastic annulus fibrosus (AF), and the cartilaginous endplate (CEP), which provides the connection to the vertebral bodies (Figure 1). These tissues are strictly interconnected and consists of a specific ECM. IVD matrix biosynthesis is performed by a cell population with distinct phenotype (whose markers have not been well identified yet) and is modulated by the mechanical loading and ATP release [Kerr et al., 2017; Berg et al., 2018; Waxenbaum and Bennet, 2018; Smith et al., 2011; Wuertz et al., 2012].

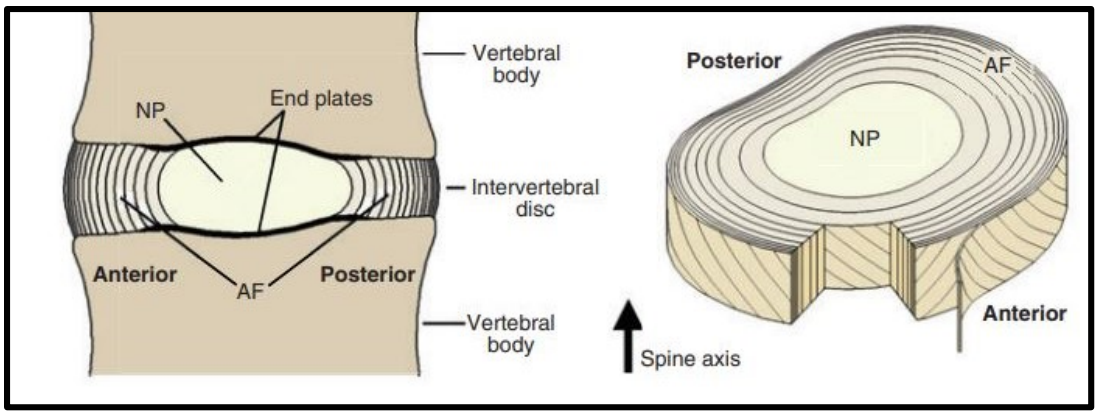


**FIGURE 1: Schematic representations of the intervertebral disc**. Cross section of disc anatomy and diagram of a transversely sliced intervertebral disc (IVD) [Smith et al., 2011].

Despite the cell density in IVD is very low (e.g. in an adult is about 55.00 cells/mm$^2$), numerous cells were found in the CEP and at the periphery of AF, being the closest regions to the limited vascular supply [Roughley, 2004; Urban and Roberts, 2006; González Martínez et al., 2017].

The IVD cell density decreases throughout life due to necrosis, apoptosis and senescence accompanied by chronic hypoxia and lack of glucose which can lead to different levels of disc degeneration [Ganey et al., 2003; Ito et al., 2002; Kalson et al., 2008; González Martínez et al., 2017; Urban, 2004].

## 1.2 INNOVATIVE METHODS FOR STUDYING SKELETAL DISEASES

Diseases of skeletal system are extensively widespread in aged population and are considered to be one of the main causes of disability and morbidity [Roberts et al., 2016; Lane, 2006; Sacitharan, 2019]. The most common disorders of the skeletal system include intervertebral osteoporosis, bone fractures, osteogenesis imperfecta (OI), osteoarthritis (OA), rheumatoid arthritis (RA) and disc degeneration (IVDD) [Roberts et al., 2016; Vos et al., 2012; Kerr et al., 2017; Lane, 2006; Sacitharan, 2019, Jones et al., 2014].

Apart from injuries and accidents, there are a number of factors predisposing to skeletal disorders that can anticipate the senescence of the skeletal system and also affect the young population. These include: genetics, dysmetabolism, environmental factors (smoking, lack of exercise, unhealthy lifestyle), sports-related overuse injuries, and occupational exposures (vibration, mechanical loading) [Jones et al., 2014].

In addition to clinical studies, the advancement of the understanding of skeletal physiological aging and pathologies, together with the development of effective therapeutic interventions is based on preclinical basic research studies employing different approaches. Among these it is worth remember:

- bone and cartilage tissue specimens of human origin to obtain primary cells for the realization of three-dimensional (3D) (culture and co-culture) *in vitro* models overcoming the limits of traditional 2D monolayer cell cultures [Baker and Chen, 2012; Cassotta et al., 2020; Owen and Reilly, 2018; Penolazzi et al., 2020];
- paying particular attention to the cell culture conditions for the realization of cell culture *in vitro* systems one step closer to natural conditions (pH, oxygen levels, glucose concentration, mechanical stimuli, dynamic condition and shear stress, calcium content, and paracrine signaling) [Penolazzi et al., 2020; Bader et al., 2011; Baker, 2016];
- adequate scaffold including biomimetic materials resembling the natural extracellular environment combined with cells at different stage of maturation [Park et al., 2018];
- drug-releasing scaffolds [Zeng et al., 2019];
- organ-on-a chip and integrated microfluidic culture platforms recapitulating the complex and dynamic (3D) environment experienced by bone and cartilage cells *in vivo* [Bader et al., 2011; Baker, 2016; Penolazzi et al., 2020];
- large animal models to assess the effectiveness of tissue engineering strategies in situations that more closely mimic the clinical scenario [Daly et al., 2016; Kuyinu et al., 2016].

## 1.3 PURINERGIC SYSTEM

Emerging evidence showed that the purinergic system, mainly through ATP and P2X7R, are involved in mechanotransduction and bone and joint diseases [Agrawal and Gartland, 2015; Kaebisch et al., 2015; Jorgensen, 2018; Koolpe et al., 1999; Kudirka et al., 2007; Varani et al., 2008; Knight et al., 2009; Burnstock et al., 2013]. A better understanding how this important system regulates the functions of skeleton may help to i.) improve the knowledge on the mechanisms that are involved in the onset and progression of skeletal diseases, and ii.) design novel repair strategies to restore bone and joint function.

The treatment of a wide range of diseases with employment of purinergic compounds is just beginning and much research in this field is needed [Burnstock, 2017]. Our purpose is to deepen the knowledge about purinergic system in skeleton with the aim of contributing to develop new effective therapeutic approaches.

### 1.3.1 Extracellular ATP, ectonucleotidases enzymes and purinergic receptors

ATP in the extracellular space regulates a variety of biological processes including cardiac function, neurotransmission, muscle contraction, vasodilatation, bone metabolism, and liver glycogen metabolism [Burnstock, 2004; Bours et al., 2006; White and Burnstock, 2006]. ATP is present in very little amounts (nmol/L) in the extracellular space under physiological conditions (healthy tissues), but increases dramatically in response to tissue damage, inflammation, hypoxia and ischaemia [Bours et al., 2006; Giuliani et al., 2019]. The release of ATP by the cells depends on the nature of the stimulus and/or on the pathophysiological condition; it occurs through different mechanisms involving: a) ATP binding cassette (ABC) transporters; b) vesicular exocytosis; c) gap junctions, connexins and/or pannexin hemichannels; d) calcium homeostasis modulator (CALMH) channel; e) P2X7R (Figure 2). In addition, ATP is released into the extracellular environment in a totally uncontrolled manner after cell damage, hypoxia, mechanical stress or necrosis [Verkhratsky et al., 2009; Eltzschig et al., 2012; Brandao-Burch et al., 2012; Idzko et al., 2014].

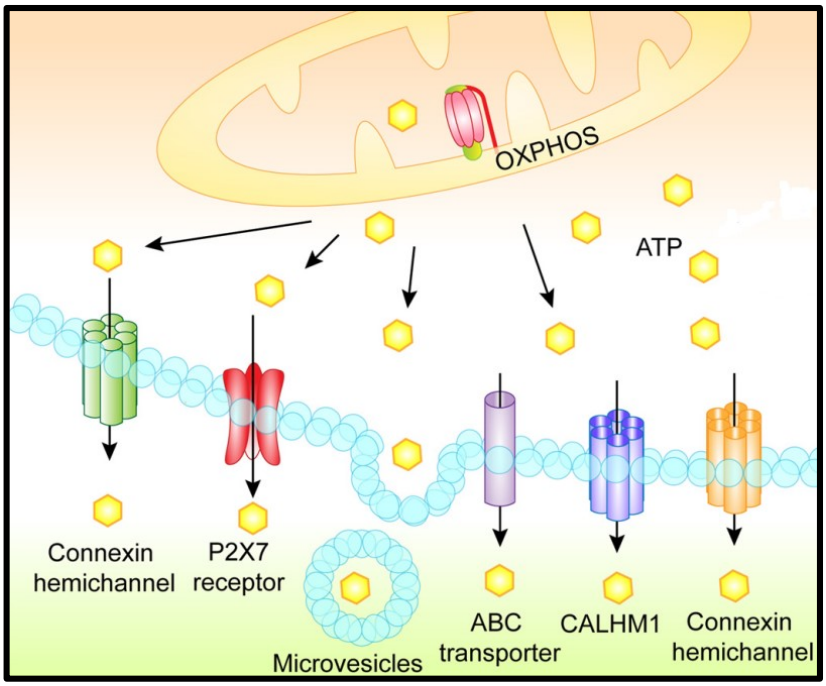


**FIGURE 2: ATP release.** The ATP generated inside the cell by glycolysis and oxidative phosphorylation (OXPHOS) can be released through vesicular exocytosis, plasma membrane-derived microvesicles, connexin or pannexin channels, ATP binding cassette (ABC) transporters, calcium homeostasis modulator (CALHM) channels or P2X7R [Giuliani et al., 2019].

The extracellular ATP degradation is controlled by the action of ectonucleotidases enzymes, including the members of the ectonucleoside triphosphate diphosphohydrolases (E-NTPDases), ectonucleotide pyrophosphatase phosphodiesterases (E-NPPs), ectoalkaline phosphatases (ALPs) and ecto-5'nucleotidase/CD73, which efficiently hydrolyze ATP, ADP and AMP to adenosine (ADO), generating phosphate (Pi) or pyrophosphate (PPi) in the extracellular space [Robson et al., 2006; Zimmermann et al., 2012; Bergamin et al., 2012]. The ALPs present specificity for numerous substrates such as phosphomonoester and phosphate compounds including adenine nucleotides, pyrophosphate, glucose-6-phosphate, and β-glycerophosphate [Zimmermann et al., 2012]. Bone ALP is a major regulator of bone mineralization [Vimalraj, 2020]. In particular, bone ALP hydrolyzes inorganic pyrophosphate which is a natural inhibitor of mineralization and provides inorganic phosphate for the synthesis of hydroxyapatite [Vimalraj, 2020].

The biological effects of extracellular nucleotides/nucleosides are mediated by purinergic receptors activation. Purinergic receptors include P1, adenosine sensitive receptors and P2, ATP and ADP sensitive receptors [Burnstock, 1978; Ralevic and Burnstock, 1998]. The P1 (metabotropic) receptors are sensitive to adenosine and are transmembrane receptors. Four subtypes have been described: A1, A2A, A2B and A3, with different pharmacological properties [Ralevic and Burnstock, 1998]. P2 receptors (P2R) include two subgroups: P2Y receptors and P2X receptors [Ralevic and Burnstock, 1998]. Eight P2Y receptors (P2YR) subtypes have been identified in mammals: P2Y1R, P2Y2R, P2Y4R, P2Y6R, P2Y11R, P2Y12R, P2Y13R and P2Y14R [White and Burnstock, 2006]. These receptors are G protein-coupled with seven transmembrane domains [Illes et al., 2000], whereas the P2X receptors (P2XR) are ligand-gated ionotropic receptors, exclusively activated by extracellular ATP [Abbracchio and Burnstock, 1994; Khakh et al., 2001; Roger et al., 2015]. The P2XR activation opens an ion channel in the cell membrane, permeable to $Na^+$ and $Ca^{+2}$ influx and $K^+$ efflux [Abbracchio and Burnstock, 1994; Khakh et al., 2001; Roger et al., 2015]. Seven P2XR subtypes have been identified: P2X1R, P2X2R, P2X3R, P2X4R, P2X5R, P2X6R and P2X7R [Di Virgilio et al., 2001]. Each receptor consists of i) N-terminus, ii) two transmembrane domains divided by a long extracellular loop, responsible for ligand interaction, and iii) a C-terminal tail varying in length depending on P2XR subtype [MacKenzie et al., 1999; Rassendren et al., 1997]. P2X7R is activated by sustained ATP exposure or higher ATP concentrations [Surprenant and North, 2009; Roger et al., 2015; North and Surprenant, 2000]. Among P2X receptors, P2X7R differs from other P2XR members and has been the subject of many studies with respect to others.

### 1.3.2 P2X7 receptor (P2X7R)

In recent years, P2X7R has been largely associated with pathological conditions where the extracellular ATP concentration rises dramatically, due to inflammation or leakage from cell damage among other pathways [Jimenez-Mateos et al., 2019]. This receptor attracts much attention by pharmacological companies and it is of emerging interest as a potential therapeutic target or new biomarker in several diseases [Jimenez-Mateos et al., 2019].

P2X7R is characterized by unique molecular structure and properties, described below:

a) **P2X7R structure:** the largest protein of the P2XR family [Surprenant et al., 1996] (595 aminoacids) with a glycosylated and cysteine-rich extracellular domain (282 aa), two transmembrane-spanning helices called TM1 and TM2 domains (about 24 aa each), a short intracellular N-terminal domain (26 aa) and a large intracellular carboxy-terminal domain (C-terminal, 239 aa). The three-dimensional monomer structure has a dolphin-like shape [Di Virgilio et al., 2018a; Di Virgilio et al., 2018b], where the large extracellular loop constitutes the main body (head, flippers and dorsal fin) and the two transmembrane helices form the dolphin tail [Hattori et al., 2012], as shown in figure 3.

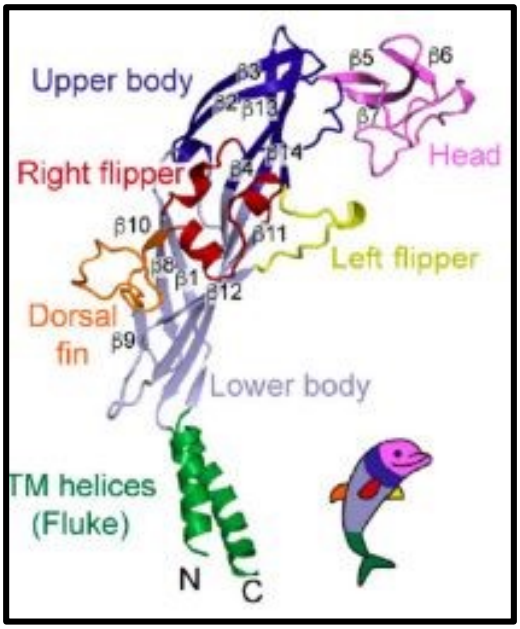


**FIGURE 3: Schematic ilustration of the P2X7R in the "dolphin-like" shape** [Di Virgilio et al., 2018a].

P2X7R has a unique long C terminus which is critical for the formation of a typical non-selective pore [Di Virgilio et al., 2018a; Di Virgilio et al., 2018b; Roger et al., 2015]. Convincing evidence suggests that: i) the pore is a consequence of dilatation of P2X7R channel [Di Virgilio et al., 2018a; Di Virgilio et al., 2018b], ii) P2X7R itself is unable to form a pore but, when activated, it can recruit accessory molecules (such as pannexin-1) that mediate pore formation [Pelegrin and

Surprenant, 2006]. Moreover, different proteins can interact with P2X7R including intracellular and heat shock proteins (HSP), cytoskeletal elements and kinases, P2X4R and pannexin-1 plasma membrane hemichannels [Pelegrin and Surprenant, 2006; Baroja-Mazo et al., 2013; Kopp et al., 2019].

b) **Single nucleotide polymorphisms (SNP):** *P2RX7* gene is highly polymorphic and more than 1500 human single nucleotide polymorphisms were identified. Two SNPs have been studied extensively: a) 1513A>C (rs3751143) that leads the substitution of glutamate for alanine at position 496 (E496A) and b) 489C>T (rs208294) that leads the substitution of histidine for tyrosine at position 155 (H155Y). The 1513A>C substitution, localized in the carboxyl-terminal cytoplasmic tail of the receptor, is associated in heterozygosis (AC) with a 50% decrease in P2X7R responses and in homozygosis (CC) to a near complete loss of P2X7R function [Gu et al., 2001; Sanz et al., 2014]. The 489C>T, localized in P2X7R ectodomain, instead, causes a gain of function [Cabrini et al., 2005; Sluyter and Stokes, 2011; Sanz et al., 2014; Di Virgilio et al., 2017].

c) **Transcriptional regulation of *P2RX7*:** human *P2RX7* gene is located on chromosome 12q24.31 [Sluyter, 2017; Jimenez-Mateos et al., 2019; Kopp et al., 2019], and its promoter region was first localized within a 2 kb DNA segment located in the gene 5'UTR region. The transcription initiation site is localized at nt 1683 of the *P2RX7* gene (GenBank Y12851), while the minimal active promoter region is localized within nt –158 to nt +32, with a TTAAA sequence at nt –32/–28 [Jimenez-Mateos et al., 2019; Bilodeau et al., 2015; Zhou et al., 2009]. Little is known about the *P2RX7* gene expression regulation. Only in the last years some evidences emerged as regards the action exercised by specific transcription factors. For example, the transcription factor specificity protein 1 (Sp1) has been reported to bind promoter region and to activate *P2RX7* gene expression in the mouse nervous system [Garcia-Huerta et al., 2012]. Bioinformatic analysis revealed that mouse *P2RX7* promoter contains putative regulatory elements including AP1 (activator protein 1), CREB (c-AMP-responsive element-binding proteins), HIF (hypoxia-inducible factor), STAT (signal transducer and activator of transcription), and T-cell factor/lymphoid enhancer factor (TCF/LEF1- involved in Wnt signal transduction pathway) binding sites [Garcia-Huerta et al., 2012; Jimenez-Mateos et al., 2019]. Human *P2RX7* promoter, contains CpGs rich islands which are potential sites for promoter methylation [Zhou et al., 2009; Jimenez-Mateos et al., 2019]. It has been recently showed that an increase in glucose concentration in intestinal epithelia cells stimulates *P2RX7* transcription via modulation of CCAAT/enhancer binding proteins (C/EBPs) [Bilodeau et al., 2015].

Today there is no evidence regarding regulation by transcription factors correlated with osteogenesis and bone metabolism.

d) **Post-transcriptional regulation of P2X7R:** Ten splice variants of human P2X7R have been described (P2X7R A–J) [Cheewatrakoolpong et al., 2005; Feng et al., 2006; Masin et al., 2012]. The canonical full-length is P2X7RA and the splice variants (P2X7RB, P2X7RC, P2X7RE, P2X7RG) are C-terminally truncated [Di Virgilio et al., 2017]. P2X7RG and P2X7RH have an inserted additional exon (exon N3), P2X7RC lacks exon 4, P2X7RD exon 5, P2X7RE exons 7 and 8, and P2X7RF exons 4 and 8. The P2X7RJ variant is truncated after exon 7 [Sluyter and Stokes, 2011, Di Virgilio et al., 2017]. The most common human splice variant is P2X7RB which acts as an ion channel but it is unable to trigger membrane permeabilization for large cationic molecules [Menkova-Garnier et al., 2016; Di Virgilio et al., 2017]. Moreover, it seems to display the same pharmacological properties of P2X7RA. In addition, the P2X7RA and P2X7RB can heterotrimerize in plasma membrane, producing the P2X7RA/P2X7RB that potentiates all P2X7RA functions, including large pore formation [Adinolfi et al., 2010]. The P2X7RB is the predominant form in many tissues and it has been related to tumor progression and mesenchymal cell differentiation [Giuliani et al., 2014; Carluccio et al., 2019], as shown in figure 4.

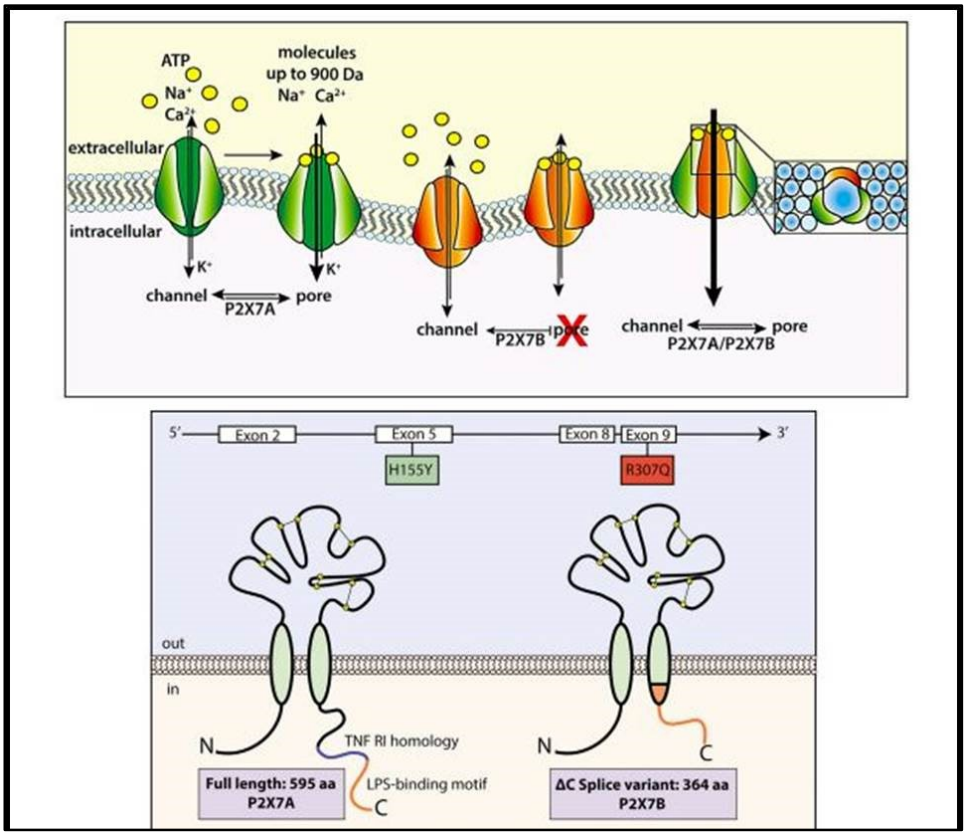


**FIGURE 4: P2X7RA and P2X7RB:** The full-length P2X7RA can function as an ion channel and a large pore (upper panel). The truncated P2X7RB is unable to generate the pore, the carboxy-terminal tail of P2X7RB lacks the last 249 aa of the full-length receptor and shows an insertion of 18 extra aa after residue 346. The P2X7RB can assemble with P2X7RA to form a heterotrimeric P2X7RA/P2X7RB receptor [Di Virgilio et al., 2018a; Di Virgilio et al., 2017].

e) **P2X7R activation:** this receptor presents an affinity for ATP (natural agonist), even if drastically lower than other P2XR receptors ($EC_{50} \geq 100$ μM) [Surprenant et al., 1996]. Another, and the most potent P2X7R agonist available, is 2,3'-(4-benzoil)-ATP (BzATP) being 10–30 times more potent than ATP. The activation of P2X7R opens, within milliseconds, a transmembrane ion-conducting channel that is selectively permeable to small cations such $Ca^{2+}$ and $Na^{+}$ (influx) and $K^{+}$ (efflux) [Surprenant et al., 1996; Rassendren et al., 1997; Roger et al., 2015]. P2X7R activation also induces membrane permeabilisation that refers to the formation of large pore that allows passage of large molecules, up to 900 Da, across the plasma membrane [Surprenant et al., 1996; Roger et al., 2015]. The pore formation is a reversible phenomenon that occurs after exposure to the agonist for prolonged application or after an exposure at a high agonist concentration (> 100 μM) [Di Virgilio et al., 1988, Roger et al., 2015]. Moreover, pore formation is associated with cytotoxic activity (apoptosis, necrosis and pyroptosis) [Adinolfi et al., 2005; Orioli et al., 2017].

f) **P2X7R functions:** P2X7R presents several functions in many distinct cell populations, or even in the same cell type, with a complex role in inflammation [Volonté et al., 2012]. The P2X7R is recognized as the main sensor for extracellular ATP during inflammation and mediates the immune response [Adinolfi et al., 2018]. Numerous cytokines and chemokines have been shown to be released upon P2X7R activation, such as: IL-1β, IL-18, tumor necrosis factor alpha (TNF-α), IL-6, monocyte chemoattractant protein 1 (MCP-1/CCL2), transforming growth factor beta (TGF-β), IL-8, CC-chemokine ligand 3 (CCL3) and CXC chemokine ligand 2 (CXCL2), and extracellular matrix remodeling factors such as: metalloproteinase-9 and tissue inhibitor of metalloproteinase (TIMP)-1 [Kopp et al., 2019; Di Virgilio, 2017; Orioli et al., 2017; Adinolfi et al., 2018; Riteau et al., 2010; Di Virgilio et al., 2020]. The P2X7R-dependend $K^{+}$ efflux induces inflammasome NLRP3 (NOD-, LRR- and pyrin domain-containing protein 3) activation [Orioli et al., 2017]. This phenomenon is involved both in host defense, and initiation and pathology of many inflammatory diseases [Coll et al., 2016]. NLRP3 can be activated by pathogen-associated molecular pattern (PAMPs: some of them are of bacterial origin), but also by damage-associated molecular pattern (DAMPs: uric acid crystals, amyloid β, asbestos, silica, alum adjuvant, cholesteral crystals, ATP) [Coll et al., 2016]. The NLRP3 inflammasome activation usually requires two steps: i) a priming signal (microbial ligands recognized by toll like receptors (TLR) or endogenous cytokines) leading to the upregulation of pro-IL-1β and NLRP3 protein levels by activating the nuclear factor kappa B (NF-kB) pathway; and ii) provided by some specific stimulus, such as ATP, to promote the assembly of C-terminal caspase recruitment domain (ASC) and pro-caspase-1 [He et al., 2016; Jo et al., 2016]. Alterations in ion homeostasis, mainly in the $K^{+}$ efflux or $Ca^{2+}$ mobilization, are the major mechanisms of NLRP3 activation [He et al., 2016;

Jo et al., 2016; Awad et al., 2018]. The extracellular ATP activates the NLRP3 inflammasome through P2X7R [Jo et al., 2016; Orioli et al., 2017]. The intracellular increase of $Ca^{2+}$ and $Na^{+}$ due to P2X7R activity induces a number of pathways such as those mediated by: NF-kB, nuclear factor of activated T-cells (NFAT), phosphoinositide 3-kinases/serine/threonine-protein kinase (PI3K/AKT), the glycogen synthase kinase 3 beta (GSK3β) down modulation. In addition, the P2X7R activation leads to the migration of HIF-1α transcription factor into the nucleus resulting in the production of vascular endothelial growth factor (VEGF) [Orioli et al., 2017; Adinolfi et al., 2018], (Figure 5).

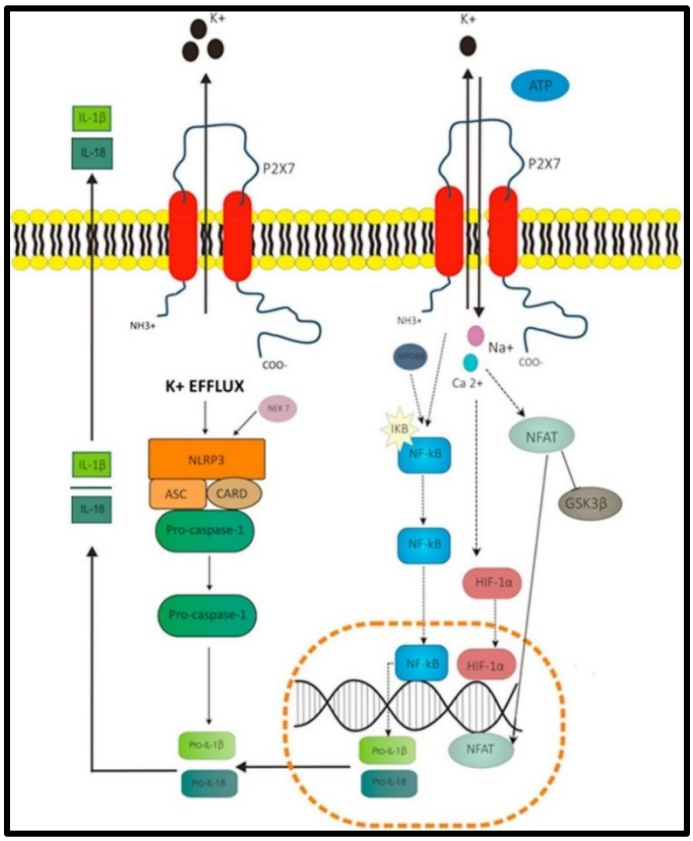


**FIGURE 5: P2X7R activation**. The $K^{+}$ efflux activates inflammasome, which causes maturation of pro-IL-1β and pro-IL-18. Moreover, P2X7R promotes the expression of some cytokines via nuclear factor kappa B (NF-κB), promotes hypoxia-inducible factor 1 (HIF-1α) activation, vascular endothelial growth factor (VEGF) release and nuclear factor of activated T-cells (NFAT) activation dependent of $Ca^{2+}$ influx [Adinolfi et al., 2018].

## 1.4 RELATION BETWEEN P2X7R AND SKELETAL SYSTEM: BONE CELLS AND INTERVERTEBRAL DISC CELLS

Over the last two decades many studies have demonstrated the presence of P2X7R in the cells of the skeletal system [Orriss et al., 2012]. Much progress has been made in understanding how P2X7R is regulated in bone and cartilage during both physiological and pathological conditions, even if much remains to be discovered and better understand [Jimenez-Mateos et al., 2019].

### 1.4.1 Bone tissue

In osteoclast cells, P2X7R exerts a profound effect on the differentiation and resorption. Increasing evidence has demonstrated that P2X7R plays a key role in osteoclast related bone erosion activity, since the inhibition of this receptor reduces the fusion of osteoclast precursors and formation of multinucleated osteoclasts *in vitro* [Dong et al., 2020]. However, conflicting data showed that P2X7R may induce osteoclast apoptosis with the formation of cytolytic pores and a decrease of bone resorption [Gartland et al., 2003a; Gartland et al., 2003b; Dong et al., 2020]. It is well known that NFATc1, the master transcription factor of osteoclast differentiation, induces the expression of numerous osteoclast differentiation markers [Ishiyama et al., 2015; Dong et al, 2020]. Inhibition of P2X7R leads to the suppression of NFATc1 impairing fusion, while the treatment with BzATP induces NFATc1 expression during osteoclastogenesis [Gartland et al., 2003a; Gartland et al., 2003b; Dong et al., 2020].

Differently from osteoclasts, the functionality of P2X7R in osteoblasts and their precursors is still debated [Agrawal and Gartland, 2015; Kaebisch et al., 2015; Jorgensen, 2018, Dong et al., 2020]. Additional studies are needed to examine whether expression of P2X7R is regulated and how such regulation might contribute to bone cell function [Grol et al., 2009]. Some studies showed that in osteoblasts, P2X7R activation increases differentiation and bone formation [Panupinthu et al., 2008], whereas, as described above, in osteoclasts can result in apoptosis [Gartland et al., 1999; Korcok et al., 2004; Grol et al., 2009]. These important differences in the effects of P2X7R in osteoblasts and osteoclasts may reflect a sophisticated mechanism through which the skeleton responds to mechanical stimulation by simultaneously enhancing bone formation and suppressing its resorption [Grol et al., 2009]. In this regard, the P2X7R might be an ideal target for the development of drugs with combined anabolic and anti-resorptive actions for use, for example, in treatment of osteoporosis and the prevention of bone loss in microgravity [Grol et al., 2009].

As mentioned, some studies indicate that activation of P2X7R by extracellular ATP leads to differentiation of osteoblasts as well as increased matrix formation and mineralization [Dong et al., 2020]. Other studies have shown that P2X7R activates phospholipase D (PLD) and increases lysophosphatidic acid, up-regulating specific osteoblastic markers (Runx2, osterix, sialoprotein and osteocalcin) and stimulating bone mineralization [Panupinthu et al., 2008; Dong et al., 2020]. On the contrary, in some experimental models, such as mesenchymal stromal cells, it was found that P2X7R increases the adipocyte marker peroxisome proliferator-activated receptor gamma (PPARγ), promoting adipogenesis at the expense of osteogenesis [Long et al., 2011; Dong et al., 2020].

Growing evidence has confirmed the participation of P2X7R in VEGF secretion and HIF-1α modulation [Orioli et al., 2017; Tafani et al., 2011], a critical phenomenon in the skeletal homeostasis.

It is in fact well known that the concentration of oxygen in the bone microenvironment is low (about 1%-8%). In the skeleton, the involvement of P2X7R in hypoxic conditions is little studied and represents, to date, an interest point to be deepened.

Another important aspect of bone metabolism where the role of P2X7R deserves deepening is the ATP-mediated purinergic signaling in the process of mechanotransduction [Dong et al., 2020; Kvist et al., 2014]. Osteoblasts and osteocytes release ATP into extracellular space in response to mechanical stimulation, such as sheer pressure and fluid flow, that is transduced into cellular responses by mechanotransduction mechanisms [Dong et al., 2020; Zeng et al., 2019]. It has been shown that P2X7R are important for a normal anabolic response to physical stimulation of the skeleton [Li et al., 2005; Kvist et al., 2014], therefore, it could be speculated that P2X7R are involved in the mechanotransductory cascade [Kvist et al., 2014]. The mechanical stimulation is an essential factor in regulating bone formation and remodeling [Dong et al., 2020; Kvist et al., 2014; Jorgensen, 2018]. It has been demonstrated that mechanical load-induced extracellular ATP activated P2X7R positively affects bone metabolism and also bone regeneration/repair in patients with bone fracture or bone inflammatory diseases [Dong et al., 2020; Jorgensen, 2018; Burnstock et al., 2013; Zeng et al., 2019; Kvist et al., 2014].

As already described, extracellular ATP can be degraded by ectonucleotidases which are present in osteoblast surface. The inorganic phosphate, generated by ATP hydrolyses, may stimulate bone mineralization and osteoblast proliferation [Grol et al., 2009; Dong et al., 2020]. However, ATP can also inhibit mineralization, in particular when hydrolyzed by E-NPPs enzymes that generate pyrophosphate which is a potent inhibitor of bone mineralization [Orriss et al., 2013; Dong et al., 2020].

High concentrations of ATP are needed to P2X7R activation and it has been controversial whether the receptor has any physiological functions in osteoblasts [Kvist et al., 2014]. *In vitro* concentrations of ATP above 1 mM partly inhibit bone formation especially mineralization [Orriss et al., 2012; Kvist et al., 2014]. This is a high concentration of ATP, and it may only occurs *in vivo* as a result of cell damage including microcracks in the bone tissue [Kvist et al., 2014]. Consequently, the effects are thought to be caused mainly by P2X7R and, like in the immune system, activation of P2X7R by ATP in the skeleton may be a danger signal of tissue or cell injury [Kvist et al., 2014]. With regard to the bone pathologies and the traumas that the skeleton can suffer, the role of P2X7R has been recently explored even if many issues still remain controversial. For example, in osteoporosis, studies showed that loss-of-function polymorphisms in the *P2RX7* gene may decrease the bone mineral density and the risk of vertebral fractures [Zeng et al., 2019]. Moreover, P2X7R can ameliorates osteoporosis by maintaining the balance between osteoclasts and osteoblasts activities [Zeng et al., 2019]. P2X7R

activation stimulates the differentiation of osteoblasts and enhances the mineralization of osteoblasts [Panupinthu et al., 2008; Zeng et al., 2019]. Knockout of P2X7R show diminished appositional growth of long bones and calvarial sutures, which cause impaired responses to mechanical loading [Zeng et al., 2019]. Therefore, P2X7R decreases fracture risk by the response to skeletal mechanotransduction [Zeng et al., 2019]. These results suggested that P2X7R can relieve osteoporosis by promoting osteogenesis and mineralization [Zeng et al., 2019]. On the other hand, the activation of P2X7R receptor can regulate osteoclast formation and activity, increasing the bone loss [Korcok et al., 2004; Zeng et al., 2019]. It reflects the complex nature of P2X7R [Zeng et al., 2019].

A possible explanation for these conflicting results could be related with the use of cell lines or animal models, that only partially represent what occurs in the human body, being necessary a more sophisticated and reliable experimental models.

### 1.4.2 IVD cells

The role of purinergic system has not been specifically investigated in IVD fibrocartilaginous microenvironment. The major information is based on chondrocytes. The chondrocytes express many P2 receptors (P2X1R, P2X2R, P2X3R, P2X4R, P2X7R, P2Y1R and P2Y2R) [Koolpe et al., 1999; Kudirka et al., 2007; Varani et al., 2008; Knight et al., 2009; Burnstock et al., 2013]. In these cells the P2R activation inhibits cartilage formation, promotes proteoglycan breakdown, increases the production of nitric oxide and prostaglandin E2 (PGE2), and the response of chondrocytes to ATP is enhanced by IL-1β and TNF-α [Burnstock et al., 2013]. In contrast, other studies demonstrated that the P2R activation stimulates proteoglycan and collagen accumulation and suppresses the nitric oxide released by the chondrocytes [Burnstock et al., 2013]. These conflicting results may be due to differential activation of purinergic receptors or to crosstalk between pathways induced by purinergic signaling [Kerr et al., 2017].

IVD cells respond to mechanical loading by converting the mechanical stimulus into a series of biochemical signals, including the production and release of extracellular ATP [Kerr et al., 2017; Fernando et al., 2011; Salvatierra et al., 2011] (Figure 6). Recent studies have demonstrated that compressive loading affects ATP production and its release by IVD cells [Fernando et al., 2011; Salvatierra et al., 2011]. High accumulated level of extracellular ATP in relation to physiological concentration was found in the NP of IVD [Gonzales et al., 2015; Trabanelli et al., 2012; Wang et al., 2013; Gonzales et al., 2014]. The extracellular ATP promotes the biosynthesis of ECM upregulating aggrecan and type II collagen expression [Gonzales et al., 2015].

Another point to be considered is the presence of an exacerbated inflammation in IVDD with the contemporary presence of some pro-inflammatory cytokines, as IL-6, MCP-1, IL-8, TNF-α, and IL-1β. All these cytokines have been correlated with P2X7R activation [Johnson et al., 2015; Di Virgilio et al., 2017; Adinolfi et al., 2018]. IL-1β plays a critical role in promoting disc degeneration [Johnson et al., 2015]. It has been reported that IL-1β mediates the induction of catabolic molecules including matrix metalloproteinases (MMP) and disintegrin and metalloproteinase with thrombospondin motifs (ADAMTS) [Johnson et al., 2015], and the release of this cytokine could be through P2X7R-NLRP3 dependent mechanism. In this scenario, the relation between this inflammatory cytokine, and P2X7R-NLRP3 in IVD cells could be a new interesting target pathway for IVD therapies.

As already mentioned, P2X7R is involved in a series of skeletal physiological activities including bone cell proliferation and differentiation [Grol et al., 2009; Dong et al., 2020]. P2X7R has also been associated in some joint diseases [Zeng et al., 2019]. For example: in osteoarthritis, the P2X7R mediates pain and inflammation: its inhibition decreases IL-1β, TNF-α, IL-6, MMP-13, and PGE2 release [Staunton et al., 2013; Chang et al., 2015; Zeng et al., 2019]. In the rheumatoid arthritis (RA), the P2X7R activation causes joint injury by producing inflammatory response in human rheumatoid synoviocytes and the inhibition of P2X7R alleviates the articular inflammation in RA [Caporali et al., 2008; Teixeira et al., 2017; Zeng et al., 2019].

In view of the need to develop new therapies aimed at regenerating/repairing the IVD and considering the role of P2X7R in inflammatory processes, it is reasonable to consider P2X7R as a potential drug target in IVDD.

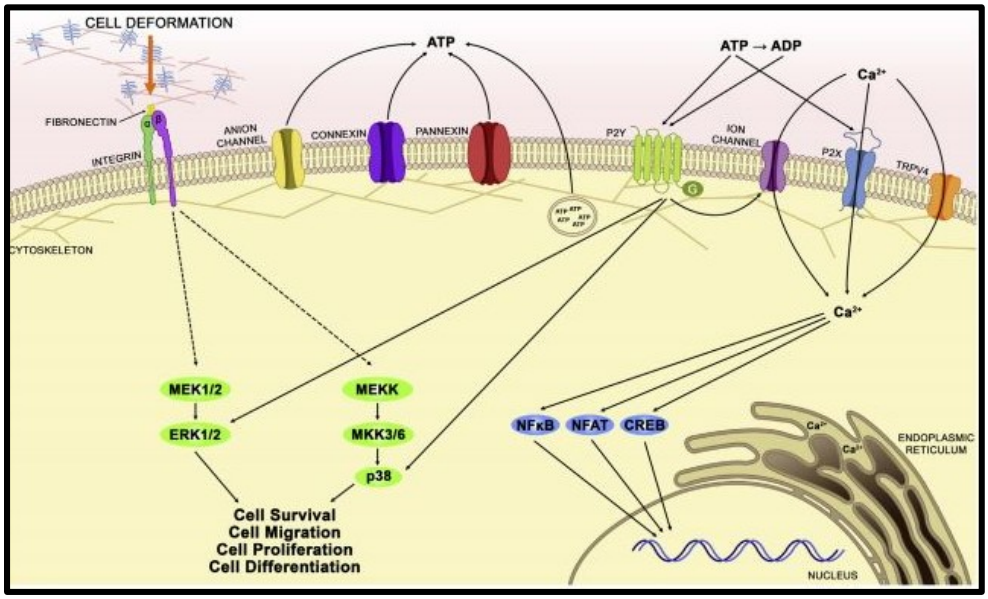


**FIGURE 6: Putative mechanotransduction pathways in intervertebral disc cells.** ATP is released from intervertebral disc cells and extracellular ATP could acts as a signaling molecule, binding to P2YR and P2XR [Kerr et al., 2017].

# 2. AIMS OF THE STUDY

The study carried out in this thesis concerns a wider scenario aimed at:

a) identifying new molecular targets for the design and development of effective drugs to be used both for the treatment of pathologies that affect bone and cartilage tissues, and for slowing the physiological degeneration process due to aging.
b) optimizing experimental cell culture conditions for mimicking the *in vivo* skeletal microenvironment.

Two major areas were investigated:

**1) *P2X7R in bone biology:*** The role of P2X7R in bone biology is only in part investigated and it is still not clear whether the P2X7R-mediated effects on bone are positive or negative. The major evidence about P2X7R and bone cells come from animal experimental models and cell lines, and these models reflect only in part what occurs in the human body. Part of the thesis has been focused: on i) the participation of P2X7R in the mineralization process, supported by mature cells (osteoblasts) and osteoblast precursor cells (mesenchymal stromal cells), and ii) the regulation of expression of *P2RX7* gene, during osteogenic differentiation.

**2) *P2X7R in intervertebral disc*:** IVD cells respond to mechanical loading by converting the mechanical stimulus into a series of biochemical signals including the production and release of extracellular ATP. In the extracellular space, the biological effects of this nucleotide are mediated by P2X7R. This receptor is related with a series of skeletal physiological activities and also in some joint diseases. As well as, the P2X7R induces the NLRP3 inflammasome activation and, as consequence, the IL-lβ release (involved in the initiation and progression of disc degeneration). The second part of the thesis has been focused on P2X7R participation in the degeneration and inflammation of intervertebral disc.

With this experimental planning, we expect that our data opens the way to deepen the knowledge on the regulation of P2X7R expression, to identify new targets in view of therapeutic approaches useful to restore the quality of bone and joint, and to improve the development of new skeleton repair strategies.

# 3. P2X7R IN BONE BIOLOGY

A first series of experiments were planned in order to contribute to the following open questions:

**1) Does the P2X7R participate significantly in the mineralization process?**
**2) Does the P2X7R respond to changes in oxygen concentration?**
**3) Is P2X7R expression modulated by transcriptional regulators that are recognized to play a role in the osteogenic differentiation process and osteoblastic function?**

For this purpose, the experiments were conducted as follows:

## 3.1 EXPERIMENTAL MODELS

We used human primary osteoblasts and human mesenchymal stromal cells.

## 3.2 METHODOLOGY

### 3.2.1 Isolation and culture of human osteblasts (hOBs)

Human bone fragments (explants) from 45 patients were employed in this study, 37 bone samples from the vertebral lamina, and 8 from skullcap (patients' age was between 30 and 86 years, mean age 62.4 years, 21 females and 24 males), as shown in table 1. The patients were operated for unstable spine disease or underwent brain surgery for intracranial tumor. The bone specimens were placed in sterile phosphate buffered solution (PBS) at 4°C and were dissected within 16 hours (h) after removal. Bone chips were minced in small fragments (2 $mm^3$) as previously reported [Lambertini et al., 2017], washed twice with PBS, placed in T25 culture flasks (Sarstedt, Nümbrecht, Germany) and cultured in 50% DMEM high glucose/50% DMEM F12 supplemented with 20% Fetal Calf Serum (FCS) (Euroclone S.p.A., Milan, Italy) and 100 µg/mL streptomycin/100 U/mL penicillin (Sigma Aldrich, St. Louis, USA) at 37°C, in a 5% $CO_2$ humidified atmosphere. Upon detection of a cell colony from the bone fragments (after 5-8 days) the cells were expanded until confluent (passage zero- P0). Then the cells were detached by trypsinization (0.05% Trypsin –EDTA solution, Sigma Aldrich) harvested, washed, counted with a hemocytometer, and plated at the confluence of 10.000 cells/$cm^2$ for further *in vitro* experiments (passage 1 (P1) to passage7 (P7)). The research protocol was approved by Ethics Committee of the University of Ferrara and S. Anna Hospital.

**Table 1:** Human osteoblasts samples information.

| Samples | Age | Sex | Type |
|---|---|---|---|
| **1** | 42 | M | vertebral lamina |
| **2** | 52 | M | vertebral lamina |
| **3** | 52 | M | vertebral lamina |
| **4** | 82 | M | vertebral lamina |
| **5** | 60 | F | vertebral lamina |
| **6** | 62 | M | vertebral lamina |
| **7** | 51 | F | vertebral lamina |
| **8** | 72 | F | vertebral lamina |
| **9** | 67 | F | vertebral lamina |
| **10** | 65 | F | vertebral lamina |
| **11** | 65 | F | vertebral lamina |
| **12** | 41 | M | vertebral lamina |
| **13** | 75 | M | vertebral lamina |
| **14** | 72 | F | vertebral lamina |
| **15** | 59 | F | vertebral lamina |
| **16** | 80 | M | vertebral lamina |
| **17** | 78 | M | vertebral lamina |
| **18** | 77 | M | vertebral lamina |
| **19** | 72 | F | vertebral lamina |
| **20** | 51 | F | vertebral lamina |
| **21** | 71 | M | vertebral lamina |
| **22** | 71 | F | vertebral lamina |
| **23** | 43 | M | vertebral lamina |
| **24** | 46 | F | vertebral lamina |
| **25** | 56 | M | vertebral lamina |
| **26** | 73 | M | vertebral lamina |
| **27** | 70 | M | Skullcap |
| **28** | 65 | M | Skullcap |
| **29** | 61 | F | Skullcap |
| **30** | 49 | F | Skullcap |
| **31** | 54 | F | Skullcap |
| **32** | 81 | F | Skullcap |
| **33** | 54 | M | vertebral lamina |
| **34** | 72 | F | vertebral lamina |
| **35** | 64 | M | vertebral lamina |
| **36** | 61 | F | vertebral lamina |
| **37** | 77 | F | vertebral lamina |
| **38** | 57 | M | vertebral lamina |
| **39** | 30 | M | vertebral lamina |
| **40** | 67 | M | vertebral lamina |
| **41** | 70 | M | vertebral lamina |
| **42** | 86 | M | vertebral lamina |
| **43** | 57 | F | Skullcap |
| **44** | 38 | M | Skullcap |
| **45** | 60 | F | vertebral lamina |

### 3.2.2 Isolation procedure and culture of Wharton's jelly mesenchymal stromal cells (hWJ-MSCs)

Human umbilical cords were collected after mothers' consent and approval of the Ethics Committee of the University of Ferrara and S. Anna Hospital. Harvesting procedures of Wharton's jelly from

umbilical cord were conducted in full accordance with the Declaration of Helsinki as adopted by the 18th World Medical Assembly in 1964 and successively revised in Edinburgh (2000) and the Good Clinical Practice guidelines. Typically, the cord was rinsed several times with PBS before processing and was cut into pieces (2–4 cm in length). Single pieces were dissected, first separating the epithelium of each section along its length, to expose the underlying Wharton's jelly. The soft gel tissue was then finely chopped. The same tissue was placed directly into a T25 flask for culture expansion in DMEM low glucose (Euroclone S.p.A.) supplemented with 10% FCS (Euroclone S.p.A.) and 100 U/mL penicillin /100 µg/mL streptomycin at 37°C in a 5% $CO_2$ humidified atmosphere. Upon detection of a cell colony, the cells were expanded until confluent (passage zero (P0)). Thereafter, cells were detached by trypsinization (0.05% Trypsin –EDTA solution, Sigma Aldrich), harvested, washed, counted with a hemocytometer, and and plated at the confluence of 10.000 cells/$cm^2$ for further *in vitro* experiments (passage 1 (P1) to passage 4 (P4)).

### 3.2.3 Flow cytometric analysis

hMSCs from Wharton's jelly were analyzed for the expression of mesenchymal and hematopoietic surface marker molecules. Briefly, cell pellets were resuspended in PBS and incubated with fluorescein isothiocyanate (FITC)– or phycoerythrin (PE)– conjugated mouse anti-human antibodies CD29-PE, CD34-FITC, CD44-FITC, CD45-PE, CD90-FITC and CD105-PE (DakoCytomation; Dako, Glostrup, Denmark) for 15 min at 4°C. Monoclonal antibodies with no specificity were used as negative control. Antibody-treated cells were then washed with PBS and spinned down. Cell pellets were resuspended in 400 µL of PBS and analyzed by FACS Scan (Becton Dickinson, Franklin Lakes, NJ). For each sample, 20.000 events were acquired and analyzed using the Cell Quest software (Becton Dickinson European HQ, Erembodegem Aalst, Belgium).

### 3.2.4 Controlled culture conditions

The experiments were performed at different partial pressures of oxygen ($pO_2$):
i) normoxic conditions, 21 % oxygen tension,
ii) hypoxic conditions, 1.5% oxygen tension.
hOBs and hWJ-MSCs were plated and cultured in normoxic conditions in a conventional incubator for 24 h at 37°C, allowing the cells to attach. Plates were then divided into two groups and incubated under either normoxic or hypoxic conditions for 48 h (early stage of differentiation). The cells were then grown in normoxic conditions and exposed to osteogenic medium (late stage of differentiation) for further *in vitro* experiments.

Hypoxic condition was obtained by using Xvivo System model X3 (BioSpherix Ltd., Parish, NY, USA) with a gas mixture composed of 1.5% $O_2$, 5% $CO_2$, and balanced $N_2$ at 37°C. The equipment consists of a modular set of closed incubator and closed hood, and allows high optimal solution for cell culture and handling under hypoxic conditions, preventing the effect of brief interruption of culture condition that can compromise the outcome of the experiments.

### 3.2.5 Immunocytochemistry

Immunocytochemical analysis was performed using the ImmPRESS kit (Vector Labs, Burlingame, USA). hOBs or hWJ-MSCs were fixed with cold 100% methanol at room temperature (RT) for 10 min; then rinsed three times with TBS 1X (Tris-buffered saline) for 5 min and permeabilized using 0.2% (v/v) Triton X-100 in TBS 1X for 5 min; then washed three times with TBS 1X for 5 min. Cells were treated with 3% $H_2O_2$ for 10 min (RT), washed once with TBS 1X for 5 min and incubated in normal horse serum (2.5 %) (Vector Labs) for 10 min at RT. After blocking, polyclonal antibodies for Runt-related transcription factor 2 (Runx2; M-70 #sc-10758, Santa Cruz Biotechnology, Dallas, USA; rabbit anti-human, 1:200 dilution), osteopontin (OPN; LF-123, a generous gift from Dr. L. Fisher, NIH, Bethesda, USA; rabbit anti-human, 1:200 dilution), type I collagen (COL1A1; H-197 #sc-28657, Santa Cruz Biotechnology; rabbit anti-human, 1:100 dilution), transcriptional repressor GATA binding 1 (TRPS1; #20003-1-AP, Proteintech, Manchester, United Kingdom; rabbit anti-human, 1:300 dilution), nuclear factor of activated T-cells, cytoplasmic 1 (NFATc1; H-110, #sc-13033, Santa Cruz Biotechnology; rabbit anti-human, 1:300 dilution) and P2X7R (#APR-004, Alomone Labs, Jerusalem, Israel; rabbit anti-human, 1:200 dilution) or isotype control (normal rabbit IgG; #2729, Cell Signaling technology, Massachusetts, USA; 1:200 dilution) were added and the incubation carried out overnight (4°C). Then, the cells were rinsed three times with TBS 1X for 5 min at RT, were incubated in Vecstain ABC (Vector Labs) and stained with DAB solution (Vector Labs). After washing, cells were mounted in glycerol/TBS 9:1 and observed with a Nikon Eclipse 50i optical microscope.

### 3.2.6 Cell viability

hOBs and hWJ-MSCs were seeded in 96 multi-well plates at density of 3.500 cells/well and 3.000 cells/well respectively. The cells were exposed to: the selective P2X7R antagonists A740003 (1 μM, 5 μM or 10 μM; Tocris Bioscience, Bristol, UK) or AZ 10606120 (300 nM and 1 μM; Tocris Bioscience) or 1 U/mL or 2 U/mL apyrase, an ATP and ADP scavenger (Sigma-Aldrich, USA). After 72 h of treatment, cell viability was assessed by 3-(4,5-dimethylthiazol-2-yl)-2,5 diphenyltetrazolium bromide (MTT) assay (Sigma-Aldrich). Briefly, MTT was added to each well,

the plate was incubated at 37°C for 2 h, and then the MTT crystals were solubilized with lysis buffer (10% SDS). The plate was incubated at RT for 24 h, and absorbance was measured at 570 nm with a spectrophotometer (Sunrise™ Absorbance Reader; Tecan Group Ltd., Männedorf, Switzerland). Live cells were calculated as a percentage of control (untreated cells).

For CalceinAM/propidium iodide (PI), hOB cells were seeded in 12 multi-well plates at density of 20.000 cells/well, and treated with A740003 (1 μM, 5 μM or 10 μM) for 72 h. Before staining, the medium was removed from the wells, and 500 μL of the staining solution was added to each well. The samples were incubated in the dark at room temperature for 15 min, thereafter the wells were rinsed with PBS and immediately visualized under a fluorescence microscope (Nikon, Optiphot-2; Nikon Corporation, Tokyo, Japan). Dead cells stained red, while viable ones appeared green.

### 3.2.7 Osteogenic induction

hOBs were seeded in 24 multi-well plates at density of 20.000 cells/well, representing about 80% of cell confluence, were kept in 50% DMEM high glucose (Euroclone S.p.A.) and 50% DMEM F12 (Euroclone S.p.A.) supplemented with 10% FCS (Euroclone S.p.A.) and cultured for 48-72 h, referred as the early stage of differentiation (ES). After this time, hOBs were exposed to osteogenic medium (DMEM high glucose supplemented with 10% FCS, in presence of 10 mM β-glycerophosphate, $10^{-7}$ M dexamethasone and 100 μM ascorbate, all from Sigma-Aldrich) for either 7-11 days, referred to as middle stage of differentiation (MS) or 11-28 days, referred to as late stage of differentiation (LS). Where indicated the cells were treated twice a week with A740003 (1 μM or 5 μM), AZ 10606120 (300 nM and 1 μM) or 2 U/mL apyrase, an ATP and ADP scavenger or 2 U/mL denaturated apyrase (Sigma-Aldrich, USA) until the late stage of differentiation (LS). Vehicle control group cells were exposed to DMSO 0.05% (Sigma-Aldrich).

hWJ-MSCs were seeded in 24 multi-well plates at density of 20.000 cells/well, representing about 80% of the cell confluence, were kept in DMEM low glucose medium (Euroclone S.p.A.) supplemented with 10% FCS (Euroclone S.p.A.) and cultured for 72 h, referred as the early stage of differentiation (ES). After this time, cells were exposed to osteogenic medium and cultured for further 18-32 days, referred as late stage of differentiation (LS). The osteogenic medium was changed and the cells were treated twice a week with 5 μM A740003 or DMSO (0.05%).

### 3.2.8 Mineralization assay

The extent of mineralized matrix was determined by Alizarin Red S staining (ARS) (Sigma-Aldrich). Cells were fixed in 70% ethanol for 45 min at room temperature, washed with PBS, stained with 40 mM ARS (pH 4.2) for 15 min at 37°C, and washed with deionized water. A solution of

cetylpyridinium 10% (p/v) in sodium phosphate was then added for 20 min. Absorbance was measured at 570 nm. Percentage of mineral matrix was expressed as percentage of control cells (untreated) and normalized over μg/μL of protein content.

### 3.2.9 Western blot

Cell lysates were prepared in lysis buffer (50 mMTris-HCl, pH 7.6, 1% NP-40, 150 mM NaCl, 1 mM NaF) supplemented with protease inhibitors. Proteins were quantified using the Coomassie blue method [Bradford, 1976]. Thirty μg of protein were resolved on Bolt Mini Gels 4–12% (Life Technologies, Carlsbad, USA). After electrophoresis, proteins were transferred to nitrocellulose membranes (GE Healthcare Life Sciences, Milan, Italy). Membranes were incubated overnight with the primary antibody (Ab) at 4°C. The anti-P2X7R antibody (#APR-004, Alomone labs) was used at a concentration of $1.6x10^{-3}$ mg/mL in 5% non-fat dry milk. The anti-actin antibody (#MA5-11869, Thermo Fisher Scientific) was used at a concentration of $2.0x10^{-5}$ mg/mL in 5% non-fat milk. Nitrocellulose membranes were incubated with the corresponding horseradish peroxidase-conjugated secondary antibody. The goat anti-rabbit (# 1706515, Bio-Rad, Milan, Italy) was used at a 1:3000 diluition, and goat anti-mouse (#1706516, Bio-Rad, Milan, Italy) was used at a 1:3000 diluition. Densitometric analysis was performed by ImageJ software (with NIH USA ImageJ software, public domain available at: http://rsb.info.nih.gov/nih-image/).

### 3.2.10 Cytosolic free calcium concentration measurements

The cytosolic free $Ca^{2+}$ concentration was measured using the fluorescent $Ca^{2+}$ indicator Fura-2-acetoxymethyl ester (Fura-2/AM) (Thermo Fisher Scientific, Waltham, USA) [Falzoni et al., 1995; Di Virgilio et al., 2019]. Cells at early stage of differentiation were incubated at 37°C for 20 min in saline solution (125 mM NaCl, 5 mM KCl, 1 mM $MgSO_4$, 1 mM $NaH_2PO_4$, 20 mM HEPES, 5.5 mM glucose, and 5 mM $NaHCO_3$, pH 7.4), in presence of 1 mM $CaCl_2$, and supplemented with 4.0 μM Fura-2/AM and 250 μM sulfinpyrazone (Sigma-Aldrich). Then, the cells were centrifuged at 300 x g for 5 min. The supernatant was discarded and the pellet was resuspended in the above saline solution. The cell suspension was placed in a thermostat-controlled (37°C) and magnetically-stirred cuvette of a Cary Eclipse Fluorescence Spectophotometer (Agilent Technologies, Milan, Italy). The $[Ca^{2+}]_i$ was determined at the 340/380 nm excitation ratio and at 505 nm emission wavelengths. The P2X7R agonist, 2', 3'-(4-benzoil)-ATP (BzATP) (500 μM; Sigma-Aldrich), was added to investigate P2X7R responses. Ionomycin 1 μM was added to trigger a maximal $Ca^{2+}$ increase.

### 3.2.11 Luciferase reporter assay

Two fragments of the human *P2RX7* gene (-2500/+34 P2X7R-Luc and -1500/+34 P2X7R-Luc) were cloned into the promoterless pGL4.10 [*luc2*] vector (pGL4.10-Luc Vector) containing a firefly luciferase cDNA (gift from Dr. Fernand-Pierre Gendron, Université de Sherbrooke, Quebec, Canada [Bilodeau et al., 2015]. For luciferase experiments, human cervical carcinoma HeLa cells were seeded in 24 multi-well plates at density of 64.000 cells/well and co-transfected using Lipofectamine 2000 (Thermo Fisher Scientific) with 0.125 µg of the different expression vectors (pBlight-FLAG TRPS1, pRSV NFATc1/A or pcDNA3.1 cbfa1) in combination with 0.25 µg of the different *P2RX7* promoter constructs or 0.25µg of pGL4.10-Luc Vector. Thirty hours after transfection, the medium was replaced with fresh medium and stimulated, where required, with 20 nM Phorbol 12-myristate 13-acetate (PMA; Sigma Aldrich) and 1 µM ionomycin (Thermo Fisher Scientific), for another 18 h. Thereafter, cells were washed once with PBS 1X and lysed in 120 µL of 1X reporter lysis buffer (Promega). Luciferase activity was measured using the Luciferase Assay System (Promega) in a GloMax 20/20 single tube Luminometer (Promega) and corrected for µg/µL of protein content. Luciferase output was expressed as fold change of the promoterless pGL4.10-Luc Vector emission, arbitrarly defined as 1.

To verify the effect of hypoxia on regulation of *P2RX7* gene, HeLa cells were transfected with 0.25 µg of -2500/+34 P2X7R-Luc or -1500/+34 P2X7R-Luc using Lipofectamine 2000 Reagent (Thermo Fisher Scientific). Twenty-four hours after transfection, the medium was replaced and the cells were cultured in presence or absence of 0.5 mM of hypoxia mimicking agent, $CoCl_2$, for 24 hours. Cells were then washed once with PBS 1X and lysed in 120 µL of 1X reporter lysis buffer (Promega, Milan, Italy). The luciferase activity was measured using the Luciferase Assay System (Promega) as mentioned above.

### 3.2.12 Chromatin immunoprecipitation assay (ChIP)

ChIP assays were performed as previously described [Lambertini et al., 2008]. Briefly, $5x10^6$ SaOS-2 cells (an osteosarcoma cell line with osteoblastic like phenotype) were cultured for 72 h in normoxic condition or $5x10^6$ hOB cells were incubated for 48 h under hypoxia or normoxia. Crosslinking of DNA-bound protein was achieved by 10 min incubation of the cells in a 1% formaldehyde solution at 37°C. Cells were then washed in ice-cold PBS, and resuspended in SDS lysis buffer supplemented with 1X protease inhibitor cocktail (Sigma Aldrich) for 15 min on ice. The isolated chromatin was sonicated to an average size of about 200–1000 bp. An equal amount of chromatin was immunoprecipitated at 4°C overnight with 5 µg of the following antibodies: NFATc1 (H-110, #sc-13033, Santa Cruz Biotechnology), Runx2 (M-70, #sc-10758, Santa Cruz

Biotechnology), β-catenin (#ab196204, Abcam, Cambridge, UK), Osterix (#ab22552, Abcam), TRPS1 (#20003-1-AP, Proteintech) and HIF-1α (#NB100-134 Novus Biologicals, CO, USA). Incubation with pre-immune rabbit IgG served as a negative control. Antibody-bound proteins were precipitated for 1h 30 min at 4°C using 60 µl of Protein A-conjugated agarose beads (Merck Millipore, Darmstadt, Germany). Immunoprecipitated chromatin complexes were sequentially washed with the following buffers: low salt wash buffer (0.1 % SDS, 1 % Triton X-100, 2 mM EDTA, 20 mM Tris–HCl pH 8.1, 150 mM NaCl), high salt wash buffer (0.1 % SDS, 1 % Triton X-100, 2 mM EDTA, 20 mM Tris–HCl pH 8.1, 500 mM NaCl), LiCl wash buffer (0.25 mM LiCl, 1% IGEPAL-CA630, 1% deoxycholic acid, 1 mM EDTA, 10 mM Tris-pH 8.1), and TE buffer. The immunocomplexes were eluted by adding a 200 µl aliquot of a freshly prepared solution of 1 % SDS in 0.1 M $NaHCO_3$ followed by incubation at room temperature for 30 min. Crosslinking was reversed by addition of 0.2 M NaCl (final concentration) followed by incubation at 65°C for 16 h. Samples were then digested with proteinase K at 45°C for 1 h and DNA was purified using PCR purification kit (Promega, Milan, Italy) according to the manufacturer's instructions. Two primers were used to detect the DNA segment located at −479/−162 within the *P2RX7* core promoter region: Fw 5′-CCAACTGCAGACCAGAGTATTA- 3′ and Rev 5′-CCCAGATGCCTACACAAAGA- 3′. Quantitative real-time PCR was performed with CFX96 Real-Time Detection System (Bio-Rad, California, USA) using iTaqUniversal SYBR Green SuperMix (Bio-Rad). The Input fractions (4% of the cell lysate before immunoprecipitation) were used as the internal positive control. Quantification of DNA binding was calculated as a fold enrichment using the $2^{(-\Delta\Delta Ct)}$ method and normalized against the pre-immune IgG sample.

### 3.2.13 Statistical analysis

The data were analyzed for statistical significance by Student's *t*- test or one way ANOVA followed by a post-hoc test for multiple comparisons (Tukey test). The data are expressed as the mean±SD. Differences were considered significant at $p<0.05$.

## 3.3 RESULTS

### 3.3.1 Characterization of human Wharton's jelly mesenchymal stromal cells and osteoblasts

The immunophenotypical profile of hWJ-MSCs was determined by flow cytometric analysis using a panel of antibodies against cell surface markers to attribute an MSC-like immunophenotype. As

shown in figure 7a hWJ-MSC samples were positive for CD90, CD29, CD44, and CD105 (mesenchymal cell markers), but negative for CD34 and CD45 (haematopoietic cell markers).

Cells from bone fragments were cultured in osteogenic medium and assessed for their intrinsic properties by immunocytochemistry to demonstrate the presence of typical osteoblast markers, i.e. Runx2, OPN (osteopontin), and COL1. Expression of two additional transcription factors acting at different stages in osteoblast proliferation and modulating different functions, such as NFATc1 and TRPS1 (tricho-rhino-phalangeal syndrome type I; an atypical member of GATA transcriptional factor family) was also investigated (Figure 7b). Furthermore, ability to deposit mineralized matrix was tested by Alizarin Red staining (ARS) in both cell types (Figure 7c). Based on these specific features, samples intrinsically more prone to generate typical hOBs were used for experiments, as reported in the scheme shown in figure 7d.

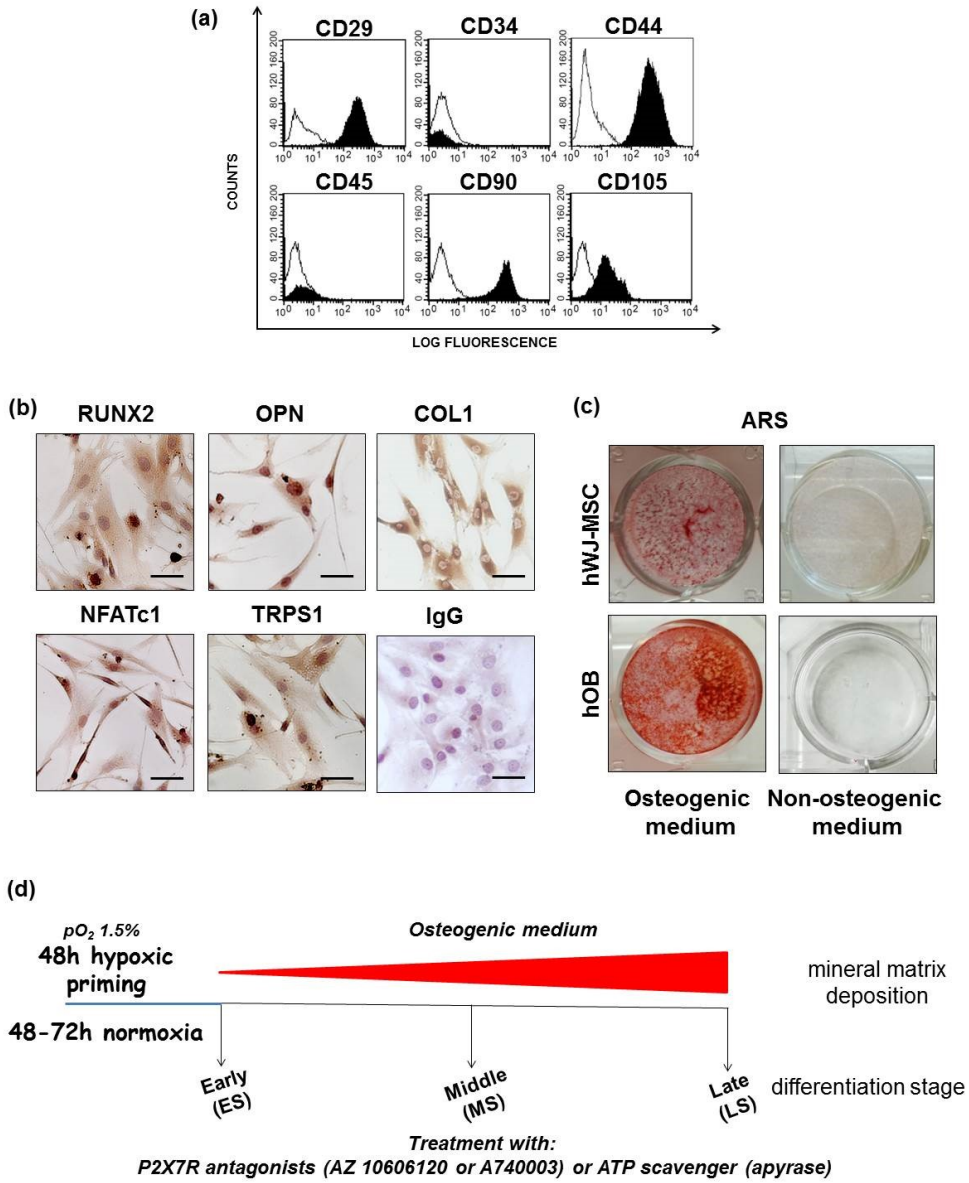


**FIGURE 7: Characterization of human Wharton's jelly mesenchymal stromal cells (hWJ-MSC) and human osteoblasts (hOBs)**. (a) The expression of typical mesenchymal stromal cells (MSC) surface markers (CD29, CD44,

CD90, and CD105) and hematopoietic markers (CD45 and CD34) were investigated by flow cytometric analysis. Isotype controls are represented by the white curves. (b) Representative images of human osteoblastic cells. The expression of runt-related transcription factor 2 (Runx2), osteopontin (OPN), type I collagen (COL1), nuclear factor of activated T-cells (NFATc1), and tricho-rhino-phalangeal syndrome type I (TRPS1) was evaluated by immunocytochemistry. The isotype control (IgG) was reported. Scale bars: 50 µm. (c) Deposition of mineral matrix was evaluated by Alizarin Red staining (ARS) in presence of osteogenic medium and non-osteogenic medium in both cell types. (d) Experimental planning. After a cell expansion in growth medium (early stage of differentiation, ES), hWJ-MSC and hOBs were cultured in osteogenic medium and, when required, the cells were treated twice a week with P2X7R antagonist (A740003, AZ 10606120) or apyrase for 7-11 days (middle stage of differentiation, MS) or 11-28 days in culture until the mineral matrix deposition (late stage of differentiation, LS).

### 3.3.2 P2X7R expression

Immunocytochemistry analysis revealed the presence of P2X7R on freshly isolated hOBs (Figure 8a). When the cells were cultured in osteogenic medium in normoxia, Western blot analysis revealed a slight increase of P2X7R expression, suggesting a positive correlation between P2X7R expression and osteoblast (Figure 8b). Hypoxic priming did not alter the P2X7R protein expression (Figure 8b). To test whether the P2X7R was functional, hOBs at early stage of differentiation were stimulated with the P2X7R semi-selective agonist BzATP. BzATP triggered a sharp increase in the cytoplasmic $Ca^{2+}$ concentration followed by a sustained plateau, suggestive of a prolonged influx from the extracellular space through the P2X7R channel (Figure 8c,g). Notably, mesenchymal stromal cells from Wharton' jelly (hWJ-MSCs), despite expressing P2X7R (Figure 8d,e), showed no response to BzATP stimulation (Figure 8f,g), suggesting that either the P2X7R was not functional or was not exposed on the plasma membrane. Unlike, hOBs, P2X7R levels decrease during hWJ-MSCs osteogenic differentiation in both conditions (normoxia or hypoxic priming) (Figure 8e).

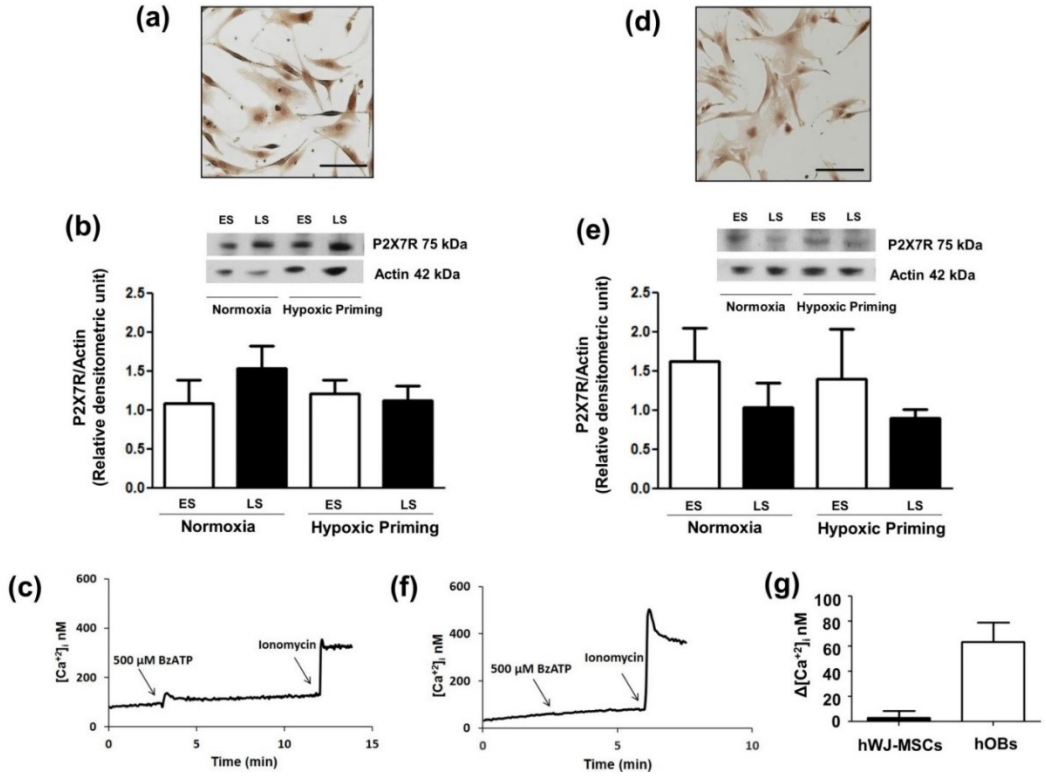

**FIGURE 8: Expression and function of P2X7R in human osteoblasts (hOBs) and human Wharton's jelly mesenchymal stromal cells (hWJ-MSCs).** (a) Representative immunostaining of P2X7R in freshly isolated hOBs. (b) Representative Western blot in the early stage (ES) and in the late stage of hOBs differentiation (LS) in normoxic or hypoxic priming condition is reported with densitometric analysis of samples analyzed. Data are expressed as mean±SD of P2X7R/Actin ratio. Data were analyzed byANOVA followed by Tukey test, $p<0.05$. (c) Representative trace showing the intracellular $Ca^{2+}$ rise following hOBs stimulation with 500 μM BzATP. (d) Representative immunostaining of P2X7R in hWJ-MSCs. (e) Representative Western blot in the early stage (ES) and in the late stage of differentiation (LS) of hWJ-MSCs in normoxic or hypoxic priming condition is reported with densitometric analysis of all samples analyzed. Data are expressed as mean±SD of P2X7R/Actin ratio. (f) Representative trace showing the intracellular $Ca^{2+}$ rise following hWJ-MSCs stimulation with 500 μM BzATP. (g) Intracellular $Ca^{2+}$ rise following stimulation with 500 μM of P2X7R agonist (BzATP). All experiments were carried out at least three times.

### 3.3.3 Effect of P2X7R antagonist

To further investigate the role of the P2X7R in the hOB maturation we tested the effect of the potent and selective P2X7R antagonist A740003 on mineral matrix deposition by hOBs cultured in osteogenic medium in normoxia or hypoxic priming. Blockage of P2X7R with 5 μM A740003, but not 1 μM decreased deposition of mineralized matrix in the late stage of hOB differentiation in both conditions (Figure 9a), while no effect was observed in osteo-differentiated hWJ-MSCs (Figure 10a). Blockage of P2X7R with A740003 did not cause toxicity in hOBs (Figure 9b) and hWJ-MSCs (Figure 10b). The effect of A740003 suggests that the P2X7R is tonically activated in culture even in the absence exogenously-added ATP and this process is independent of oxygen concentrations.
Since we found that the hypoxia seems not to affect the ability of hOBs to deposit mineral matrix in presence of A740003, we performed next experiments only in normoxia condition.
We also tested the mineral matrix deposition by hOBs in presence of another potent P2X7R antagonist (AZ 10606120) demonstrating that this molecule only slightly decreased the mineralization: there was a reduction of 12% at a concentration of 300 nM and 24% at a concentration of 1 μM (Figure 11a). Blockage of P2X7R with AZ 10606120 did not cause toxicity in hOBs (Figure 11b).

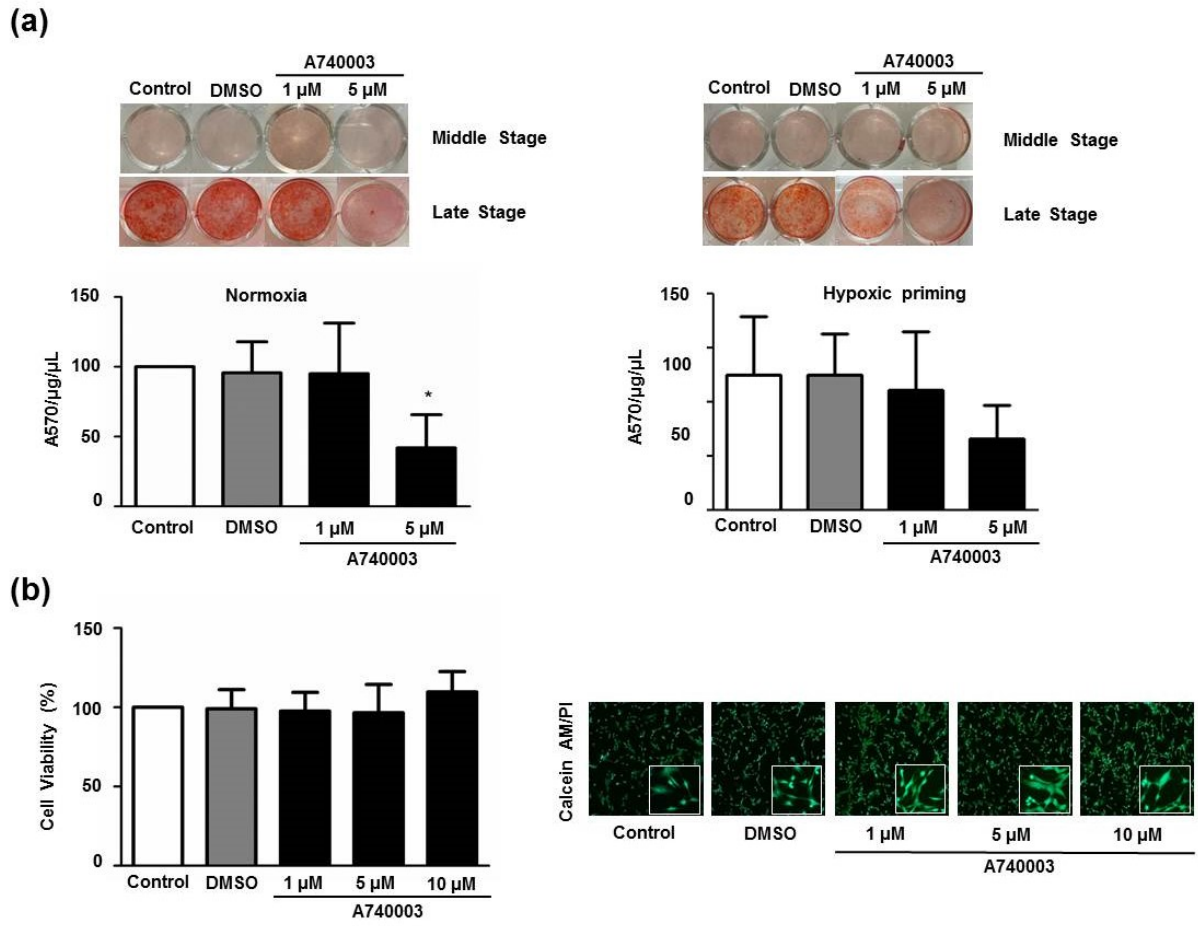


**FIGURE 9: Effect of P2X7R antagonist (A740003) on human osteoblasts (hOBs) matrix mineralization.** (a) Matrix mineralization was analyzed by Alizarin Red S staining after the treatment with 1 µM or 5 µM A740003 in osteogenic medium in normoxia or hypoxic priming. The cells were treated twice a week, until the mineral matrix deposition (late stage of differentiation). Data are expressed as mean±SD and were analyzed by one way ANOVA followed by Tukey test. The percentage was calculated in relation to control cells (untreated), considered as 100% ($p$<0.05). *different from control cells and dimethyl sulfoxide (DMSO) cells. All experiments were carried out at least three times. (b) Cell viability in presence of A740003 was measured in hOBs treated for 72 h with 1 µM, 5 µM or 10 µM A740003 by 3-(4,5-dimethylthiazol-2-yl)-2,5-diphenyltetrazolium bromide (MTT) analysis (left panel), and by double staining with Calcein AM/propidium iodide (right panel). The green fluorescence indicates the presence of calcein labeled live cells, while propidium iodide labeled dead cells are revealed by red fluorescence. Merged photomicrographs are reported. Viability is expressed as percentage of control (untreated) cells. All experiments were carried out at least three times. Data are expressed as mean±SD (untreated cells considered as 100%) and were analyzed by one way ANOVA followed by Tukey test.

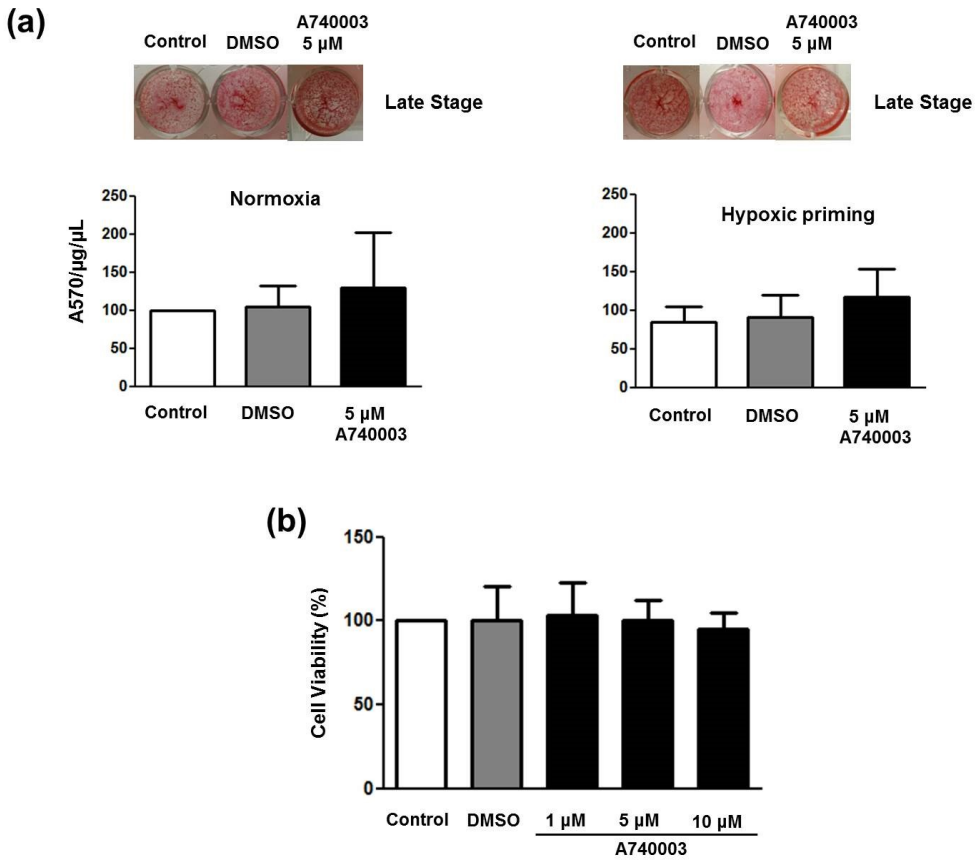


**FIGURE 10: Effect of P2X7R antagonist on human Wharton's jelly mesenchymal stromal cells (hWJ-MSCs) matrix mineralization.** (a) Mineral matrix formation was analyzed by Alizarin Red Staining after the treatment with 5 µM A740003 in normoxia and hypoxic priming. Data are expressed as mean±SD and were analyzed by one way ANOVA followed by Tukey test. The percentage was calculated in relation to control cells (untreated), considered as 100% ($p$<0.05). All experiments were carried out at least three times. (b) Cell viability was analyzed in hWJ-MSCs treated with 1 µM, 5 µM or 10 µM A740003. The percentage was calculated in relation to control cells (untreated), considered as 100% ($p$<0.05).

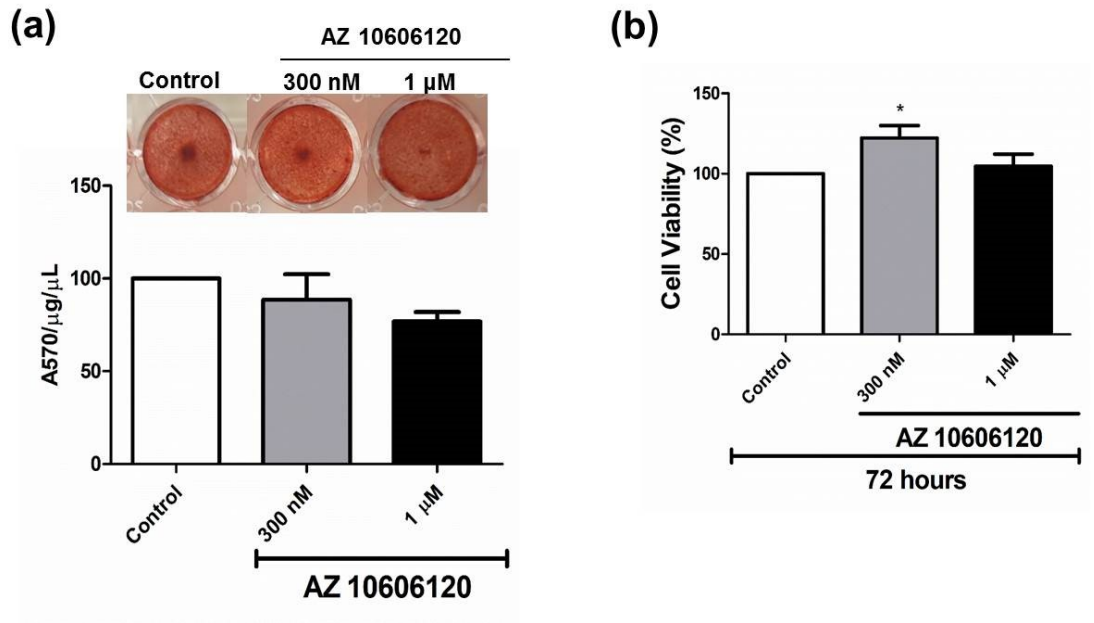


**FIGURE 11: Effect of P2X7R antagonist (AZ 10606120) on human osteoblasts (hOBs) matrix mineralization.** (a)

Mineral matrix formation was analyzed by Alizarin Red Staining after the treatment with 300 nM or 1 μM AZ 10606120. Data are expressed as mean±SD and were analyzed by one way ANOVA followed by Tukey test. The percentage was calculated in relation to control cells (untreated), considered as 100% ($p$<0.05). (b) Cell viability was analyzed in hOBs treated with 300 nM or 1 μM AZ 10606120. The percentage was calculated in relation to control cells (untreated), considered as 100% ($p$<0.05).

Since the treatment with P2X7R antagonist decreased the mineral matrix deposition, it is conceivable that removal of ATP from the culture medium should inhibit these responses. Thus we verified the effect on matrix mineralization of apyrase, a nucleotide-degrading enzyme. As shown in figure 12 mineral matrix deposition, in presence or in absence of β-glycerophosphate, as well as cell viability, was unaffected when the cells were exposed to apyrase. As expected, the presence of β-glycerophosphate in the osteogenic medium is necessary for deposition of the mineral matrix. Refractoriness of P2X7R-dependent responses to apyrase treatment is not novel. It is in fact known that apyrase, 47 kDa in size, may not easily reach the ATP halo generated in close contact with the outer part of the plasma membrane. This is even true in osteoblasts which release ATP at distinct plasma membrane sites via a strictly regulated vesicular pathway [Brandao-Burch et al., 2012].

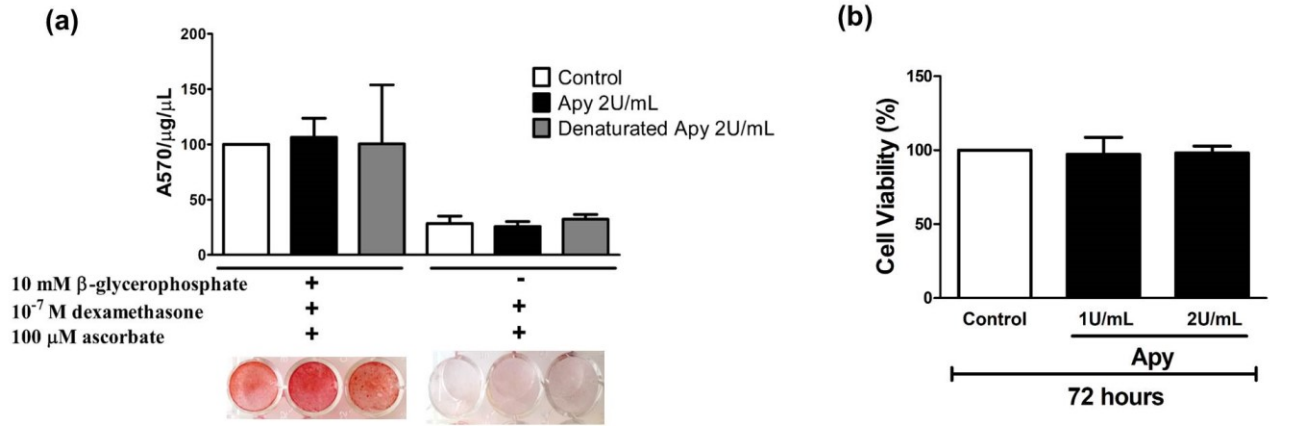


**FIGURE 12: Effect of ATP scavenger on human osteoblasts (hOBs) matrix mineralization.** (a) Mineral matrix formation was analyzed by Alizarin Red Staining after the treatment with 2 U/mL apyrase (Apy) or denatured apyrase. Data are expressed as mean±SD and were analyzed by one way ANOVA followed by Tukey test. The percentage was calculated in relation to control cells (untreated), considered as 100% ($p$<0.05). All experiments were carried out at least three times. (b) Cell viability was analyzed in hOBs treated with 1 U/mL or 2 U/mL apyrase. The percentage was calculated in relation to control cells (untreated), considered as 100% ($p$<0.05).

### 3.3.4 Characterization and activity of *P2RX7* gene promoter

Little is known about the regulation of the human *P2RX7* gene expression, today there are only a couple of studies that investigated the human *P2RX7* promoter. In the first, Zhou and collaborators [Zhou et al., 2009] identified the active promoter region and the transcription initiation site, using a series of cDNA fragments that were generated encompassing a 1.7 kb DNA segment of the human *P2RX7* gene 5′ region (Figure 13a,b). Fragments ranging from −1664/+32 to −53/+32 nt were cloned

and inserted into a luciferase vector. The P2X7R-luciferase reporter was transfected into the P2X7R negative HEK293 cells. Significant promoter activity was found in fragments ranging from −1664/+32 to −158/+32 nt, while shorter fragments lacked significant promoter activity. Maximal promoter activity was found in the −158/+32 nt fragment [Zhou et al., 2009], a second study with five different luciferase constructs [Bilodeau et al., 2015], found that the *P2RX7* (Figure 13c) promoter is regulated by the C/EBPβ.

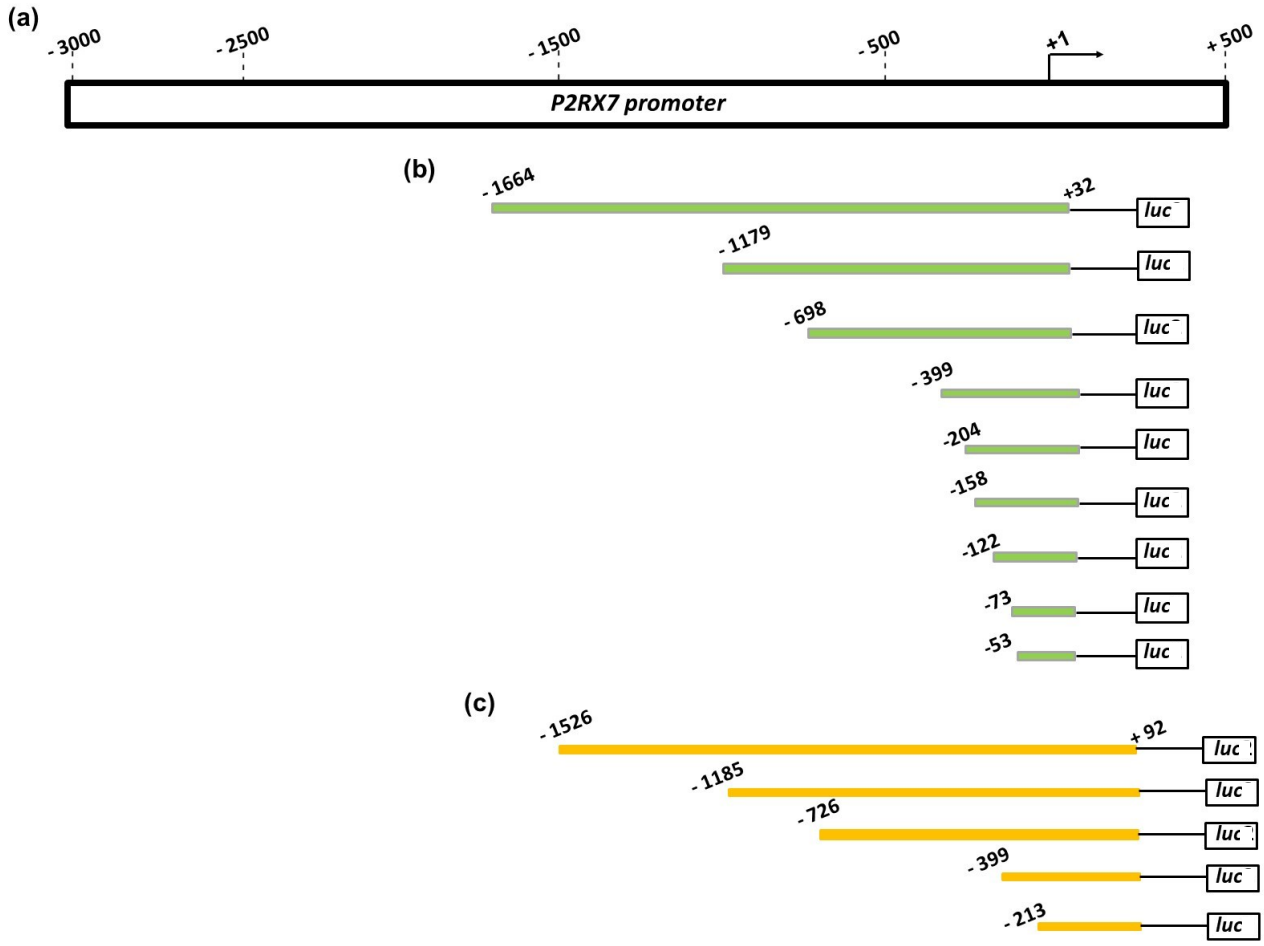


**FIGURE 13: Human *P2RX7* promoter.** (a) Schematic representation of *P2RX7* promoter. (b) The schematic representation of *P2RX7* promoter constructs used by Zhou [Zhou et al., 2009] and collaborators for elucidation of *P2RX7* active promoter region. (c) Schematic representation of the *P2RX7* promoter constructs used by Bilodeau and collaborators for elucidation of *P2RX7* regulation by CCAAT/enhancer binding proteins (C/EBP) [Bilodeau et al., 2015].

Starting from these evidences and from the data so far available on the role of the P2X7R in bone cells, we have then turned our interest to understand if the expression of P2X7R was regulated by osteogenic factors. First of all, the *P2RX7* 5'-flanking region spanning +56 to -2500 was subjected to a bioinformatics analysis by using AliBaba 2.1 public software, to identify potential binding sites for the main osteogenic transcription factors. The sequences of binding sites for transcription factors by us investigated are reported in table 2. As shown in figure 14, the *P2RX7* promoter region analyzed

contains numerous potential binding sites for transcription factors, e.g. Runx2, Osterix, TCF/LEF1, NFAT, TRPS1 and HIF-1 which are well known for their critical role in osteoblast maturation [Agrawal et al., 2017; Sindhavajiva et al., 2017; Minear et al., 2010; Penolazzi et al., 2011; Goss et al., 2019; Fan et al., 2014]. Of notice, we found nine potential binding motifs for NFAT. This is of particular interest because previous findings showed that the P2X7R couples to the $Ca^{2+}$-NFATc1 pathway [Giuliani et al., 2014], and its function is required for NFATc1 nuclear localization and transcriptional activity in rat osteoblasts [Grol et al., 2013]. Therefore, we focused our attention on investigating whether *P2RX7* was itself a NFAT target gene.

**Table 2:** Sequences of transcription factor binding sites.

| Transcription Factor | Consensus Binding Site |
|---|---|
| **SP7/Osterix** | GGGCGG |
| **TRPS-1** | (A/T)GATA(A/G) |
| **RUNX-2** | (T/C)G(T/C)GG(T/C)/ TG(T/C)GG(T/C)/ (A/G)CC(A/G)CA |
| **NFATc1** | GGAAA/ TTTCC |
| **HIF-1** | (A/G)CGTG/ CACG(T/C) |
| **TCF/LEF1** | (A/T)(A/T)CAAAGG |

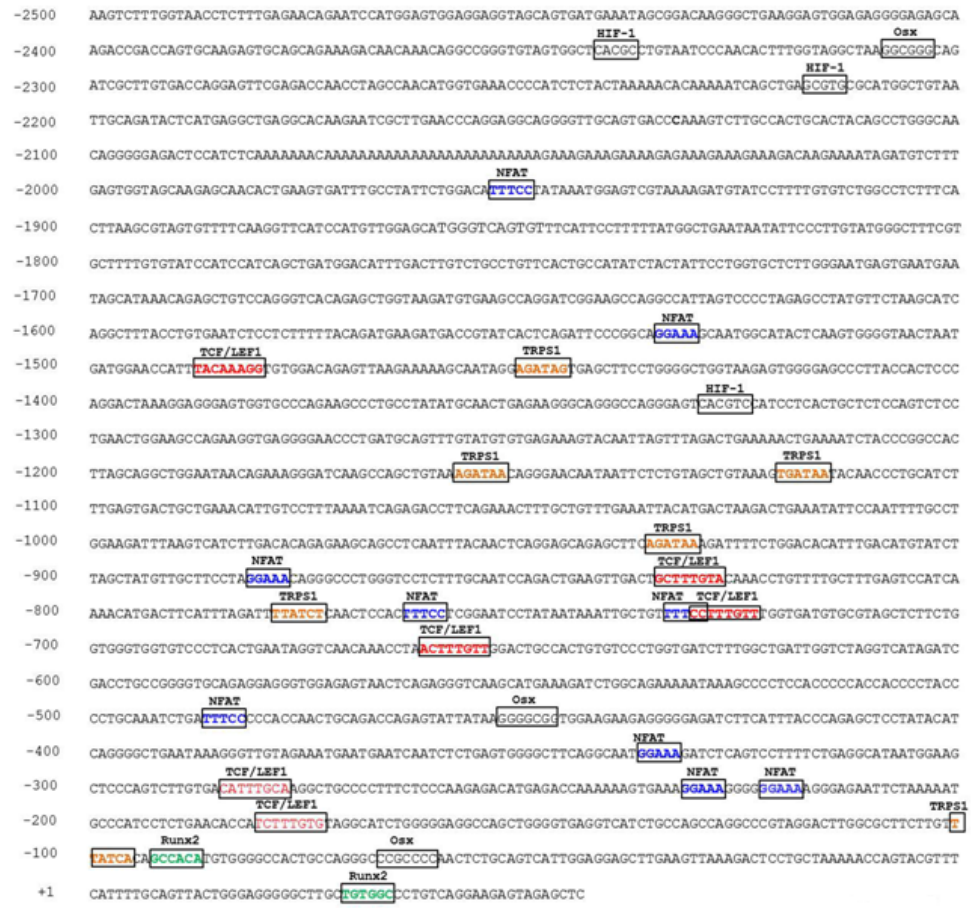


**FIGURE 14: *In silico* analysis of the human *P2RX7* gene promoter region (-2500 to +56 bp).** Nucleotide numbering

is relative to the first nucleotide (adenine +1) of the transcription start site (TSS), which is indicated in bold. The positions of putative transcription factor binding motives identified using the AliBaba 2.1 public software tool are boxed.

The involvement of NFATc1 in the modulation of the *P2RX7* promoter and in the regulation of the expression of P2X7R was investigated by Luc assays in Hela cells transfected with NFATc1/A expression vector. Two different *P2RX7* promoter constructs were used, the -2500/+34 P2X7R-Luc containing all the NFAT potential binding sites, and the -1500/+34 P2X7R-Luc lacking the two most distal sites (Figure 15a). As shown in figure 15b, the two constructs have comparable effects on the overall activity of the promoter, and were both positively affected by NFATc1 overexpression in presence of ionomycin and PMA: *P2X7R* promoter activity was enhanced by more than 13-fold both in -1500/+34 P2X7R-Luc and -2500/+34 P2X7R-Luc in relation to pGL4.10-Luc Vector. Promoter activity also increased when the cells were co-transfected with TRPS1 or Runx2 expression vector, but the increase was not statistically significant (Figure 15c,d). The hypothesis that the *P2RX7* is a direct transcriptional target of NFATc1 was confirmed by chromatin immunoprecipitation assays by using the SaOS2 osteoblastic-like cells. As shown in figure 15e, NFATc1 occupancy was demonstrated by using the specific primers positioned in the core promoter region. The same analysis was also performed to investigate the *in vivo* recruitment of Runx2, TRPS1, β-catenin and osterix in the predicted binding sites, but no binding was detected.

As described above, using bioinformatic analysis, we also identified three potential HIF-1 binding sites in the *P2RX7* promoter (Figure 16a). To determine whether HIF-1 activity plays a role in *P2RX7* transcriptional activation, HeLa cells were transfected with the above *P2RX7* promoter constructs. As shown in figure 16b, our preliminary results showed that the activity of *P2RX7* promoter was negatively affected by $CoCl_2$ (hypoxia mimicking agent). With this result, the possibility that P2X7R is a direct transcriptional target of HIF-1 was examined by ChIP assay. As reported in figure 16c, HIF-1 was specifically recruited at *P2RX7* promoter in hypoxia preconditioned hOB only in one sample of total of three samples analyzed. The results obtained by us so far are inconclusive, therefore, further investigation is necessary to conclude whether hypoxia may or may not regulate *P2RX7* promoter activity.

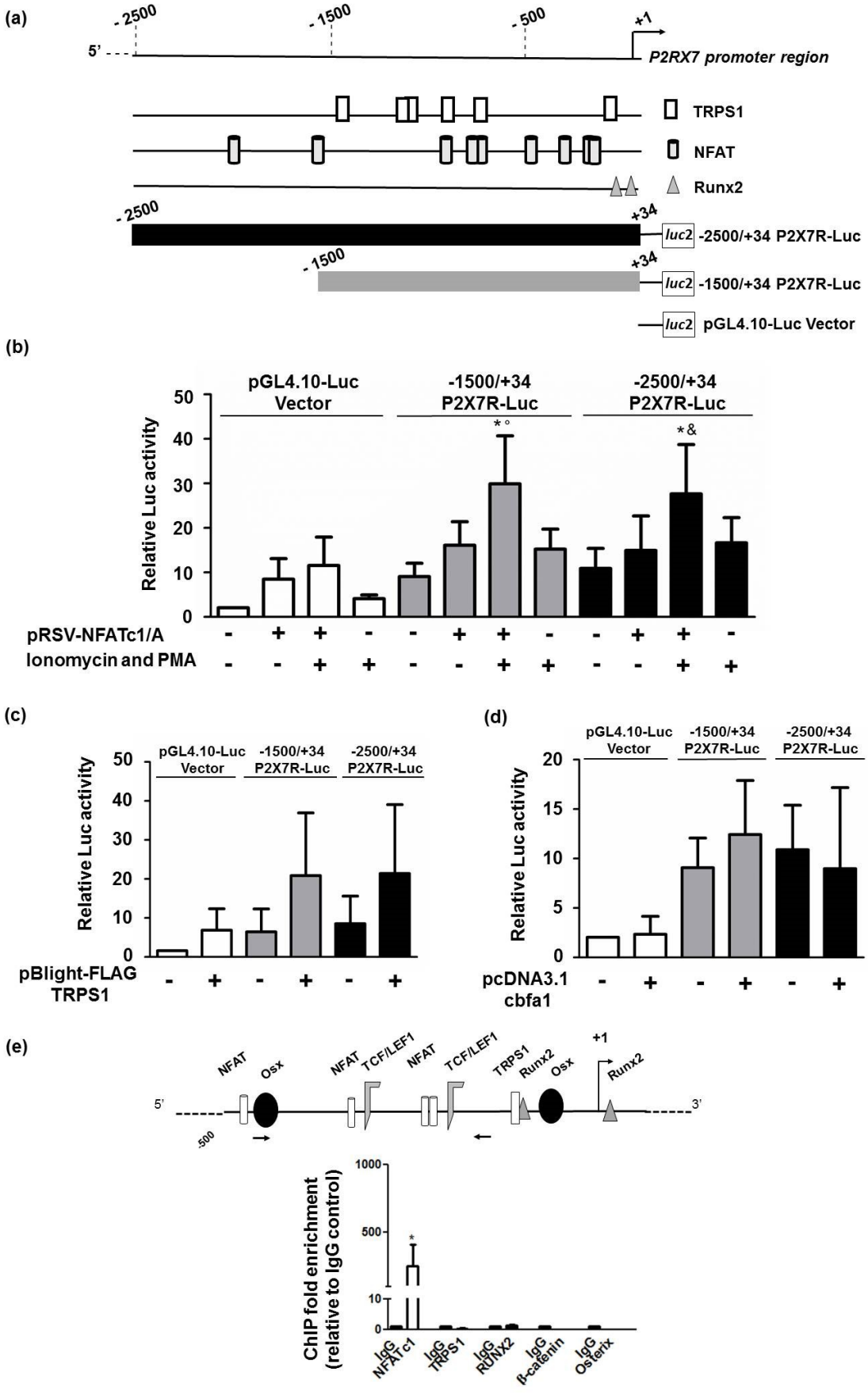
(a)
-2500
-1500
-500
+1
5'
P2RX7 promoter region
TRPS1
NFAT
Runx2
-2500
+34
luc2
-2500/+34 P2X7R-Luc
-1500
+34
luc2
-1500/+34 P2X7R-Luc
luc2
pGL4.10-Luc Vector
(b)
pGL4.10-Luc Vector
-1500/+34 P2X7R-Luc
-2500/+34 P2X7R-Luc
Relative Luc activity
50
40
30
20
10
0
*°
*&
pRSV-NFATc1/A
Ionomycin and PMA
(c)
pGL4.10-Luc Vector
-1500/+34 P2X7R-Luc
-2500/+34 P2X7R-Luc
Relative Luc activity
pBlight-FLAG TRPS1
(d)
pGL4.10-Luc Vector
-1500/+34 P2X7R-Luc
-2500/+34 P2X7R-Luc
Relative Luc activity
pcDNA3.1 cbfa1
(e)
NFAT
Osx
NFAT
TCF/LEF1
NFAT
TCF/LEF1
TRPS1
Runx2
Osx
+1
Runx2
5'
3'
-500
ChIP fold enrichment (relative to IgG control)
1000
500
10
0
*
IgG NFATc1
IgG TRPS1
IgG RUNX2
IgG β-catenin
IgG Osterix

**FIGURE 15: *P2RX7* promoter activity.** (a) Position of potential binding sites for tricho-rhino-phalangeal syndrome type I (TRPS1), nuclear factor of activated T-cells (NFAT), and runt-related transcription factor 2 (Runx2) in the *P2RX7* promoter, and the schematic representation of *P2RX7* promoter constructs. Transcriptional activity of *P2XR7* promoter was assessed by luciferase assay in HeLa cells transfected with 0.25 µg of PGL4.10-Luc Vector, -1500/+34 P2X7R-Luc or -2500/+34 P2X7R-Luc constructs, in combination with 0.125 µg of the expression vectors (b) pRSV-NFATc1/A (in presence or absence of 1 µM ionomycin and 20 nM PMA); (c) pBlight-FLAG TRPS1; (d) pcDNA3.1 cbfa1 (Runx2). Luciferase activity was corrected for protein content. Luciferase output was expressed as fold change of the promoterless pGL4.10- Luc Vector emission, arbitrarily defined as 1, (n=4). Data are expressed as mean±SD and were analyzed by one way ANOVA followed by Tukey test, $p<0.05$. * versus pGL4.10-Luc Vector control group, ° versus -1500/+34 P2X7R-Luc in the absence of NFATc1/A, ionomycin and phorbol 12-myristate 13-acetate (PMA), & versus -2500/+34 P2X7R-Luc in the absence of NFATc1/A, ionomycin and PMA. (e) Chromatin immunoprecipitation assay (ChIP) analysis of NFATc1 (in presence of 20 nM PMA and 1 µM ionomycin), TRPS1, Runx2, β-catenin, osterix recruitment to the *P2RX7* promoter. The positioning and sequences of NFATc1, TRPS1, β-catenin, osterix and Runx2 potential binding sites within the *P2RX7* core promoter together with the position of the specific primers used for real time PCR (qPCR) amplifications are reported. The graph shows the results of ChIP-qPCR analysis performed on DNA templates obtained from SaOS-2 cells. Results of real time PCR (qPCR) were analyzed by the $2^{(-\Delta\Delta Ct)}$ method after normalization to the IgG negative control and data expressed as mean±SD of at least three independent experiments. * $p<0.05$.

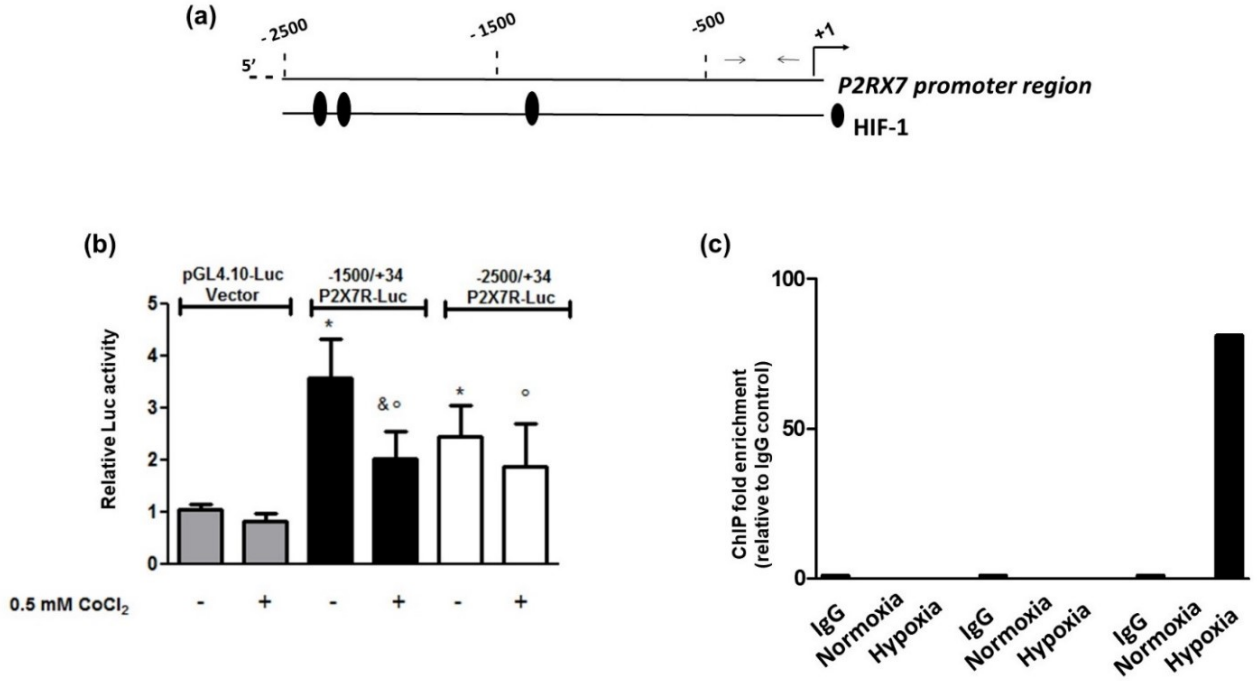


**FIGURE 16: *P2RX7* promoter activity under hypoxia** (a) Position of potential binding sites for hypoxia-inducible factor 1 (HIF-1) in the *P2RX7* promoter. Transcriptional activity of *P2XR7* promoter was assessed by luciferase assay in HeLa cells transfected with 0.25 µg of PGL4.10-Luc Vector, -1500/+34 P2X7R-Luc or -2500/+34 P2X7R-Luc constructs, in combination with 0.5 mM $CoCl_2$. Data are expressed as mean±SD and were analyzed by one way ANOVA followed by Tukey test, $p<0.05$. * versus pGL4.10-Luc, °versus pGL4.10-Luc+$CoCl_2$ and &-1500/+34 P2X7R-Luc versus -1500/+34 P2X7R-Luc+$CoCl_2$. (c) Chromatin immunoprecipitation assay (ChIP) HIF-1 (three hOBs samples analyzed). The graph shows the results of ChIP-qPCR analysis performed on DNA templates obtained from hOBs. Results of qPCR were analyzed by the $2^{(-\Delta\Delta Ct)}$ method after normalization to the IgG negative control.

## 3.4 DISCUSSION

The evidence gathered from this study is that hOBs express a functional P2X7R by conventional methods showing (a) the intracellular calcium rise following hOBs stimulation with BzATP agonist, and, consistently (b) the decrease of mineralized matrix deposition after treatment with the A740003 antagonist. In the second part of the work, we focused on characterization and activity of the *P2RX7* gene promoter, identifying in the *P2RX7* promoter several specific binding sites for transcription factors differently involved in the mineralization process in the bone microenvironment. In particular, we provided evidence demonstrating that the P2X7R is upregulated by NFATc1, a member of the NFAT family of cytosolic $Ca^{2+}$-dependent transcription factors [Sitara and Aliprantis, 2010]. By the ChIP analysis, we demonstrated for the first time that NFATc1 is recruited at the *P2RX7* promoter (Figure 17).

NFATc1 is well known as a master regulator of osteoclastogenesis [Kim et al., 2016] whilst the role of NFATc1 signaling in osteoblasts is not well understood and is still controversial [Penolazzi et al., 2011; Kim et al., 2016]. $Ca^{2+}$-NFATc1 signaling and NFAT transcriptional activity has been previously demonstrated to be activated during rat osteoblastic mineralization by high ATP concentrations acting through P2X7R [Grol et al., 2013]. Our data strengthens the importance of this axis in the bone context, and suggests a new mechanism based on a reciprocal regulatory circuit between P2X7R and NFATc1 supporting mineral ECM deposition. Our findings may help clarify the dynamics and spatial organization of multiple signals during physiological and pathological bone mineralization, as it might occur in joint cartilage, arteries and cardiovascular tissues in the course of bone diseases, metabolic disorders or physiological aging [Jørgensen, 2018; Jørgensen et al., 2015; Zeng et al., 2019].

To date, the role of P2X7R on bone homeostasis and the calcified bone matrix is incompletely understood, most likely due to the use of unsatisfactory experimental models. The *in vitro* deposition of the mineral matrix occurs both by skeletal progenitor cells (mesenchymal stromal cells, MSCs) and mature cells (OBs) at LSs of culture in osteogenic medium, likely in response to different signals specific to each given cell lineage. MSCs are proliferating cells that must remain sensitive to osteogenic differentiation stimuli, for bone remodeling, regeneration, or repair [Hayrapetyan et al., 2015]. Conversely, OBs represent terminally differentiated “steady-state cells” that will be embedded in the calcified bone. Both cell types are P2X7R positive, but the P2X7R might not be functional or plasma membrane-expressed in MSCs, as we have shown in hWJ-MSCs, regardless of the source of origin [Agrawal et al., 2017]. We hypothesized that MSCs in their physiological native environment, the stem cell niche, lack those molecules, such as P2X7R activation partners, that promote maturation only of cells located on the bone surface and committed to mineral matrix deposition, that is the

osteoblasts. Expression of nonfunctional P2X7R in skeletal progenitor cells might make these cells potentially prone to terminally osteo-differentiate, but at the same time prevent premature mineralization. This hypothesis, although as yet unsubstantiated by direct experimental evidence, is supported by the recent finding that increased P2X7R expression and activity correlate with pathologic calcification in joint and in blood vessels [Zeng et al., 2019]. Therefore, it is possible that the fine-tuning of P2X7R expression/activity plays a critical role in ECM mineralization in physiological contexts. ECM mineralization is an intrinsic property of mature osteoblasts, to be distinguished from mineral deposition, which is instead *in vitro* forced during MSC-dependent osteogenesis. This leads us to say that, as an experimental model, OBs are to be preferred over MSCs to investigate the P2X7R role and regulation in bone homeostasis. In the future, we could improve knowledge about P2X7R through experimental systems that more closely reproduce the complexity of bone microenvironment. We refer to *in vitro* models, for example, three-dimensional dynamic constructs based on coculture of osteoclasts, osteoblasts, and endothelial cells under controlled cell culture conditions, such as microgravity, hypoxia, and mechanical stimulation. Such experimental systems, relying on the paracrine effect of the various cell populations, are self-sustaining in terms of proliferation and differentiation for a time appropriate to the investigations. Therefore, they could also help in the interpretation and validation of data that we found overcoming the limitations related to the low number of cells. For example, we found it difficult to highlight a clear cut correlation between the ChIP data and a specific response during hOB osteogenic induction, or in the presence of P2X7R agonists or antagonists (BzATP or A740003). A crucial limiting factor is the low cell yield from any given biopsy, which does not allow to carry out a thorough molecular assay in the same sample. In most cases, we detected only weak signals by using chromatin from hOBs, suggesting weak or unstable interaction between the specific transcription factors and the *P2RX7* promoter. The bioinformatic analysis we performed suggests that it is reasonable to further investigate the role performed by other factors such as Runx2, TRPS1, HIF-1, or TCF/β-catenin in the regulation of *P2RX7* expression, for the reasons mentioned below. Runx2 is the master regulator of osteogenesis [Vimalraj et al., 2015], and TRPS1 has been recently correlated with the mineralization process [Goss et al., 2019]. In addition, low oxygen tension is the physiological condition of the bones, and it leads to an increased expression of HIF-1α. HIF-1α is a crucial factor in the control of energy metabolism recently found upregulated in cells overexpresing the P2X7R [Amoroso et al., 2012]. TCF/β-catenin is an important component of canonical Wnt signaling that plays a critical role in transmitting mechanosignals within the bone cell network [Baron and Kneissel, 2013; Grol et al., 2016]. Mechanical loading is essential to preserve bone health [Baron and Kneissel, 2013]. Recent studies have demonstrated that the P2X7R, together with pannexin 1 (Panx1), αVβ3 integrin, and T-type

calcium channel Cav3.2-1, acts as a unique mechanosensory complex in bone [Seref-Ferlengez et al., 2019] and coordinates load-induced Wnt/β-catenin signaling essential for proper skeletal response to mechanical stimulation.

The results we obtained open the way for further investigations regarding the role of the purinergic system, mainly P2X7R, in bone cells. This will require the optimization of some analysis to be designed for a low number of cells, in order to clarify especially the following:

- the epigenetic control of P2X7R transcription. Epigenetic marks include DNA methylation, histone modifications, microRNA, and chromatin remodeling. A growing number of studies have indicated that these mechanisms participate in all aspects of osteogenesis [Ghorbaninejad et al., 2020; Delgado-Collen et al., 2012]. Therefore, it will be interesting to explore these issues also for the P2X7R having been demonstrated its participation in bone metabolism;
- normal osteoblasts versus osteoblasts from patients with bone diseases: the ability of the cells to deposit mineral matrix in relation with P2X7R activity, ATP metabolites and the activity of ectonucleotidase enzymes;
- since P2X7R participates in the differentiation of osteoclasts and osteoblasts, the role of this receptor in the communication of these two cells needs to be furthered in more adequate experimental models such as three dimensional dynamic cellular constructs based on co-culture of osteoclasts and osteoblasts;
- recent studies on relationship between bone cells and energy metabolism aimed to identify the key players in this relationship. Interestingly, recent evidence demonstrates that P2X7R is involved in the management of energy homeostasis [Coccurello and Volonté et al., 2020] therefore it could play an interesting role in this context also in bone microenvironment.

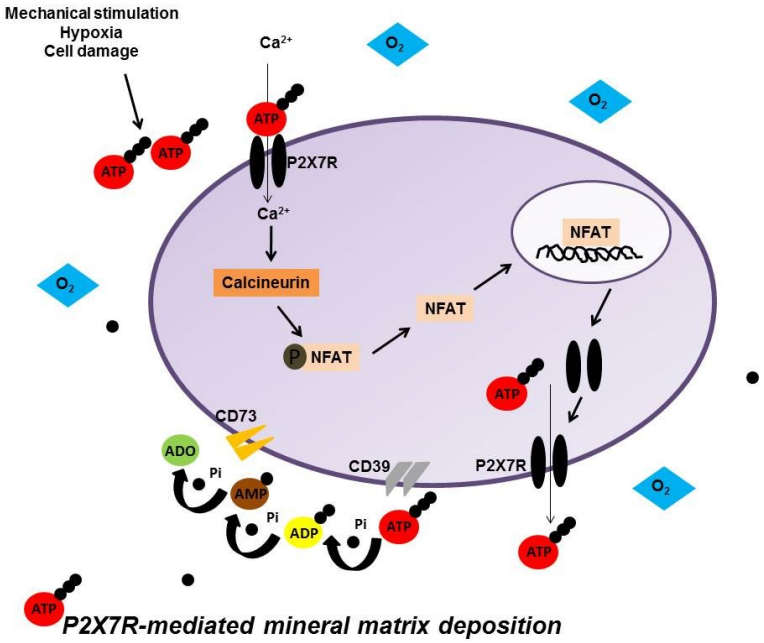


***P2X7R-mediated mineral matrix deposition***

**FIGURE 17:** ATP is released from osteoblasts into the extracellular space in response to mechanical stimulation, hypoxia or cell damage (microcracks and fractures), or by P2X7R, creating high extracellular ATP concentrations [Dong et al., 2020; Jorgensen, 2018; Burnstock et al., 2013]. The hydrolyses of extracellular ATP by ectonucleotidases enzymes (E-NTPDases and ecto-5'nucleotidase/CD73) provides a source of phosphate, essential to mineralization. In addition, biological effects of high extracellular ATP are mediated by P2X7R, that opens a cation permeable membrane channel [Di Virgilio et al., 2019]. The $Ca^{2+}$influx induces the calcineurin action, activating the NFAT by its dephosphorization. The nuclear factor of activated T-cells (NFAT) traslocated into the nucleus, upregulating the P2X7R expression, and inducing the bone mineralization. We also verified that this phenomenon is independent of oxygen concentration. Our findings contribute to understand the significance of P2X7R action and extracellular ATP in the bone context, and suggest that the P2X7R could be a new target for bone tissue regeneration/repair.

In conclusion, our data extend our understanding of P2X7R expression and function in bone, and pave the way to study the relationship between this receptor and mineralization process in more sophisticated experimental models, with the aim to identify new targets to prevent bone loss and promote bone repair.

Part of the results presented in this chapter have already been published [Bergamin LS, Penolazzi L, Lambertini E, et al. Expression and function of the P2X7 receptor in human osteoblasts: The role of NFATc1 transcription factor. Journal of Cellular Physiology. 2021 Jan;236(1):641-652. DOI: 10.1002/jcp.29891]. Acknowledgement: Wiley and Journal of Cellular Physiology.

# 4. P2X7R IN INTERVERTEBRAL DISC

A first series of experiments have been planned with the intention of making a contribution to the following open questions:

**1) Is the P2X7R expressed in IVD?**
**2) Is the P2X7R and NLRP3 expression correlated with IVD degeneration grade?**
**3) Is the NLRP3 inflammasome a target for P2X7R activation?**
**4) Could P2X7R be a new therapeutic target for intervertebral disc degeneration (IVDD)?**

For this purpose, the experiments were conducted as follows:

## 4.1 EXPERIMENTAL MODELS

In this study, biopsy samples of human intervertebral disc were used as a source of progenitor cells able to represent an excellent *in vitro* model for studying the role of P2X7R. At the same time, tissue samples were used to conduct a rigorous histological analysis in which the expression levels of P2X7R and the NLRP3 inflammasome were associated to the degeneration grade on the basis of the clinical data. For this purpose human lumbar disc tissues from a total of 83 donors were used (patients' age was between 33 and 83 years, mean age 57 years, see Table 3). Patients were operated for the herniated lumbar disc and the level of disc degeneration is evaluated according to Pfirrmann classification [Pfirrmann et al., 2001].
Several experiments with freshly isolated IVD cells (passage 0, P0) and subcultured cells (passage 2, P2) were performed. Recently, Penolazzi and collaborators [Penolazzi et al., 2018; Penolazzi et al., 2019] demonstrated that P0 cells have a morphology very similar to that found in the histological preparation. The cell morphology changed in expanded P2 cells, where the predominant form became the flattened one. P0 cells can be considered an adequate experimental model mimicking the IVD degeneration since resemble the characteristics of IVD from which derived. After monolayer culture expansion IVD cells (P2) lose the chondrocyte-like phenotype and undergo de-differentiation process regardless of the Pfirrmann grade from which the cells were originally obtained, resembling the degeneration process. It is therefore reasonable to assume that P2 cells represent a good compromise as de-differentiated cells, without becoming senescent [Penolazzi et al., 2018; Penolazzi et al., 2019].
A variety of cells coexist in the degenerated IVD microenvironment such as neurons, chondrocytes, and osteoblasts [Penolazzi et al., 2018]. For this reason, in order to obtain the most informative results from the endogenous degenerated microenvironment, we chose to preserve the whole cell population using a relatively quick protocol (mild enzymatic digestion) to minimize artifacts without selecting

the different types of cells from IVD or completely disrupting extracellular matrix (ECM). With this technique, it is possible i.) to produce P0 cells really resembling IVD microenvironment, ii.) to minimize artifacts from extended *in vitro* culture, and iii.) to obtain viable cells [Penolazzi et al., 2018; Penolazzi et al., 2019].

**Table 3:** Human intervertebral disc (IVD) samples information (NA: Not Available).

| Samples | Age | Sex | Level | Degeneration | Duration of symptoms prior to surgery |
|---|---|---|---|---|---|
| 1 | 63 | M | L4L5 | PF III | 4 months |
| 2 | 57 | M | L5S1 | PF IV | 5 months |
| 3 | 56 | M | L2L3 | PF II | 2 months |
| 4 | 49 | F | L4L5 | PF II | 2 months |
| 5 | 52 | M | L4L5 | PF III | 1 month |
| 6 | 79 | M | L4L5 | PF IV | 5 months |
| 7 | 50 | M | L5S1 | PF III | 2 months |
| 8 | 54 | F | L4L5 | PF IV | 5 months |
| 9 | 44 | M | L5S1 | PF III | 2 months |
| 10 | 63 | F | L5S1 | PF V | 12 months |
| 11 | 57 | F | L4L5 | PF V | 24 months |
| 12 | 70 | M | L4L5 | PF IV | 1 month |
| 13 | 40 | F | L4L5 | PF II | 5 months |
| 14 | 38 | M | L5S1 | PF IV | 12 months |
| 15 | 74 | M | L4L5 | PF III | 2 months |
| 16 | 70 | M | L4L5 | PF IV | 2 months |
| 17 | 56 | M | L3L4 | PF I | 3 months |
| 18 | 46 | M | L4L5 | PF III | 12 months |
| 19 | 47 | F | L5S1 | PF IV | 2 months |
| 20 | 51 | M | L5S1 | PF IV | 6 months |
| 21 | 41 | M | L2L3 | NA | 1 month |
| 22 | 51 | M | L4L5 | PF III | 3 months |
| 23 | 52 | F | L5S1 | NA | 12 months |
| 24 | 63 | F | L5S1 | PF III | 1 month |
| 25 | 37 | M | L4L5 | PF II | 2 months |
| 26 | 49 | M | L5S1 | PF III | 9 months |
| 27 | 44 | M | L5S1 | PF III | 4 months |
| 28 | 54 | M | L4L5 | PF III | 2 months |
| 29 | 64 | M | L4L5 | PF IV | 3 months |
| 30 | 64 | M | L3L4 | PF IV | NA |
| 31 | 77 | M | L4L5 | PF III | NA |
| 32 | 72 | F | L4L5 | PF III | NA |
| 33 | 48 | F | L4L5 | PF II | NA |
| 34 | 75 | F | L4L5 | PF V | NA |

| | | | | | |
|---|---|---|---|---|---|
| **35** | **67** | **F** | **L3** | **NA** | **NA** |
| **36** | **67** | **F** | **L4** | **NA** | **NA** |
| **37** | **57** | **M** | **L4L5** | **PF IV** | **NA** |
| **38** | **77** | **F** | **L4L5** | **PF IV** | **24 months** |
| **39** | **51** | **M** | **L5S1** | **PF IV** | **1 month** |
| **40** | **56** | **M** | **L4L5** | **PF III** | **NA** |
| **41** | **56** | **NI** | **L4L5** | **PF IV** | **NA** |
| **42** | **72** | **M** | **L5S1,** | **PF II** | **NA** |
| **43** | **60** | **F** | **L4L5** | **PF III** | **NA** |
| **44** | **61** | **F** | **L3L4** | **PF III** | **36 months** |
| **45** | **80** | **M** | **L4L5** | **PF IV** | **11 months** |
| **46** | **36** | **M** | **L2L3** | **PF III** | **3 months** |
| **47** | **70** | **M** | **L3L4** | **PF III** | **NA** |
| **48** | **54** | **M** | **L4L5** | **PF IV** | **12 months** |
| **49** | **57** | **M** | **L4L5** | **PF III** | **3 months** |
| **50** | **54** | **M** | **L3L4** | **PF III** | **1 month** |
| **51** | **48** | **F** | **L4L5** | **PF III** | **1 month** |
| **52** | **59** | **M** | **L3L4** | **PF IV** | **NA** |
| **53** | **72** | **F** | **L4L5** | **PF II** | **36 months** |
| **54** | **80** | **M** | **L4L5** | **PF V** | **NA** |
| **55** | **47** | **F** | **L5S1** | **PF IV** | **24 months** |
| **56** | **51** | **M** | **L4L5** | **PF I** | **2 months** |
| **57** | **43** | **M** | **L4L5** | **PF III** | **12 months** |
| **58** | **51** | **M** | **L3L4** | **PF III** | **3 weeks** |
| **59** | **71** | **M** | **L5L5** | **PF II** | **10 months** |
| **60** | **81** | **M** | **L3L4** | **PF III** | **18 months** |
| **61** | **63** | **F** | **L5S1** | **PF IV** | **4 months** |
| **62** | **53** | **M** | **L4L5** | **PF IV** | **5 months** |
| **63** | **36** | **M** | **L3L4** | **PF II** | **2 months** |
| **64** | **44** | **M** | **L5S1** | **PF II** | **2 weeks** |
| **65** | **43** | **M** | **L5S1** | **PF III** | **3 months** |
| **66** | **38** | **F** | **L5S1** | **PF II** | **6 months** |
| **67** | **33** | **M** | **L5S1** | **PF III** | **3 weeks** |
| **68** | **48** | **F** | **L5S1** | **PF III** | **7 months** |
| **69** | **56** | **M** | **L5S1** | **PF IV** | **5 months** |
| **70** | **33** | **M** | **L4L5** | **PF III** | **2 months** |
| **71** | **73** | **M** | **L4L5** | **PF III** | **6 months** |
| **72** | **83** | **M** | **L3L4** | **PF IV** | **12 months** |
| **73** | **69** | **M** | **L5S1** | **PF IV** | **12 months** |
| **74** | **47** | **M** | **L5S1** | **PF III** | **1 month** |
| **75** | **82** | **M** | **L4L5** | **PF IV** | **5 months** |
| **76** | **43** | **F** | **L5S1** | **PF IV** | **2 months** |
| **77** | **76** | **F** | **L5S1** | **PF IV** | **2 months** |

| | | | | | |
|---|---|---|---|---|---|
| **78** | **55** | **F** | **L4L5** | **PF III** | **10 months** |
| **79** | **48** | **F** | **L5S1** | **PF IV** | **4 months** |
| **80** | **81** | **F** | **L3L4** | **PF II** | **1 month** |
| **81** | **66** | **F** | **L4L5** | **PF III** | **2 months** |
| **82** | **70** | **M** | **L3L4** | **PF III** | **2 months** |
| **83** | **42** | **F** | **L5S1** | **PF IV** | **3 months** |

## 4.2 EXPERIMENTAL PLANNING

The expression of P2X7R and NLRP3 in IVD tissues was investigated by immunohistochemistry in several samples with different grades of lumbar disc degeneration (Pfirrmann grade I-V). In the IVD cells, we evaluated the P2X7R functionality and the ability of the cells to release IL-1β in presence of LPS (inflammation inductor) and P2X7R antagonist (A740003). Furthermore, we assessed the cell proliferation in presence of P2X7R antagonist (A740003) or P2X7R agonists (BzATP or ATP), as shown in figure 18.

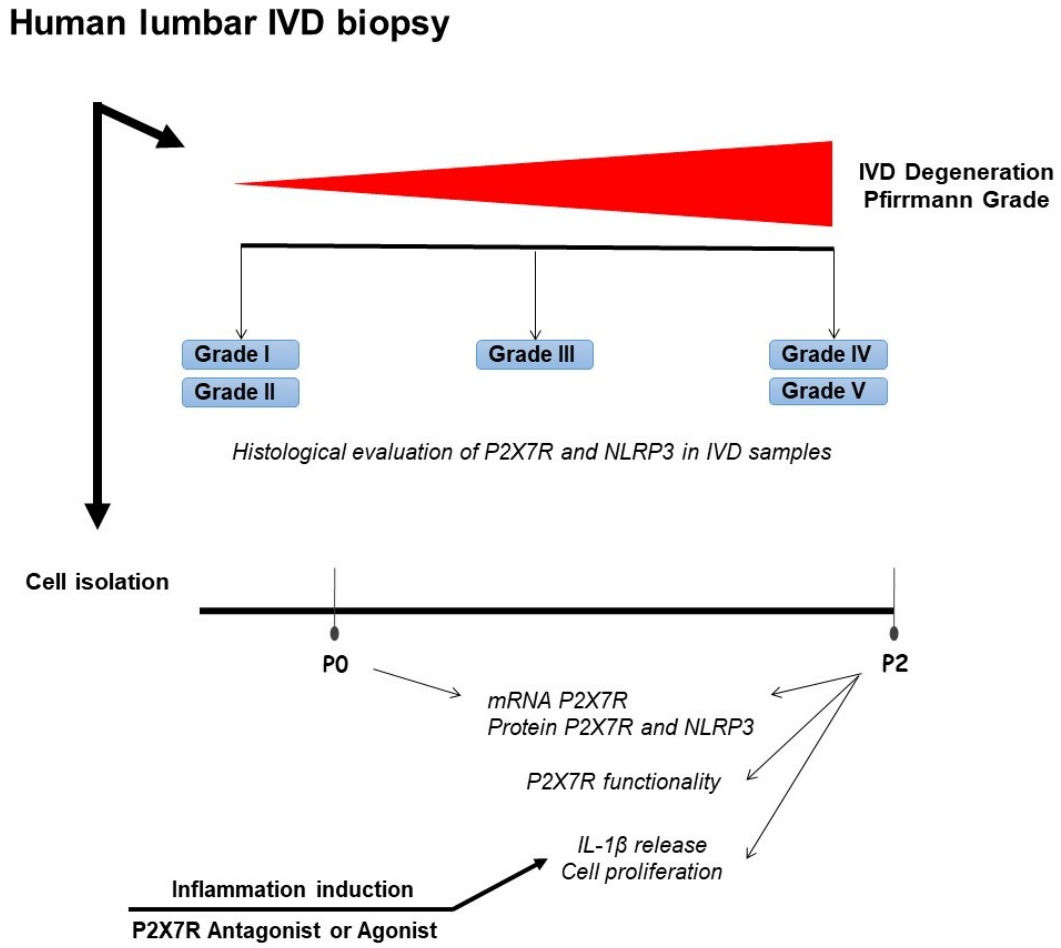


**FIGURE 18: Experimental planning.**

## 4.3 METHODOLOGY

### 4.3.1 Isolation of human IVD cells

Lumbar intervertebral disc tissues (1-2 $cm^3$) were collected, cut into small pieces, and subjected to mild digestion in 15 ml centrifuge tube with only 1 mg/mL type IV collagenase (Sigma Aldrich, St. Louis, USA) for 5 h at 37°C in Dulbecco's Modified Eagle's Medium (DMEM)/F12 (Euroclone S.p.A., Milan, Italy) as previously described [Penolazzi et al., 2018]. Once the digestion was terminated, cell suspension was filtered with a Falcon™ 70 µm Nylon Cell strainer (BD Biosciences, Franklin Lakes, NJ, USA). Subsequently 300 x g centrifugation was conducted for 10 min, the supernatant discarded, the cells resuspended in basal medium (DMEM/F12 containing 10% fetal calf serum, 100 µg/mL streptomycin, 100 U/mL penicillin, and 1% Glutamine) (Euroclone) and seeded in polystyrene culture plates (Sarstedt, Nümbrecht, Germany) at 10.000 cells/$cm^2$. The cells that were released from the dissected tissue and maintained in culture at 37°C in a humidified atmosphere with 5 % $CO_2$ within the first 48 h were referred to as passage zero (P0) cells. P0 cells were expanded by growing for a period not exceeding a week until subconfluent, detaching by trypsinization, and maintained in culture for two passages to obtain P2 cells that were used for later experiments.

### 4.3.2 Histochemical analysis

Small fragments of each IVD sample were rinsed with PBS, fixed in 4% buffered paraformaldehydefor 24 h at 4°C, embedded in paraffin and cross-sectioned (5 µm thick). Sections were deparaffinized, rehydrated and heated in sodium citrate (pH 6) for antigen retrieval. Slides were then processed with 3% $H_2O_2$ in PBS for 10 min and with blocking solution in PBS (1% BSA/10% FCS) for 30 min at room temperature. Then the slides were incubated over night with P2X7R antibody (#APR-004, Alomone Labs, Jerusalem, Israel; 1:50 dilution) at 4°C, followed by treatment with Vectastain ABC solution (Vector Labs, Burlingame, USA) for 30 min. For histological evaluation of NLRP3/NALP3 the slides were incubated with 0.3% $H_2O_2$ in PBS without any antigen retrieval. After three rinses in wash buffer (0.025% Triton X-100 in PBS), tissue sections were kept for 2 h at RT with a blocking solution (1% BSA/10% FCS), and then incubated overnight at 4°C with the primary antibody (NLRP3/NALP3, #NBP2-12446, Novus Biologicals, Colorado, USA; 1:50 diluition) and followed by treatment with Vectastain ABC solution (Vector Labs) for 30 min. All reactions were developed using DAB solution (Vector Labs), the sections were counterstained with hematoxylin and mounted in glycerol. Sections were then observed in the NikonEclipse 50i optical microscope (Nikon Corporation, Tokyo, Japan) and protein levels were expressed as % of positive cells evaluated in 10 fields per section of each sample.

### 4.3.3 RNA Extraction and Quantitative Real-Time (qRT)-PCR

Total RNA was extracted from IVD cells using the PureLink RNA Mini Kit (Thermo Scientific, Milan, Italia) according to the manufacturer's instructions and RNA content was determined with a Nanodrop 2000 spectrophotometer (Thermo Scientific). RNA was added to each cDNA synthesis reaction using the High Capacity cDNA Reverse Transcription Kit (Applied Biosystems, California, USA). Real Time PCRs were carried out in the AB StepOne Real Time PCR (Applied Biosystems) with TaqMan Gene Expression Master Mix (Applied Biosystems). Amplification was performed with TaqMan® MGB probes (Applied Biosystem) for pan-P2X7R (Hs00175721_m1); ecto-5'nucleotidase/CD73 (Hs00159686_m1); E-NTPDase1/CD39 (Hs00969559_m1); GAPDH (4326317E) all from Applied Biosystems whereas TaqMan Gene Expression custom assays were purchased to identify P2X7RA and P2X7RB previously described by [Adinolfi et al., 2010]. All results were analyzed by the $2^{(-\Delta\Delta CT)}$ method [Livak and Schmittgen, 2001].

### 4.3.4 Immunocytochemistry

Immunocytochemistry was performed using the ImmPRESS kit (Vector Labs). IVD cells (P0 and P2) were fixed with cold 100% methanol at room temperature (RT) for 10 min; then rinsed three times with PBS 1X (phosphate-buffered saline) for 5 min and permeabilized using 0.2% (v/v) Triton X-100 in PBS 1X for 5 min; then washed three times with PBS 1X for 5 min. Cells were treated with 3% $H_2O_2$ for 10 min (RT), washed once with PBS 1X for 5 min and incubated in blocking solution containing 1% BSA/2.5% FCS for 20 min at RT. After blocking, antibodies against P2X7R (#APR-004; rabbit anti-human, 1:1000 dilution, Alomone Labs), NLRP3/NALP3 (#NBP2-12446, Novus Biologicals; 1:1000 diluition), COL2A1 (#Ab3092; mouse anti-human, 1:200 dilution, Abcam, Cambridge, UK), SOX9 (#sc-20095; rabbit anti-human, Santa Cruz Biotechnology, Texas, USA), ACAN (#sc-33695; mouse anti-human, 1:200 dilution, Santa Cruz Biotechnology), or isotype control (normal rabbit IgG; #2729, 1:1000 dilution, Cell Signaling technology, Massachusetts, USA) were added and the incubation carried out overnight (4°C). Then, the cells were rinsed three times with PBS 1X for 5 min at RT, were incubated in Vectastain ABC (Vector Labs) and stained with DAB solution (Vector Labs). After washing, cells were mounted in glycerol/TBS 9:1 and observed with a Leitz microscope (Wetzlar, Germany). Quantitative image analysis of immunostained cells was obtained by a computerized video-camera-based image-analysis system (with NIH USA ImageJ software, public domain available at: http://rsb.info.nih.gov/nih-image) under bright field microscopy. Briefly, images were taken with single stain, without carrying out nuclear counterstaining with hematoxylin and unaltered TIFF images were digitized and converted to black and white picture to evaluate the distribution of relative gray values (i.e., number of pixels in the

image as a function of gray value), which reflected chromogen stain intensity. The results were expressed by the quantification of pixels per 100 cells.

### 4.3.5 Immunofluorescence

Cells were seeded on glass coverslips put into 24 well plates/ and fixed in 4% paraformaldehyde for 15 min. After three washes with PBS 1X, the cells were permeabilized using 0.05% (v/v) Triton X-100 in PBS 1X for 10 min; then cells were incubated inthe blocking solution containing 2% nonfat dry milk -NFDM/0.05% Triton X-100 in PBS 1X for 40 min. After that, cells were incubated overnight at 4°C with the primary antibody P2X7R (#P8232, Sigma Aldrich, rabbit anti-human, 1:100 dilution). Then, cells were incubated with the fluorescent secondary antibody donkey anti-rabbit IgG Alexa Fluor (#ab150064; Abcam, 1:1000 dilution) in 2% NFDM/0.05% Triton X-100 in PBS 1X for 1 h at RT, mounted in Fluoroshield Mounting Medium (Abcam). Samples with no primary antibody were also included as control.

### 4.3.6 Cytosolic free calcium concentration measurements

Cytosolic free calcium was measured using the fluorescent $Ca^{2+}$ indicator Fura-2-acetoxymethyl ester (Fura-2/AM) (Thermo Scientific) [Falzoni et al., 1995; Di Virgilio et al., 2019]. IVD cells (P2) were incubated at 37°C for 20 min in saline solution (125 mM NaCl, 5 mM KCl, 1 mM $MgSO_4$, 1 mM $NaH_2PO_4$, 20 mM HEPES, 5.5 mM glucose, and 5 mM $NaHCO_3$, pH 7.4), in presence of 1 mM $CaCl_2$, and supplemented with 4.0 μM Fura-2/AM and 250 μM sulfinpyrazone (Sigma-Aldrich). Then, the cells were centrifuged at 300 x g for 5 min. The supernatant was discarded and the pellet was resuspended in the above saline solution. The cell suspension was placed in a thermostat-controlled (37°C) and magnetically-stirred cuvette of a Cary Eclipse Fluorescence Spectophotometer (Agilent Technologies, Milan, Italy). The $[Ca^{2+}]_i$ was determined at the 340/380 nm excitation ratio and at 505 nm emission wavelengths. The P2X7R agonist, BzATP (500 μM) (Sigma-Aldrich), was added to investigate P2X7R responses. Ionomycin 1 μM was added to trigger a maximal $Ca^{2+}$ increase.

### 4.3.7 Ethidium bromide uptake

Changes in plasma membrane permeability after exposure to BzATP (500 μM) (Sigma-Aldrich) were studied by ethidium bromide uptake. IVD cells were kept at 37°C in a thermostat-controlled and magnetically stirred cuvette of a Cary Eclipse Fluorescence Spectophotometer (Agilent Technologies) in the presence of 20 μM ethidium bromide (Sigma-Aldrich). Fluorescence changes were acquired at 360 nm and 580 nm excitation and emission wavelengths, respectively. Full

permeabilization was obtained with 100 μM digitonin.

### 4.3.8 Cytokines release

The evaluation of IL-1β release in cell supernatant was measured with Quantikine Immunoassay for human IL-1β/IL-1F2, purchased from R&D Systems (Minneapolis, USA), as described by the manufacturer. The results were expressed by pg/mL of cytokine/μg/μL of protein.

We tested two protocols for analyzing the IL-1β release in IVD cells:

Protocol 1: cells cultured in presence of 10% FCS and exposed to:

i) 10 μg/mL LPS (lipopolysaccharide; Sigma-Aldrich) for a total of 25 h. One hour before the end of treatment, the cells were exposed to 500 μM BzATP;

Protocol 2: IL-1β release was also evaluated in the IVD cells in presence of 1% fetal calf serum and treated with:

i) 1 μg/mL LPS for a total of 25 h. One hour before the end of treatment, the cells were exposed to 500 μM BzATP.

The supernatants were collected and frozen at − 20 °C until use for determination of cytokine concentrations.

### 4.3.9 Proliferation assay

IVD cells were seeded and, once at the subconfluence stage, were treated with 100 μM BzATP (a synthetic P2X7R agonist), or 1 mM ATP (natural P2X7R agonist), all reagents purchased from Sigma-Aldrich, or 5 μM A740003 (a selective P2X7R antagonist; Tocris Bioscience, Bristol, UK), or DMSO (0.05%) (Sigma-Aldrich) in DMEM high glucose/F12 containing 10% FCS. The IVD cells were treated three times (0 h, 48 h and 96 h) with agonist or antagonist of P2X7R for a total of 168 h. In the times 0 h, 72 h, 96 h and 168 h cells were rinsed, stained with crystal violet and cell proliferation was analyzed by optical density (OD, 570 nm) in a microplate reader. The % of cell growth was calculated using the value of absorbance in relation to control (untreated cells).

### 4.3.10 Statistical analysis

The data were analyzed for statistical significance by Student's *t*- test or one way ANOVA followed by a post-hoc test for multiple comparisons (Tukey test). The data are expressed as the mean±S.D or mean±S.E.M. Differences were considered significant at $p<0.05$.

## 4.4 RESULTS

### 4.4.1 The expression level of P2X7R and NLRP3 in lumbar degenerated IVD tissue

Although IL-1β is known to be involved in the pathogenesis of IVD degeneration, the role of the P2X7R and its downstream target (NLRP3 inflammasome) in this process remains unknown. For this reason, we investigated their expression in degenerated IVD tissue by immunohistochemistry. As shown in figure 19, both P2X7R and NLRP3 are more expressed in IVD tissues with mild (PF III) and high (PF IV-V) Pfirrmann grades than in IVD tissues with low grade (I-II).

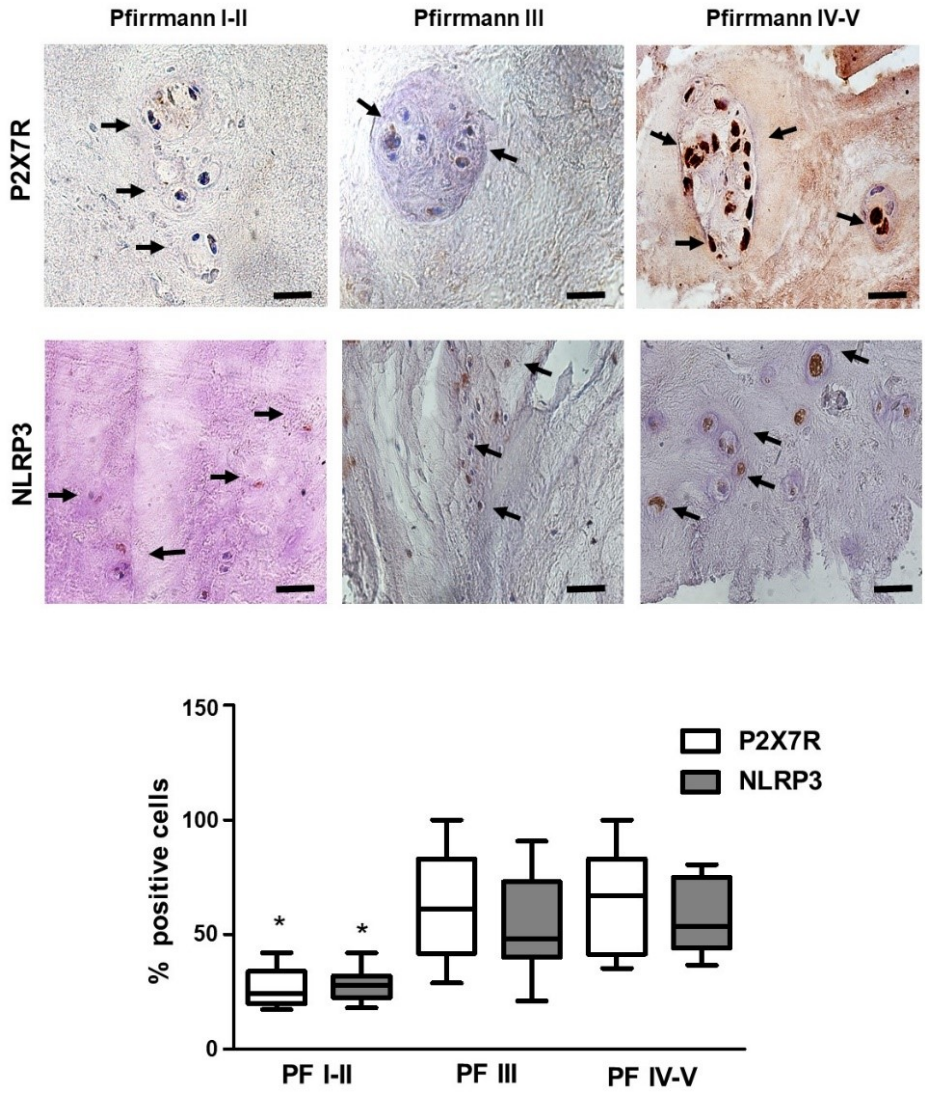


**FIGURE 19: P2X7R and NOD-, LRR- and pyrin domain-containing protein 3 (NLRP3) expression in intervertebral disc specimens.** Immunohistochemistry was performed on IVD tissues with different Pfirrmann grades. Representative optical photomicrographs and quantification of the protein level of P2X7R and NLRP3. The results are reported as a whisker box plot representing the min to max (line indicates median) and data were analyzed by ANOVA followed by Tukey's test *versus Pfirrmann III and IV-V (Pfirrmann I-II, n = 6; Pfirrmann III, n = 8; Pfirmann IV-V, n = 12). IVD cells are indicated by arrows. Scale bars: 20 µm.

### 4.4.2 Characterization of P2X7R espression and functionality in IVD cells

Further experiments were carried out using progenitors isolated from IVD samples (see the experimental protocol described in the methodology section). In order to obtain the most informative results from the endogenous degenerated microenvironment, we chose to preserve the whole cell population deriving from the biopsy without performing cell sorting. As demonstrated in a previous paper [Penolazzi et al., 2018], IVD cells cultured *in vitro* show different morphological and phenotypic characteristics during different passages. In particular, as shown in figure 20, during cell expansion it is possible to observe a decrease of expression of typical chondrogenic markers, including collagen type II alpha 1 chain (Col2A1), SRY-box 9 (SOX9) and aggrecan (ACAN), suggesting that the cells underwent de-differentiation process. Although disc cell phenotype still remains to be defined in detail, it is in fact accepted that IVD cells exhibit a chondrocyte-like phenotype.

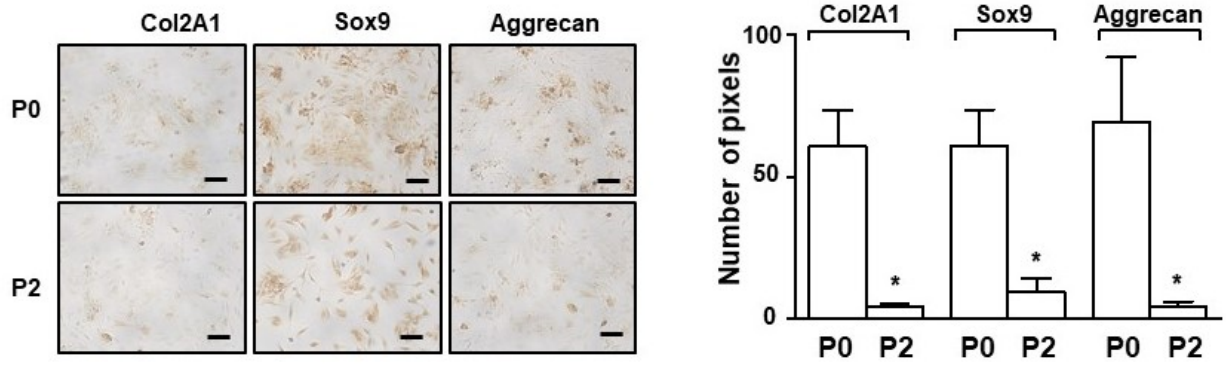


**FIGURE 20: IVD cell characterization in passage 0 (P0) and passage 2 (P2).** Representative optical photomicrographs of collagen type II alpha 1 chain (Col2A1), SRY-box 9 (SOX9) and aggrecan (ACAN) immunostaining performed in P0 and P2 cells are reported. Protein expression levels were quantified by densitometric analysis of immunocytochemical pictures using ImageJ software and expressed as means of pixels per one hundred cells ±SD. Scale bars: 20 μm.

We then verified whether P2X7R and NLRP3 expression profile we found in the histological samples was also maintained by the IVD cells isolated from the same tissue sample. This was the case: as shown by immunocytochemical detection **(**Figure 21a,b), P0 cells from IVD tissues with mild (PF III) and high (PF IV-V) Pfirrmann grades expressed P2X7R and NLRP3 at higher level than P0 cells from IVD tissues with low Pfirrmann grade (I-II). Furthemore, the same analysis conducted in IVD P2 cells revealed that the expression of P2X7R and NLRP3 increased, on average, with de-differentiation process (Figure 21c,d) supporting that in this context i.) cell de-differentiation resembles tissue degeneration, and ii.) the role of P2X7R and NLRP3 in IVDD deserves to be investigated.

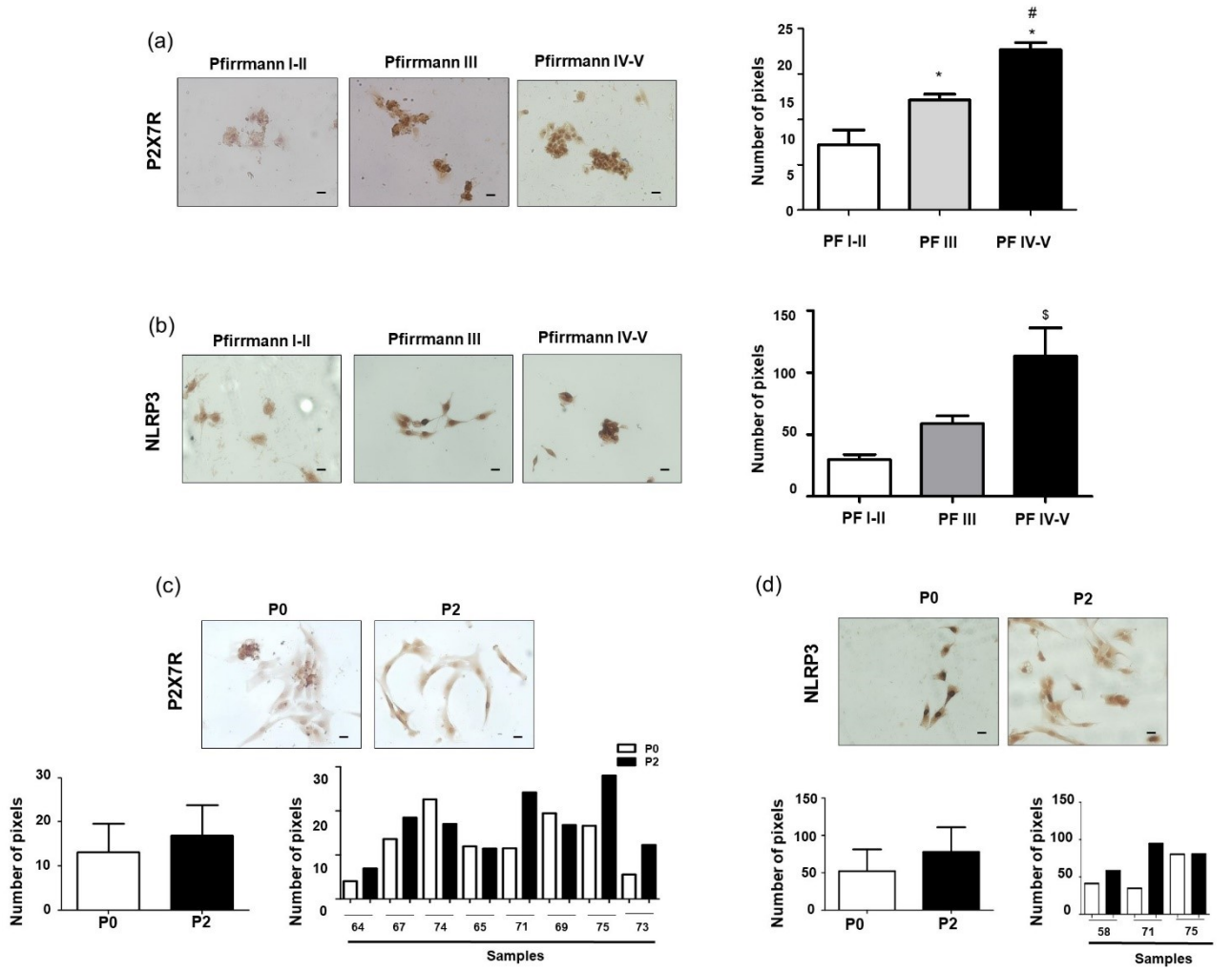


**FIGURE 21: P2X7R and NLRP3 protein expression.** Immunocytochemistry was performed in passage 0 (P0) IVD cells with different Pfirrmann grades for (a) P2X7R. Data were analyzed by ANOVA followed by Tukey's test, $p<0.05$ *Pfirrmann I-II versus Pfirrmann III and Pfirrmann IV-V; #Pfirrmann III versus Pfirrmann IV-V. (Pfirrmann I-II, n = 3; Pfirrmann III, n = 6; Pfirrmann IV-V, n = 4) and (b) NLRP3. Data were analyzed by ANOVA followed by Tukey's test, $p<0.05$ $Pfirrmann IV-V versus Pfirrmann I-II and III. Immunocytochemistry for (c) P2X7R and (d) NLRP3 was performed in P0 and P2 IVD cells. Representative optical photomicrographs and densitometric quantification of the P2X7R and NLRP3 protein level are reported (both as average and for each IVD sample). For P2X7R, sample's number (64: PF I-II; 67, 74, 65 and 71: PF III; 69, 75 and 73: PF IV-V; P0 and P2 group, n = 8); for NLRP3 samples' number (58 and 71: PF III; 75: PF IV-V, n = 3). Data were analyzed by Student's *t*- test, $p<0.05$. Densitometric analysis was performed by using ImageJ software and expressed as means of pixels per one hundred cells. Scale bars: 20 µm

We also investigated at mRNA level the expression of P2X7R in order to distinguish the expression of the two functional splice variants, P2X7RA and P2X7RB. This analysis confirm what found at protein level: P2X7R mRNA levels were significantly higher in P2 cells than in P0 cells, namely they increased during de-differentiation process (Figure 22a). As regards the two isoforms, the full length P2X7RA is the predominant one with respect to the truncated isoform P2X7RB. Both mRNA isoforms, in particular P2X7RA, increased during de-differentiation process (Figure 22b).

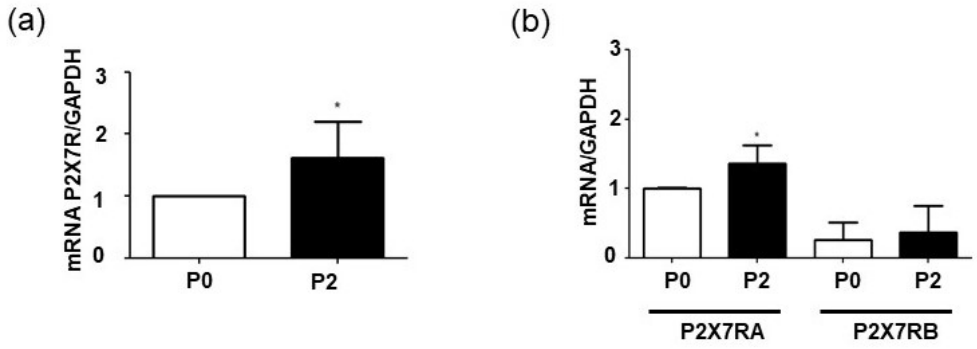


**FIGURE 22: Expression of mRNA P2X7R in intervertebral disc (IVD) cells.** mRNA expression was analyzed in IVD cells during de-differentiation process from passage 0 (P0) to passage 2 (P2) by Real Time-PCR. (a) P2X7R mRNA levels were normalized by using the house keeping GAPDH as endogenous control. Data are expressed as fold change relative to passage 0 (P0) cells and presented as mean± SD. Data were analyzed by Student's *t*- test, $p<0.05$. *Significantly different from P0 (n=10) (b) P2X7RA and P2X7RB mRNA isoforms were expressed as fold change relative to P2X7RA in P0 cells and presented as mean± SD. Data were analyzed by Student's *t*- test, $p<0.05$. *Significantly different from P2X7RA in P0 cells (n=7).

In a next step P2X7R functionality was tested. It is in fact very important that the P2X7R is able to open the channel and/or pore in the membrane. At this purpose, P2 IVD cells were stimulated with the P2X7R semi−selective agonist BzATP. Notably, we found that IVD cells are differently responsive. Some IVD samples are responsive to BzATP stimulation with increasing in the cytoplasmic $Ca^{2+}$ followed by a sustained plateau (suggestive of a prolonged influx from the extracellular space through the P2X7R channel, Figure 23a). Other IVD samples are unresponsive or poorly responsive to BzATP stimulation (Figure 23b). This result suggests that in some cases the P2X7R is not functional or is not exposed on the plasma membrane.

Likewise, we were unable to detect responses suggestive of large pore opening in all samples analyzed (e.g. ethidium bromide uptake, Figure 23c).

As regards P2X7R cellular localization, a preliminary analysis performed on some IVD samples revealed a weak cytoplasmic localization (Figure 23d).

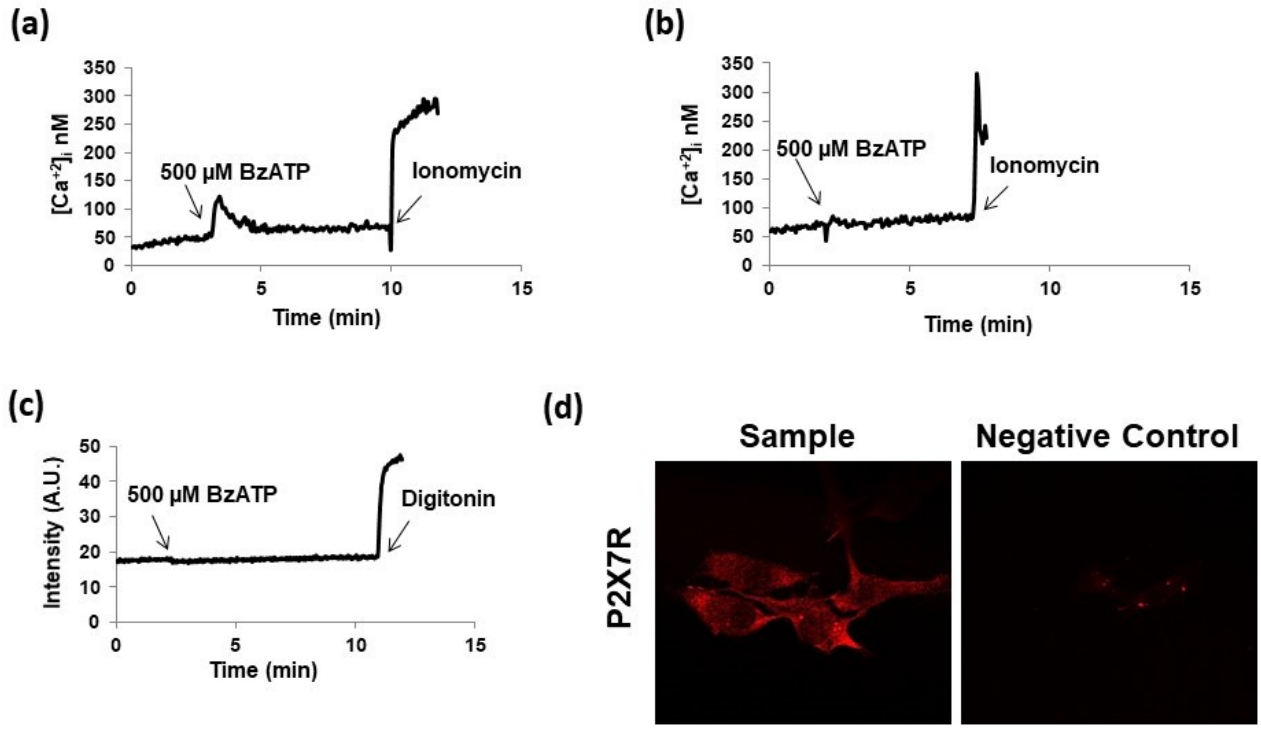


**FIGURE 23: P2X7R functionality in intervertebral disc (IVD) cells.** Representative trace of IVD cells (passage 2-P2) that (a) respond to 500 µM BzATP stimulation (n=1) and (b) representative trace evaluated in IVD cells that did not respond to 500 µM BzATP or poorly respond to BzATP (n=3). (c) Representative trace showing 500 µM BzATP-induced ethidium bromide uptake (n=4). (d) Immunofluorescence was performed in P0 IVD cells labeling with anti-P2X7R.

### 4.4.3 IL-1β release by IVD cells

Another interesting issue is the inflammation that occurs in the IVDD and the role that P2X7R may have in supporting this phenomenon. Among pro-inflammatory cytokines, IL-1β plays a key role in mediating disc degeneration [Johnson et al., 2015]. It has been previously described that IL-1β release during inflammation occurs by the P2X7R-NLRP3 dependent mechanism [Adinolfi et al., 2018]. In this scenario, a possible relation between this inflammatory cytokine and P2X7R-NLRP3 signaling in IVD cells deserves to be studied as an interesting target pathway for innovative IVDD therapies. With this in mind, we quantified the IL-1β release by IVD cells after treatment with LPS (inflammation inductor, mimicking the IVD microenvironment) and BzATP (P2X7R agonist). The results revealed that the stimulation with LPS and BzATP slightly increased IL-1β release compared to non-treated cells or LPS alone treated cells (Figure 24). This suggests that, although the level of IL-1β release in all samples is very low, it is necessary the presence of both molecules for stimulating the cells, demonstrating that the P2X7R is probably involved in this process.

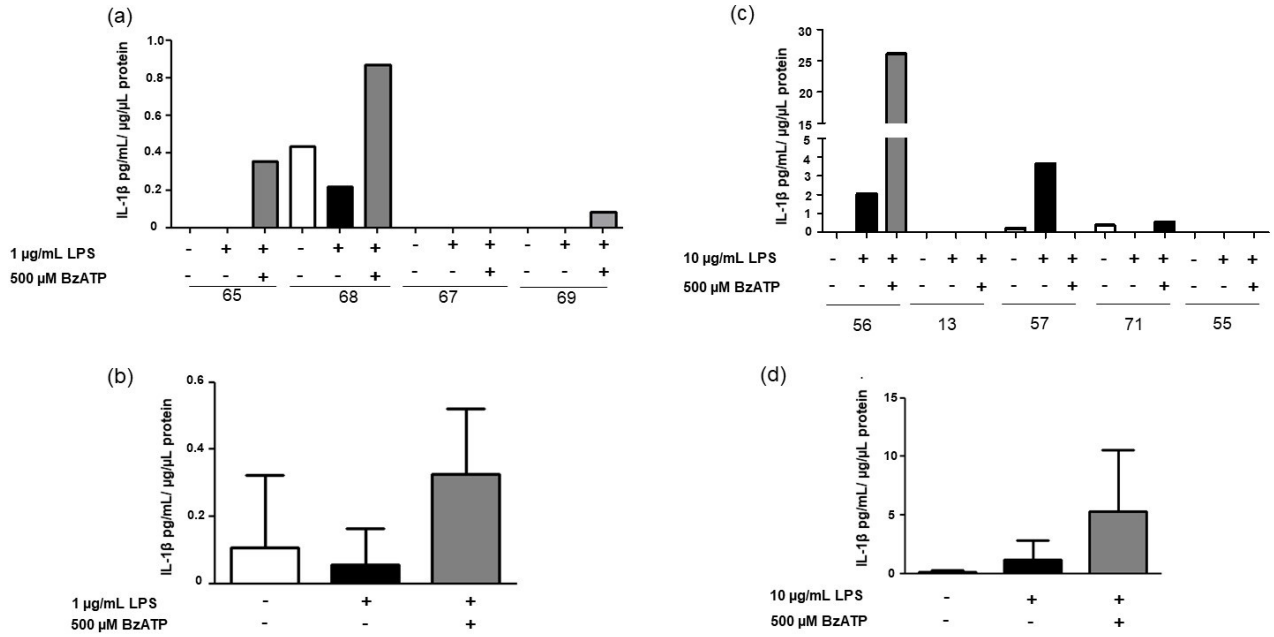


**FIGURE 24: IL-1β release in intervertebral disc (IVD) cells.** IL-1β release in presence of 1 µg/mL lipopolysaccharide (LPS) for a total of 25 h. One hour before the end of treatment, the cells were exposed to 500 µM BzATP. Data are reported for each IVD sample **(**a) and as average±SD (b). Data were evaluated by ANOVA followed by Tukey test, $p$ <0.05, (n=4). IL-1β release in presence of 10 µg/mL LPS for a total of 25 h. One hour before the end of treatment, the cells were exposed to 500 µM BzATP. Data are reported for each IVD sample (**c)** and as average±SD (d). Sample's number was also reported (56 and 13: PF I-II; 57 and 71: PF III; 55: PF IV-V). Data were analyzed by ANOVA followed by Tukey test, $p$ <0.05, (n=5).

### 4.4.4 Growth kinetics in IVD cells in presence of P2X7R antagonist and agonists

Some events as increased cell death seem to be involved in IVDD [Ding et al., 2013]. Considering that the P2X7R supports cell proliferation [Di Virgilio et al., 2017], we verified whether the treatment with P2RX7 agents alters IVD cells growth. In all samples analyzed, we observed that there was no difference in cell proliferation when the cells were treated with 5 µM A740003 compared to DMSO or control or BzATP 100 µM (Figure 25a). These results indicate that P2X7R in IVD cells does not influence *in vitro* cell proliferation. On the other hand, the presence of 1 mM ATP induced a growth advantage compared to control or BzATP, suggesting that a metabolite of ATP, probably adenosine, may be involved in the proliferation of IVD cells (Figure 25b).

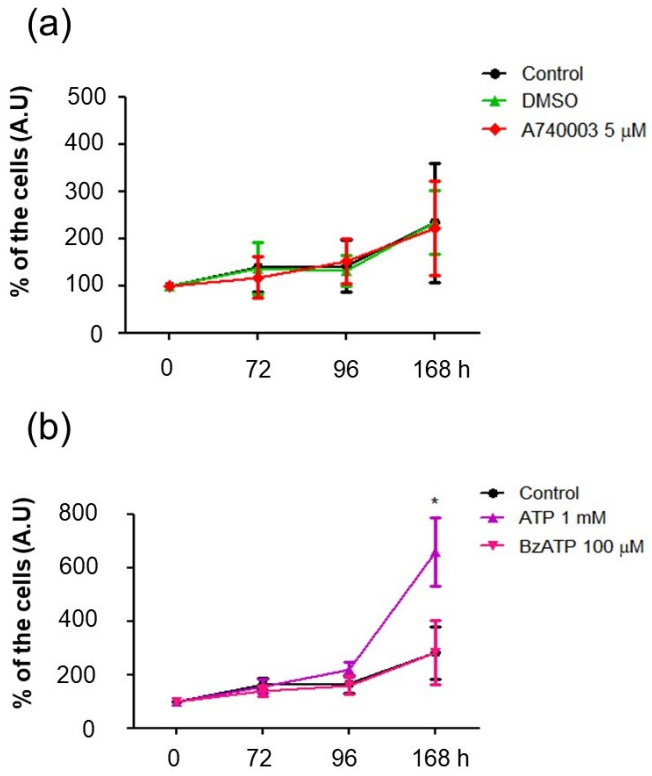


**FIGURE 25: Effect of P2X7R agonist and antagonist in intervertebral disc (IVD) cell proliferation.** The IVD cells were treated three times (0 h, 48 h and 96 h) with agonist or antagonist of P2X7R for a total of 168 h. At 0 h, 72 h, 96 h and 168 h cells were rinsed, stained with crystal violet and cell proliferation analyzed by optical density as reported in material and methods paragraphs. (a) The IVD cell proliferation after treatment with antagonist of P2X7R (5 µM A740003), or vehicle control (dimethyl sulfoxide- DMSO). The results were expressed as the percentage of cells in relation to control. Data were analyzed by ANOVA followed by Tukey test, $p < 0.05$, (n=4). (b) The IVD cell proliferation after treatment with agonist of P2X7R (100 µM BzATP; or 1 mM ATP). The results were expressed as the percentage of cells compared to control. Data were analyzed by ANOVA followed by Tukey test, $p < 0.05$, (n=3). *ATP 1 mM versus control 72 h, 96 h, 168 h; ATP 1 mM 72 h; BzATP 100 µM 168 h. (A.U. arbitrary unit).

ATP is constantly released from IVD cells [Fernando et al., 2011; Salvatierra et al., 2011]. Extracellular ATP can be rapidly hydrolyzed in ADP and AMP by E-NTPDase1/CD39 enzymes, whereas ecto-5'nucleotidase/CD73 hydrolyzes AMP in adenosine [Zimmermann et al., 2012]. We are also interested in investigating this aspect. Preliminary experiments were performed evaluating at mRNA level the expression of E-NTPdase1/CD39 and ecto-5'nucleotidase/CD73. As shown in figure 26, IVD cells expressed more ecto-5'nucleotidase/CD73 than E-NTPDase1/CD39, without significant changes during the de-differentiation process.

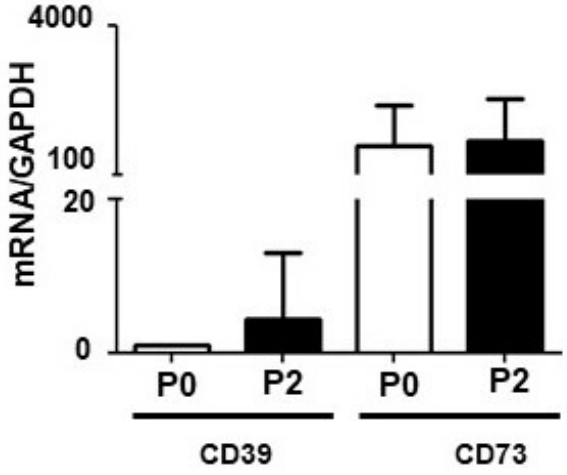


**FIGURE 26:** mRNA expression of E-NTPdase1/CD39 and ecto-5'nucleotidase/CD73 were evaluated during de-differentiation process from passage 0 (P0) to passage 2 (P2) in IVD cells by Real Time-PCR. Data are expressed as fold change relative to CD39 in P0 cells and presented as mean ±SD (n=5). Data were analyzed by ANOVA followed by Tukey test, $p<0.05$.

## 4.5 DISCUSSION

IVD degeneration is triggered by ageing, mechanical stress, traumatic injury, infection and inflammation, but the exact mechanisms are still not clear, despite intense investigation [Shapiro and Risbud, 2014; Richardson et al., 2014; Penolazzi et al., 2019]. Several pro-inflammatory cytokines and inflammatory mediators are present in degenerated IVD microenvironment [Shamji et al., 2010; Penolazzi et al., 2019]. The knowledge of specific key regulators that support the degenerative process is very important [Penolazzi et al., 2019]. With this in mind, we focused here on this aspect and conducted preliminary experiments on a potential correlation between P2X7R and NLRP3 inflammasome in human IVDD in order to understand how P2X7R and NLRP3 may impact on the discogenic phenotype. The data of this chapter are very promising, and allow us to hypothesize that the blocking P2X7R by specific antagonists may prevent the degeneration of IVD. It is worth mentioning that working with a human experimental model such as IVD from surgical biopsy inevitably comes with some limitations such as those listed below:

i) in the immunohistological analysis, due to the scarcity of biological material and poor tissue cellularity, it is difficult to obtain 10 fields for each sample section. Moreover, patients with Pfirrmann I-II are numerically lower than the Pfirrmann III-V, as they are rarely operated;

ii) Italian legislation does not allow the use of anatomical parts from cadaver; thus, it is not possible to have healthy IVD control group;

iii) the IVD cell number obtained from tissue is very low and it makes impossible to perform many experiments on the same sample;

iv) the experiment for cytosolic free calcium concentration measurements requires a high number of cells, therefore this analysis was realized only on a few samples.

Despite the weakness above described, this study may help to better understand the pathogenesis of IVD degeneration. P2X7R is the P2 receptor most consistently associated with inflammation, and one of the most potent inducers of NLRP3 inflammasome activation and IL-1β maturation and release [Adinolfi et al., 2018; Giuliani et al., 2017]. During inflammation, a release of ATP, the major activator of P2X7R, is a critical event involved in the modulation of the immune response in several joint diseases as osteoarthritis and rheumatoid arthritis [Zeng et al., 2019; Staunton et al., 2013; Chang et al., 2015; Caporali et al., 2008; Teixeira et al., 2017]. As previous mentioned, IL-1β appears to be strongly related to IVD degeneration modulating matrix metalloproteinase family, increasing the degradation of extracellular matrix, and perpetuating the inflammation [Baptista et al., 2020; Johnson et al., 2015; Chen et al., 2015]. In our study, we observed that the expression of P2X7R and NLRP3 increased during IVD degeneration. Thus, P2X7R- and NLRP3-dependent intracellular signalling pathways might be relevant to IVDD.

Finally, we also investigated the effect of P2X7R antagonist and agonist on cell proliferation. Our results indicate that BzATP was unable to open pores in the plasma membranes and to alter cell duplication. On the other hand, the natural P2X7R agonist induces a growth advantage in relation to BzATP, suggesting that a metabolite of ATP is involved in the cell proliferation of IVD cells. Moreover, we verified that the IVD cells expressed the E-NTPDase1/CD39 and ecto-5'nucleotidase/CD73 [Robson et al., 2006; Zimmermann et al., 2012]. Therefore, it is possible to hypothesize that ATP and ADP breakdown by E-NTPDase1/CD39, and AMP breakdown in adenosine by the ecto-5'nuceotidase/CD73 activity promote a complete enzymatic cascade.

In light of these, data of present study are promising in the definition of new molecules useful as potential intradiscal injectable therapeutics. The scenario of biological treatment approaches for degenerated disc repair is widely expanding, and the use of specific molecules that aim to revert/to block the inflammation present in degenerated IVD microenvironment combinated with adequate delivery systems into a degenerating disc appears promising [Penolazzi et al., 2018; Clouet et al., 2019].

The results obtained by us open the way for further investigations on the role of the purinergic system, mainly P2X7R, in intervertebral disc microenvironment. In this regard, future planning is aimed at:

i) the analysis of IL-1β expression in IVD tissues;

ii) the increase of sample number for P2X7R and NLRP3 immunohistochemical analysis;

iii) the improvement of the protocol of the exposure to LPS and P2X7R agonists in IVD cells;

iv) the analysis of the ectonucleotidases enzymes activity;

v) the analysis of pro-inflammatory cytokines such as IL-6 and TNF-α, and anti-inflammatory cytokines such as IL-10 and TGF-β after cell exposure to P2X7R agonist or antagonist;
vi) the improvement of knowledge through experimental systems that more closely reproduce the complexity of IVD microenvironment, using, for example, 3D systems in hypoxic condition.
In conclusion, for the first time, we demonstrated that P2X7R and its downstream target (NLRP3 inflammasome) are involved in pathogenesis of IVD degeneration and are more expressed in IVD tissues with mild and high Pfirrmann grades than in IVD tissues with low grade.

# 5. REFERENCES

Abbracchio MP, Burnstock G. 1994. Purinoceptors: are there families of P2X and P2Y purinoceptors? Pharmacol Ther. 64(3):445-75.

Adinolfi E, Cirillo M, Woltersdorf R, Falzoni S, Chiozzi P, Pellegatti P, Callegari MG, Sandonà D, Markwardt F, Schmalzing G, Di Virgilio F. 2010. Trophic activity of a naturally occurring truncated isoform of the P2X7 receptor. FASEB J. 24(9):3393-404.

Adinolfi E, Giuliani AL, De Marchi E, Pegoraro A, Orioli E, Di Virgilio F. 2018. The P2X7 receptor: A main player in inflammation. Biochem Pharmacol.151:234-244.

Adinolfi E, Callegari MG, Ferrari D, Bolognesi C, Minelli M, Wieckowski MR, Pinton P, Rizzuto R, Di Virgilio F. 2005. Basal Activation of the P2X7 ATP Receptor Elevates Mitochondrial Calcium and Potential, Increases Cellular ATP Levels, and Promotes Serum-Independent Growth. Mol Biol Cell. 16(7):3260-72.

Agrawal A, Henriksen Z, Syberg S, Petersen S, Aslan D, Solgaard M, Nissen N, Larsen TK, Schwarz P, Steinberg TH, Jørgensen NR. 2017. P2X7Rs are involved in cell death, growth and cellular signaling in primary human osteoblasts. Bone. 95:91-101.

Agrawal A, Gartland A. 2015. P2X7 receptors: role in bone cell formation and function. J Mol Endocrinol. 54(2):R75-88.

Amini AR, Laurencin CT, Nukavarapu SP. 2012. Bone Tissue Engineering: Recent Advances and Challenges. Crit Rev Biomed Eng. 40(5): 363–408.

Amoroso F, Falzoni S, Adinolfi E, Ferrari D, Di Virgilio F. 2012. The P2X7 receptor is a key modulator of aerobic glycolysis. Cell Death Dis. 3:e370.

Anderson HC. 1995. Molecular biology of matrix vesicles. Clin Orthop Relat Res (314):266–280.

Arboleya L, Castañeda S. 2013. Osteoimmunology: the study of the relationship between the immune system and bone tissue. Reumatol Clin. 9(5):303-15.

Archer CW, Francis-West P. 2003. The chondrocyte. Int J Biochem Cell Biol. 35(4):401-4.

Armiento AR, Alini M, Stoddart MJ. 2019.Articular fibrocartilage - Why does hyaline cartilage fail to repair? Adv Drug Deliv Rev. 146:289-305.

Awad F, Assrawi E, Louvrier C, Jumeau C, Giurgea I, Amselem S, Karabina SA. 2018. Photoaging and skin cancer: Is the inflammasome the missing link? Mech Ageing Dev. 172:131-137.

Bader DL, Salter DM, Chowdhury TT. 2011. Biomechanical influence of cartilage homeostasis in health and disease. Arthritis. 2011:979032.

Baker M. 2016. Reproducibility: respect your cells. Nature 537:433–435.

Baker BM, Chen CS. 2012. Deconstructing the third dimension - how 3D culture microenvironments alter cellular cues. J Cell Sci. 125:3015–3024.

Baptista JS, Traynelis VC, Liberti EA, Fontes RBV. 2020. Expression of degenerative markers in intervertebral discs of young and elderly asymptomatic individuals. PLoS One. 15(1):e0228155.

Baroja-Mazo A, Barbera-Cremades M, Pelegrin P. 2013. The participation of plasma membrane hemichannels to purinergic signaling. Biochim Biophys Acta. 1828(1):79- 93.

Baron R, Kneissel M. 2013. WNT signaling in bone homeostasis and disease: from human mutations to treatments. Nat Med. 19:179– 192.

Berg EJ, Ashurst JV. 2018. Anatomy, Back, Cauda Equina. StatPearls [Internet]. Treasure Island (FL): StatPearls Publishing.

Bergamin LS, Braganhol E, Zanin RF, Edelweiss MI, Battastini AM. 2012. Ectonucleotidases in in tumor cells and tumor-associated immune cells: An overview. J Biomed Biotechnol. 2012:959848.

Bilodeau MS, Arguin G, Gendron FP. 2015. C/EBPβ regulates P2X7 receptor expression in response to glucose challenge in intestinal epithelial cells. Biochem Cell Biol. 93(1):38-46.

Boonrungsiman S, Gentleman E, Carzaniga R, Evans ND, McComb DW, Porter AE, Stevens MM. 2012. The role of intracellular calcium phosphate in osteoblast-mediated bone apatite formation. Proc Natl Acad Sci U S A. 109(35):14170–14175.

Bours MJ, Swennen EL, Di Virgilio F, Cronstein BN, Dagnelie PC. 2006. Adenosine 5'- triphosphate and adenosine as endogenous signaling molecules in immunity and inflammation. Pharmacol Ther. 112(2):358-404.

Bradford MM. 1976. A rapid and sensitive method for the quantification of microgram quantities of protein utilizing the principle of protein-dye binding. Anal Biochem. 72:248-54.

Brandao-Burch A, Key ML, Patel JJ, Arnett TR, Orriss IR. 2012. The P2X7 Receptor is an Important Regulator of Extracellular ATP Levels. Front Endocrinol (Lausanne). 19;3:41.

Buckwalter JA, Glimcher MJ, Cooper RR, Recker R. 1996. Bone biology. I: structure, blood supply, cells, matrix, and mineralization. Instr Course Lect. 45:371–86.

Burnstock G, Arnett TR, Orriss IR. 2013. Purinergic signalling in the musculoskeletal system. Purinergic Signal. 9(4):541-72.

Burnstock G. 1978. A Basis for Distinguishing Two Types of Purinergic Receptor, in Cell Membrane Receptors for Drugs and Hormones. Raven Press. 107-118.

Burnstock G. 2004. Introduction: P2 receptors. Curr Top Med Chem. 4(8):793-803.

Burnstock G. 2017. Purinergic Signalling: Therapeutic Developments. Front Pharmacol. 8:661.

Cabrini G, Falzoni S, Forchap SL, Pellegatti P, Balboni A, Agostini P. 2005. A His-155 to Tyr polymorphism confers gain-of-function to the human P2X7 receptor of human leukemic lymphocytes. J Immunol. 175(1):82–89.

Camarero-Espinosa S, Rothen-Rutishauser B, Foster EJ, Weder C. 2016. Articular cartilage: from formation to tissue engineering. Biomater Sci. 4(5):734-67.

Caporali F, Capecchi PL, Gamberucci A, Lazzerini PE, Pompella G, Natale M, Lorenzini S, Selvi E, Galeazzi M, Laghi Pasini F. 2008. Human rheumatoid synoviocytes express functional P2X7 receptors. J Mol Med (Berl). 86(8):937-49.

Capulli M, Paone R, Rucci N. 2014. Osteoblast and osteocyte: games without frontiers. Arch Biochem Biophys. 561:3-12.

Carluccio M, Zuccarini M, Ziberi S, Giuliani P, Morabito C, Mariggio MA, Lonardo MT, Adinolfi E, Orioli E, Di Iorio P, Caciagli F, Ciccarelli R. 2019. Involvement of P2X7 Receptors in the Osteogenic Differentiation of Mesenchymal Stromal/Stem Cells Derived from Human Subcutaneous Adipose Tissue. Stem Cell Rev Rep. 15(4): 574-589.

Cashman K D, Ginty F. 2003. Bone. Encyclopedia of Food Sciences and Nutrition. 557–565.

Cassotta M, Pistollato F, Battino M. 2020. Rheumatoid arthritis research in the 21st century: limitations of traditional models, new technologies, and opportunities for a human biology-based approach. ALTEX Alternat Anim Exp. 37:223–242.

Chang X, He H, Zhu L, Gao J, Wei T, Ma Z, Yan T. 2015. Protective effect of apigenin on Freund's complete adjuvant-induced arthritis in rats via inhibiting P2X7/NF-κB pathway. Chem Biol Interact. 236:41-6.

Cheewatrakoolpong B, Gilchrest H, Anthes JC, Greenfeder S. 2005. Identification and characterization of splice variants of the human P2X7 ATP channel. Biochem Biophys Res Commun. 332(1):17-27.

Chen ZH, Jin SH, Wang MY, Jin XL, Lv C, Deng YF, Wang JL. 2015. Enhanced NLRP3, caspase-1, and IL- 1β levels in degenerate human intervertebral disc and their association with the grades of disc degeneration. Anat Rec (Hoboken). 298(4):720-6.

Clarke B. 2008. Normal bone anatomy and physiology. Clin J Am Soc Nephrol. Suppl 3:S131-9.

Clouet J, Fusellier M, Camus A, Le Visage C, Guicheux J. 2019. Intervertebral disc regeneration: From cell therapy to the development of novel bioinspired endogenous repair strategies. Adv Drug Deliv Rev.146:306-324.

Coccurello R, Volonté C. 2020. P2X7 Receptor in the Management of Energy Homeostasis: Implications for Obesity, Dyslipidemia, and Insulin Resistance. Front Endocrinol (Lausanne). 11: 199.

Coll RC, O'Neill L, Schroder K. 2016. Questions and controversies in innate immune research: what is the physiological role of NLRP3? Cell Death Discov. 2:16019.

Daly C, Ghosh P, Jenkin G, Oehme D, Goldschlager T. 2016. A Review of Animal Models of Intervertebral Disc Degeneration: Pathophysiology, Regeneration, and Translation to the Clinic. Biomed Res Int. 2016:5952165.

Delgado-Calle J, Garmilla P, Riancho JA. 2012. Do Epigenetic Marks Govern Bone Mass and Homeostasis?Curr Genomics. 13(3): 252–263.

Demer LL, Tintut Y. 2014. Inflammatory, metabolic, and genetic mechanisms of vascular calcification. Arterioscler Thromb Vasc Biol. 34(4):715-723.

Di Virgilio F, Chiozzi P, Ferrari D, Falzoni S, Sanz JM, Morelli A, Torboli M, Bolognesi G, Baricordi OR. 2001. Nucleotide receptors: an emerging family of regulatory molecules in blood cells. Blood. 97(3):587-600.

Di Virgilio F, Dal Ben D, Sarti AC, Giuliani AL, Falzoni S. 2017. The P2X7 Receptor in Infection and Inflammation. Immunity 47(1): 15-31.

Di Virgilio F, Giuliani AL, Vultaggio-Poma V, Falzoni S, Sarti AC. 2018. Non-nucleotide agonists triggering P2X7 receptor activation and pore formation. Front Pharmacol. 9:39. (a)

Di Virgilio F, Schmalzing G, Markwardt F. 2018. The Elusive P2X7 Macropore. Trends Cell Biol. 28:392–404. (b)

Di Virgilio F, Jiang LH, Roger S, Falzoni S, Sarti AC, Vultaggio-Poma V, Chiozzi P, Adinolfi E. 2019. Structure, function and techniques of investigation of the P2X7 receptor (P2X7R) in mammalian cells. Methods Enzymol. 629:115-150.

Di Virgilio F, Tang Y, Sarti AC, Rossato M. 2020. A rationale for targeting the P2X7 receptor in Coronavirus disease 19. Br J Pharmacol. 177(21):4990-4994.

Di Virgilio F, Steinberg TH, Swanson JA, Silverstein SC. 1988. Fura-2 Secretion and Sequestration in Macrophages. A Blocker of Organic Anion Transport Reveals That These Processes Occur via a Membrane Transport System for Organic Anions. J Immunol. 140(3):915-20.

Ding F, Shao ZW, Xiong LM. 2013. Cell death in intervertebral disc degeneration. Apoptosis. 18:777–785.

Dong Y, Chen Y, Zhang L, Tian Z, Dong S. 2020. P2X7 receptor acts as an efficient drug target in regulating bone metabolism system. Biomed Pharmacother. 125:110010.

Eltzschig HK, Sitkovsky MV, Robson SC. 2012. Purinergic signaling during inflammation. N Engl J Med. 367(24):2322-33.

Fakhry M, Hamade E, Badran B, Buchet R, Magne D. 2013. Molecular mechanisms of mesenchymal stem cell differentiation towards osteoblasts. World J Stem Cells. 5(4):136-48.

Falzoni S, Munerati M, Ferrari D, Spisani S, Moretti S, Di Virgilio F. 1995. The purinergic P2Z receptor oh human macrophage cells. Characterization and possible physiological role. J Clin Invest. 95(3):1207-16.

Fan L, Li J, Yu Z, Dang X, Wang K. 2014. The hypoxia-inducible factor pathway, prolyl hydroxylase domain protein inhibitors, and their roles in bone repair and regeneration. Biomed Res Int. 2014:239356.

Feng YH, Li X, Wang L, Zhou L, Gorodeski GI. 2006. A truncated P2X7 receptor variant (P2X7-j) endogenously expressed in cervical cancer cells antagonizes the full-length P2X7 receptor through hetero-oligomerization. J Biol Chem. 281(25):17228-37.

Fernando HN, Czamanski J, Yuan TY, Gu W, Salahadin A, Huang CY. 2011. Mechanical loading affects the energy metabolism of intervertebral disc cells. J Orthop Res. 29:1634– 1641.

Findlay DM, Kuliwaba JS. 2016. Bone–cartilage crosstalk: a conversation for understanding osteoarthritis. Bone Res. 4:16028.

Florencio-Silva R, Sasso GR, Sasso-Cerri E, Simões MJ, Cerri PS. 2015. Biology of Bone Tissue: Structure, Function, and Factors That Influence Bone Cells. Biomed Res Int. 2015:421746.

Fuchs RK, Thompson WR, Warden SJ. 2019. Bone Repair Biomaterials (Second Edition). Regeneration and Clinical Applications. Woodhead Publishing Series in Biomaterials. 15-52.

Ganey T, Libera J, Moos V, Alasevic O, Fritsch KG, Meisel HJ, Hutton WC. 2003. Disc chondrocyte transplantation in a canine model: a treatment for degenerated or damaged intervertebral disc. Spine (Phila Pa 1976). 28(23):2609-20.

García-Huerta P, Díaz-Hernandez M, Delicado EG, Pimentel-Santillana M, Miras-Portugal MT, Gómez-Villafuertes R. 2012. The specificity protein fator Sp1 mediates transcriptional regulation of P2X7 receptors in the nervous system. J Biol Chem. 287(53):44628-44.

Gartland A, Buckley KA, Bowler WB, Gallagher JA. 2003. Blockade of the poreforming P2X7 receptor inhibits formation of multinucleated human osteoclasts in vitro. Calcif Tissue Int. 73(4):361–369 (a).

Gartland A, Buckley KA, Hipskind RA, Perry MJ, Tobias JH, Buell G, Chessell I, Bowler WB, Gallagher JA. 2003. Multinucleated osteoclast formation in vivo and in vitro by P2X7 receptor-deficient mice. Crit Rev Eukaryot Gene Expr. 13 (2-4):243-53 (b).

Gartland A, Ginty AF, Gallagher JA, Bowler WB. 1999. Activation of P2X7 receptors expressed by human osteoclastoma modulates bone resorption. Calci Tissue Int. 64:S56.

Ghorbaninejad M, Khademi-Shirvan M, Hosseini S, Eslaminejad MB. 2020. Epidrugs: novel epigenetic regulators that open a new window for targeting osteoblast differentiation. Stem Cell Research & Therapy. 11(456).

Giuliani AL, Colognesi ALD, Ricco T, Roncato C, Capece M, Amoroso F, Wang QG, De Marchi E, Gartland A, Di Virgilio F. and Adinolfi E. 2014. Trophic activity of human P2X7 receptor isoforms A and B in osteosarcoma. PLoS One. 9(9): e107224.

Giuliani AL, Sarti AC, Falzoni S, Di Virgilio F. 2017.The P2X7 Receptor-Interleukin-1 Liaison.Front Pharmacol. 8:123.

Giuliani AL, Sarti AC, Di Virgilio F. 2019. Extracellular nucleotides and nucleosides as signalling molecules. Immunol Lett. 205:16-24.

Glimcher MJ. 1984. Recent studies of the mineral phase in bone and its possible linkage to the organic matrix by protein-bound phosphate bonds. Philos Trans R Soc Lond B Biol Sci. 304:479–508.

Gonzales S, Wang C, Levene H, Cheung HS, Huang CC. 2015. ATP promotes extracellular matrix biosynthesis of intervertebral disc cells. Cell Tissue Res. 359(2):635-642.

Gonzales S, Rodriguez B, Barrera C, Huang CY. 2014. Measurement of ATP-Induced Membrane Potential Changes in IVD cells. Cellular and Molecular Bioengineering. 7(4):598-606.

González Martínez E, García-Cosamalón J, Cosamalón-Gan I, Esteban Blanco M, García-Suarez O, Vega JA. 2017. Biology and mechanobiology of the intervertebral disc.Neurocirugia (Astur). 28(3):135-140.

Goss M, Socorro M, Monier D, Verdelis K, Napierala D. 2019. Trps1 transcription factor regulates mineralization of dental tissues and proliferation of tooth organ cells. Mol Genet Metab. 126(4):504-512.

Grol MW, Panupinthu N, Korcok J, Sims SM, Dixon SJ. 2009. Expression, Signaling, and Function of P2X7 Receptors in Bone. Purinergic Signal. 5(2):205-21.

Grol MW, Pereverzev A, Sims SM, Dixon SJ. 2013. P2 receptor networks regulate signaling duration over a wide dynamic range of ATP concentrations. J Cell Sci. 126(Pt 16):3615-26.

Grol MW, Brooks PJ, Pereverzev A, Dixon SJ. 2016. P2X7 nucleotide receptor signaling potentiates the Wnt/β-catenin pathway in cells of the osteoblast lineage. Purinergic Signal. 12(3):509-20.

Gu BJ, Zhang WY, Worthington RA. 2001. A Glu-496 to Ala polymorphism leads to loss of function of the human P2X7 receptor. J Biol Chem. 276:11135–11142.

Hattori M, Gouaux E. 2012. Molecular mechanism of ATP binding and ion channel activation in P2X receptors. Nature. 485(7397):207-12.

Hayrapetyan A, Jansen JA, van den Beucken JJ. 2015. Signaling pathways involved in osteogenesis and their application for bone regenerative medicine. Tissue Eng Part B Rev. 21(1):75-87.

He Y, Hara H, Nunez G. 2016. Mechanism and regulation of NLRP3 inflammasome activation. Trends Biochem Sci. 41:1012–1021.

Huang YC, Hu Y, Li Z, Luk KDK. 2018. Biomaterials for intervertebral disc regeneration: Current status and looming challenges. J Tissue Eng Regen Med. 12(11):2188-2202.

Hutchings G, Moncrieff L, Dompe C, Janowicz K, Sibiak R, Bryja A, Jankowski M, Mozdziak P, Bukowska D, Antosik P, Shibli JA, Dyszkiewicz-Konwińska M, Bruska M, Kempisty B, Piotrowska-Kempisty H. 2020. Bone Regeneration, Reconstruction and Use of Osteogenic Cells; from Basic Knowledge, Animal Models to Clinical Trials. J Clin Med. 9(1). pii: E139.

Idzko M, Ferrari D, Eltzschig HK. 2014. Nucleotide signalling during inflammation. Nature. 509(7500):310-7.

Illes P, Klotz KN, Lohse MJ. 2000. Signaling by extracellular nucleotides and nucleosides. Naunyn Schmiedebergs Arch Pharmacol. 362(4-5):295-8.

Infante A, Rodríguez CI. 2018. Osteogenesis and aging: lessons from mesenchymal stem cells. Stem Cell Res Ther. 9(1):244.

Ishiyama K, Yashiro T, Nakano N, Kasakura K, Miura R, Hara M, Kawai F, Maeda K, Tamura N, Okumura K, Ogawa H, Takasaki Y, Nishiyama C. 2015. Involvement of PU.1 in NFATc1 promoter function in osteoclast development. Allergol. Int. 64(3):241–247.

Ito K, Aebi M, Alini M. 2002. Aging and degeneration. Cause and effect of intervertebral disc damage? In: Gunzburg RSM, Szpalski M, editors. Lumbar disc herniation. Philadelphia: Lippincott Williams & Wilkins. 72–81.

Jimenez-Mateos EM, Smith J, Nicke A, Engel T, 2019. Regulation of P2X7 receptor expression and function in the brain. Brain Res Bull. 151:153-163

Jo EK, Kim JK, Shin DM, Sasakawa C. 2016. Molecular mechanisms regulating NLRP3 inflammasome activation. Cell Mol Immunol. 13(2):148-59.

Johnson ZI, Schoepflin ZR, Choi H, Shapiro IM, Risbud MV. 2015. Disc in flames: Roles of TNF-α and IL-1β in intervertebral disc degeneration. Eur Cell Mater. 30:104-16; discussion 116-7.

Johnstone B, Alini M, Cucchiarini M, Dodge GR, Eglin D, Guilak F, Madry H, Mata A, Mauck RL, Semino CE, Stoddart MJ. 2013. Tissue engineering for articular cartilage repair-the state of the art. Eur Cell Mater. 25:248-67.

Jones G, Winzenberg TM, Callisaya ML, Laslett LL. 2014. Lifestyle modifications to improve musculoskeletal and bone health and reduce disability-a life-course approach. Best Pract Res Clin Rheumatol. 28(3):461-78.

Jørgensen NR, Syberg S, Ellegaard M. 2015. The role of P2X receptors in bone biology. Curr Med Chem. 22(7):902-14.

Jørgensen NR. 2018. The purinergic P2X7 ion channel receptor-a 'repair' receptor in bone. Curr Opin Immunol. 52:32-38.

Kaebisch C, Schipper D, Babczyk P, Tobiasch E. 2015. The role of purinergic receptors in stem cell differentiation. Comput Struct Biotechnol J. 13:75-84.

Kalson NS, Richardson S, Hoyland JA. 2008. Strategies for regeneration of the intervertebral disc. Regen Med. 3:717–29.

Katsimbri P. 2017. The biology of normal bone remodelling. Eur J Cancer Care (Engl). 26(6).

Kerr GJ, Veras MA, Kim MK, Séguin CA. 2017. Decoding the intervertebral disc: Unravelling the complexities of cell phenotypes and pathways associated with degeneration and mechanotransduction. Semin Cell Dev Biol. 62:94-103.

Khakh BS, Burnstock G, Kennedy C, King BF, North RA, Séguéla P, Voigt M, Humphrey PP. 2001. International union of pharmacology. XXIV. Current status of the nomenclature and properties of P2X receptors and their subunits. Pharmacol Rev. 53(1):107-18.

Kim JH, Kim K, Kim I, Seong S, Jeong BC, Nam KI, Kim KK, Molkentin JD, Kim N. 2016. RCANs regulate the convergent roles of NFATc1 in bone homeostasis. Sci Rep. 6:38526.

Kirkham GR, Cartmell SH. 2007. Genes and Proteins Involved in the Regulation of Osteogenesis. Topics in Tissue Engineering, Vol. 3, 2007. Eds. N Ashammakhi, R Reis & E Chiellini.

Knight MM, McGlashan SR, Garcia M, Jensen CG, Poole CA. 2009 Articular chondrocytes express connexin 43 hemichannels and P2 receptors-a putative mechanoreceptor complex involving the primary cilium? J Anat. 214:275–283.

Koolpe M, Pearson D, Benton HP. 1999. Expression of both P1 and P2 purine receptor genes by human articular chondrocytes and profile of ligand-mediated prostaglandin E2 release. Arthritis Rheum. 42:258–267.

Korcok J, Sims SM, Dixon SJ. 2004. P2X7 nucleotide receptors act through two distinct mechanisms to regulate osteoclast survival. J Bone Miner Res. 19(Suppl. 1):S418–S419.

Kopp R, Krautloher A, Ramírez-Fernández A, Nicke A. 2019. P2X7 Interactions and Signaling - Making Head or Tail of It. Front Mol Neurosci. 12:183.

Kudirka JC, Panupinthu N, Tesseyman MA, Dixon SJ, Bernier SM. 2007. P2Y nucleotide receptor signaling through MAPK/ERK is regulated by extracellular matrix: involvement of β3 integrins. J Cell Physiol. 213:54–64.

Kuyinu EL, Narayanan G, Nair LS, Laurencin CT. 2016. Animal models of osteoarthritis: classification, update, and measurement of outcomes. J Orthop Surg Res. 2:11-19.

Kvist TM, Schwarz P, Jørgensen NR. 2014. The P2X7 Receptor: A Key Player in Immune-Mediated Bone Loss? Sientific World Journal. 2014:954530.

Lambertini E, Penolazzi L, Angelozzi M, Grassi F, Gambari L, Lisignoli G, De Bonis P, Cavallo M, Piva R. 2017. The expression of cystathionine gamma-lyase is regulated by estrogen receptor alpha in human osteoblasts. Oncotarget. 8:101686-101696.

Lambertini E, Tavanti E, Torreggiani E, Penolazzi L, Gambari R, Piva R. 2008. ER alpha and AP-1 interact in vivo with a specific sequence of the F promoter of the human ER alpha gene in osteoblasts. J Cell Physiol. 216:101–110.

Lane NE. 2006. Epidemiology, etiology, and diagnosis of osteoporosis Am J Obstet Gynecol. 194(2 Suppl):S3-11.

Li J, Liu D, Ke HZ, Duncan LR, Turner CH. 2005. The P2X7 nucleotide receptor mediates skeletal mechanotransduction. Journal of Biological Chemistry. 280(52):42952– 42959.

Liu Y, Guangdong Z, Yilin C. 2017. Recent Progress in Cartilage Tissue Engineering-Our Experience and Future Directions. Engineering. 3(1):28-35.

Livak KJ, Schmittgen TD. 2001. Analysis of relative gene expression data using real-time quantitative PCR and the 2 (-Delta Delta C(T)) method. Methods. 25:402–408.

Long F. 2011. Building strong bones: molecular regulation of the osteoblast lineage. Nat Rev Mol Cell Biol. 13(1):27-38.

MacKenzie AB, Surprenant A, North RA. 1999. Functional and molecular diversity of purinergic ion channel receptors. Ann N Y Acad Sci. 868:716-29.

Mackie EJ, Tatarczuch L, Mirams M. 2011. The skeleton: a multi-functional complex organ: the growth plate chondrocyte and endochondral ossification. J Endocrinol. 211(2):109-21.

Mackie EJ, Ahmed YA, Tatarczuch L, Chen KS, Mirams M. 2008. Endochondral ossification: how cartilage is converted into bone in the developing skeleton. Int J Biochem Cell Biol. 40(1):46-62.

Masin M, Young C, Lim K, Barnes SJ, Xu XJ, Marschall V, Brutkowski W, Mooney ER, Gorecki DC, Murrell-Lagnado R. 2012. Expression, assembly and function of novel C-terminal truncated variants of the mouse P2X7 receptor: re-evaluation of P2X7 knockouts. Br J Pharmacol. 165(4):978-93.

Menkova-Garnier I, Hocini H, Foucat E, Tisserand P, Bourdery L, Delaugerre C, Benne C, Lévy Y, Lelièvre JD. 2016, P2X7 Receptor Inhibition Improves CD34 T.cell Differentiation in HIV-Infected Immunological Nonresponders on c-ART. PLoS Pathog 12(4):e1005571

Minear S, Leucht P, Jiang J, Liu B, Zeng A, Fuerer C, Nusse R, Helms JA. 2010. Wnt proteins promote bone regeneration. Sci Transl Med. 2(29):29ra30.

North RA, Surprenant A. 2000. Pharmacology of cloned P2X receptors. Annu Rev Pharmacol Toxicol. 40:563-80.

Orioli E, De Marchi E, Giuliani AL, Adinolfi E. 2017. P2X7 Receptor Orchestrates Multiple Signalling Pathways Triggering Inflammation, Autophagy and Metabolic/Trophic Responses. Curr Med Chem. 24(21):2261-2275.

Orriss IR, Key ML, Hajjawi MO, Arnett TR. 2013. Extracellular ATP released by osteoblasts is a key local inhibitor of bone mineralization. PLoS One. 8(7): e69057.

Orriss IR, Key ML, Brandao-Burch A, Patel JJ, Burnstock G, Timothy R ArnettTR. 2012. The regulation of osteoblast function and bonemineralisation by extracellular nucleotides: The role of p2x receptors. Bone. 51(3):389-400.

Owen R, Reilly GC. 2018. In vitro models of bone remodelling and associated disorders. Front Bioeng Biotechnol. 6:134.

Pakyasa M, Alverdy A, Mostafa S, Wang E, Fu L, Li A, Oliveira L, Athiviraham A, Lee MJ, Wolf JM, He TC, Ameer GA, Reid RR. 2017. Neural EGF-like protein 1 (NELL-1): Signaling crosstalk in mesenchymal stem cells and applications in regenerative medicine. Genes Dis. 4(3):127-137.

Panupinthu N, Rogers JT, Zhao LP, L.P. Solano-Flore F, Possmayer SM, Sims SJ, Dixon. 2008. P2X7 receptors on osteoblasts couple to production of lysophosphatidic acid: a signaling axis promoting osteogenesis. J. Cell Biol. 181(5):859–871.

Park JY, Park SH, Kim MG, Park SH, Yoo TH, Kim MS. 2018. Biomimetic scaffolds for bone tissue engineering. Adv Exp Med Biol. 1064:109–121.

Pelegrin P, Surprenant A. 2006. Pannexin-1 mediates large pore formation and interleukin-1beta release by the ATP-gated P2X7 receptor. EMBO J. 25(21):5071-82.

Penolazzi L, Lambertini E, Bergamin LS, Roncada T, De Bonis P, Cavallo M, Piva R. 2018. MicroRNA-221 silencing attenuates the degenerated phenotype of intervertebral disc cells. Aging (Albany NY). 10(8):2001-2015.

Penolazzi L, Lambertini E, Scussel Bergamin L, Gandini C, Musio A, De Bonis P, Cavallo M, Piva R. 2019. Reciprocal Regulation of TRPS1 and miR-221 in Intervertebral Disc Cells. Cells. 8(10). pii: E1170.

Penolazzi L, Lisignoli G, Lambertini E, Torreggiani E, Manferdini C, Lolli A, Vecchiatini R, Ciardo F, Gabusi E, Facchini A, Gambari R, Piva R. 2011. Transcription factor decoy against NFATc1 in human primary osteoblasts. Int J Mol Med. 28(2):199-206.

Penolazzi L, Lambertini E, Piva R. 2020. The Adequacy of Experimental Models and Understanding the Role of Non-coding RNA in Joint Homeostasis and Disease.Front Genet. 2020 11:563637.

Pfirrmann CW, Metzdorf A, Zanetti M, Hodler J, Boos N. 2001. Magnetic resonance classification of lumbar intervertebral disc degeneration. Spine. 26:1873–1878.

Raggatt LJ, Partridge NC. 2010. Cellular and molecular mechanismsof bone remodelling. J Biol Chem. 285:25103–25108.

Ralevic V, Burnstock G. 1998. Receptors for Purines and Pyrimidines. Pharmacological Reviews. 50(3):413-492.

Rassendren F, Buell GN, Virginio C, Collo G, North RA, Surprenant A. 1997. The permeabilizing ATP receptor, P2X7. Cloning and expression of a human cDNA. J Biol Chem. 272(9):5482-6.

Raouf A, Seth A. 2000. Ets transcription factors and targets in osteogenesis. Oncogene. 19(55):6455-63.

Rico-Llanos GA, Becerra J, Visser R. 2017. Insulin-like growth factor-1 (IGF-1) enhances the osteogenic activity of bone morphogenetic protein-6 (BMP-6) in vitro and in vivo, and together have a stronger osteogenic effect than when IGF-1 is combined with BMP-2. J Biomed Mater Res A. 105(7):1867-1875.

Richardson SM, Freemont AJ, Hoyland JA. 2014. Pathogenesis of intervertebral disc degeneration. In The Intervertebral Disc-Molecular and Structural Studies of the Disc in Health and Disease. Shapiro, I.M., Risbud, M.V., Eds.; Springer: Vienna, Austria.177–200.

Riteau N, Gasse P, Fauconnier L, Gombault A, Couegnat M, Fick L, Kanellopoulos J, Quesniaux VF, Marchand-Adam S, Crestani B, Ryffel B, Couillin I. 2010. Extracellular ATP is a danger signal activating P2X7 receptor in lung inflammation and fibrosis. Am J Respir Crit Care Med. 182(6):774-83.

Roberts S, Pauline Colombier P, Aneka Sowman A, Claire Mennan C, Jan HD Rölfing JHD, Jérôme Guicheux J, Edwards JR. 2016. Ageing in the musculoskeletal system. Acta Orthop. 87(eSuppl 363):15–25.

Robson SC, Sévigny J, Zimmermann H. 2006. The ENTPDase family of ectonucleotidases: Structure function relationships and pathophysiological significance. Purinergic Signal. 2(2):409-30.

Roger S, Jelassi B, Couillin I, Pelegrin P, Besson P, Jiang LH. 2015. Understanding the roles of the P2X7 receptor in solid tumour progression and therapeutic perspectives. Biochim Biophys Acta. 1848 (10 Pt B):2584-602.

Roughley PJ. 2004. Biology of intervertebral disc aging and degeneration: involvement of the extracellular matrix. Spine (Phila Pa 1976). 29:2691–9.

Sacitharan PK. 2019. Ageing and Osteoarthritis. Subcell Biochem. 91:123-159.

Salvatierra JC, Yuan TY, Fernando H, Castillo A, Gu WY, Cheung HS, Huant CY. 2011. Difference in energy metabolism of annulus fibrosus and nucleus pulposus cells of the intervertebral disc. Cell Mol Bioeng. 4:302–310.

Sanz JM, Falzoni S, Rizzo R, Cipollone F, Zuliani G, Di Virgilio F. 2014. Possible protective role of the 489C>T P2X7R polymorphism in Alzheimer's disease. Exp Gerontol. 60:117-9.

Seref-Ferlengez Z, Urban-Maldonado M, Sun HB, Schaffler MB, Suadicani SO, Thi MM. 2019. Role of pannexin 1 channels in load-induced skeletal response. Ann N Y Acad Sci. 1442(1):79-90.

Sindhavajiva PR, Sastravaha P, Arksornnukit M, Pavasant P. 2017. Purinergic 2X7 receptor activation regulates WNT signaling in human mandibular-derived osteoblasts. Arch Oral Biol. 81:167-174.

Sitara D, Aliprantis AO. 2010. Transcriptional regulation of bone and joint remodeling by NFAT. Immunol Rev. 233(1):286-300.

Shamji MF, Setton LA, Jarvis W, So S, Chen J, Jing L, Bullock R, Isaacs RE, Brown C, Richardson WJ. 2010. Proinflammatory cytokine expression profile in degenerated and herniated human intervertebral disc tissues. Arthr. Rheum. 62:1974–1982.

Shapiro IM, Risbud MV. 2014. Introduction to the structure, function, and comparative anatomy of the vertebrae and the intervertebral disc. In The Intervertebral Disc-Molecular and Structural Studies

of the Disc in Health and Disease. Shapiro, I.M., Risbud, M.V., Eds.; Springer: Vienna, Austria. 3–16.

Sluyter R, Stokes L. 2011. Significance of P2X7 receptor variants to human health and disease. Recent Pat DNA Gene Seq. 5(1):41–54.

Sluyter R. 2017. The P2X7 Receptor. Adv Exp Med Biol. 1051:17-53.

Smith LJ, Nerurkar NL, Choi KS, Harfe BD, Elliott DM. 2011. Degeneration and regeneration of the intervertebral disc: lessons from development. Dis Model Mech. 4(1):31-41.

Song B, Estrada KD, Lyons KM. 2009. Smad Signaling in Skeletal Development and Regeneration. Cytokine Growth Factor Rev. 20(5-6):379–388.

Staunton CA, Lewis R, Barrett-Jolley R. 2013. Ion channels and osteoarthritic pain: potential for novel analgesics. Curr Pain Headache Rep. 17(12):378.

Surprenant A, Rassendren F, Kawashima E, North RA, Buell G. 1996. The cytolytic P2Z receptor for extracellular ATP identified as a P2X receptor (P2X7). Science. 272(5262):735-8.

Surprenant A, North RA. 2009. Signaling at purinergic P2X receptors. Annu Rev Physiol. 71:333-59.

Tafani M, Schito L, Pellegrini L, Villanova L, Marfe G, Anwar T, Rosa R, Indelicato M, Fini Massimo, Pucci B, Russo MA. 2011. Hypoxia-increased RAGE and P2X7R expression regulates tumor cell invasion through phosphorylation of Erk1/2 and Akt and nuclear translocation of NF-kappaB. Carcinogenesis. 32:1167–1175.

Teitelbaum SL. 2007. Osteoclasts: what do they do and how do they do it? Am J Pathol. 170(2):427-35.

Teixeira JM, Dias EV, Parada CA, Tambeli CH. 2017. Intra-Articular Blockade of P2X7 Receptor Reduces the Articular Hyperalgesia and Inflammation in the Knee Joint Synovitis Especially in Female Rats. J Pain. 18(2):132-143.

Toosi S, Behravan J. 2020. Osteogenesis and bone remodeling: A focus on growth factors and bioactive peptides. Biofactors. 46(3):326-340.

Trabanelli S, Ocadlikova D, Gulinelli S, Curti, A, Salvestrini V, Viera RP, Idzko M, Di Virgilio F, Ferrare D, Lemoli, RM. 2012. Extracellular ATP exerts opposite effects on activated and regulatory CD4+ T cells via purinergic P2 receptor activation. Journal of immunology (Baltimore, Md: 1950). 189(3):1303–10.

Urban J, Roberts S. 2006. The intervertebral disc: normal, aging, and pathologic. In: Herkowitz HN, Garfin SR, Eismont FJ, Bell GR, Balderston RA, editors. Rothman-Simeone The Spine. Philadelphia: Saunders. 71–83.

Urban J. 2004. The physiology of intervertebral disc degeneration. In: Gunzburg R, Szpalski M, Anderson G, editors. Degenerative disc disease. Lippincott Williams & Wilkins. 22–30.

Varani K, De Mattei M, Vincenzi F, Tosi A, Gessi S, Merighi S, Pellati A, Masieri F, Ongaro A, Borea PA. 2008. Pharmacological characterization of P2X1 and P2X3 purinergic receptors in bovine chondrocytes. Osteoarth Cart. 16:1421–1429.

Verkhratsky A, Krishtal OA, Burnstock G. 2009. Purinoceptors on neuroglia. Mol Neurobiol. 39(3):190-208.

Vimalraj S, Arumugam B, Miranda PJ, Selvamurugan N. 2015. Runx2: Structure, function, and phosphorylation in osteoblast differentiation. Int J Biol Macromol. 78:202-8.

Vimalraj S. 2020. Alkaline phosphatase: Structure, expression and its function in bone mineralization. Gene. 754:144855.

Volonté C, Apolloni S, Skaper SD, Burnstock G. 2012. P2X7 receptors: channels, pores and more. CNS Neurol Disord Drug Targets. 11(6):705-21.

Vos T, Flaxman AD, Naghavi M, Lozano R, Michaud C, Ezzati M, Shibuya K, Salomon JA, Abdalla S, Aboyans V, Abraham J, Ackerman I, Aggarwal R, Ahn SY, Ali MK, Alvarado M, Anderson HR,

Anderson LM, Andrews KG, Atkinson C, Baddour LM, Bahalim AN, Barker-Collo S, Barrero LH, Bartels DH, Basáñez MG, Baxter A, Bell ML, Benjamin EJ, Bennett D, Bernabé E, Bhalla K, Bhandari B, Bikbov B, Bin Abdulhak A, Birbeck G, Black JA, Blencowe H, Blore JD, Blyth F, Bolliger I, Bonaventure A, Boufous S, Bourne R, Boussinesq M, Braithwaite T, Brayne C, Bridgett L, Brooker S, Brooks P, Brugha TS, Bryan-Hancock C, Bucello C, Buchbinder R, Buckle G, Budke CM, Burch M, Burney P, Burstein R, Calabria B, Campbell B, Canter CE, Carabin H, Carapetis J, Carmona L, Cella C, Charlson F, Chen H, Cheng AT, Chou D, Chugh SS, Coffeng LE, Colan SD, Colquhoun S, Colson KE, Condon J, Connor MD, Cooper LT, Corriere M, Cortinovis M, de Vaccaro KC, Couser W, Cowie BC, Criqui MH, Cross M, Dabhadkar KC, Dahiya M, Dahodwala N, Damsere-Derry J, Danaei G, Davis A, De Leo D, Degenhardt L, Dellavalle R, Delossantos A, Denenberg J, Derrett S, Des Jarlais DC, Dharmaratne SD, Dherani M, Diaz-Torne C, Dolk H, Dorsey ER, Driscoll T, Duber H, Ebel B, Edmond K, Elbaz A, Ali SE, Erskine H, Erwin PJ, Espindola P, Ewoigbokhan SE, Farzadfar F, Feigin V, Felson DT, Ferrari A, Ferri CP, Fèvre EM, Finucane MM, Flaxman S, Flood L, Foreman K, Forouzanfar MH, Fowkes FG, Franklin R, Fransen M, Freeman MK, Gabbe BJ, Gabriel SE, Gakidou E, Ganatra HA, Garcia B, Gaspari F, Gillum RF, Gmel G, Gosselin R, Grainger R, Groeger J, Guillemin F, Gunnell D, Gupta R, Haagsma J, Hagan H, Halasa YA, Hall W, Haring D, Haro JM, Harrison JE, Havmoeller R, Hay RJ, Higashi H, Hill C, Hoen B, Hoffman H, Hotez PJ, Hoy D, Huang JJ, Ibeanusi SE, Jacobsen KH, James SL, Jarvis D, Jasrasaria R, Jayaraman S, Johns N, Jonas JB, Karthikeyan G, Kassebaum N, Kawakami N, Keren A, Khoo JP, King CH, Knowlton LM, Kobusingye O, Koranteng A, Krishnamurthi R, Lalloo R, Laslett LL, Lathlean T, Leasher JL, Lee YY, Leigh J, Lim SS, Limb E, Lin JK, Lipnick M, Lipshultz SE, Liu W, Loane M, Ohno SL, Lyons R, Ma J, Mabweijano J, MacIntyre MF, Malekzadeh R, Mallinger L, Manivannan S, Marcenes W, March L, Margolis DJ, Marks GB, Marks R, Matsumori A, Matzopoulos R, Mayosi BM, McAnulty JH, McDermott MM, McGill N, McGrath J, Medina-Mora ME, Meltzer M, Mensah GA, Merriman TR, Meyer AC, Miglioli V, Miller M, Miller TR, Mitchell PB, Mocumbi AO, Moffitt TE, Mokdad AA, Monasta L, Montico M, Moradi-Lakeh M, Moran A, Morawska L, Mori R, Murdoch ME, Mwaniki MK, Naidoo K, Nair MN, Naldi L, Narayan KM, Nelson PK, Nelson RG, Nevitt MC, Newton CR, Nolte S, Norman P, Norman R, O'Donnell M, O'Hanlon S, Olives C, Omer SB, Ortblad K, Osborne R, Ozgediz D, Page A, Pahari B, Pandian JD, Rivero AP, Patten SB, Pearce N, Padilla RP, Perez-Ruiz F, Perico N, Pesudovs K, Phillips D, Phillips MR, Pierce K, Pion S, Polanczyk GV, Polinder S, Pope CA 3rd, Popova S, Porrini E, Pourmalek F, Prince M, Pullan RL, Ramaiah KD, Ranganathan D, Razavi H, Regan M, Rehm JT, Rein DB, Remuzzi G, Richardson K, Rivara FP, Roberts T, Robinson C, De Leòn FR, Ronfani L, Room R, Rosenfeld LC, Rushton L, Sacco RL, Saha S, Sampson U, Sanchez-Riera L, Sanman E, Schwebel DC, Scott JG, et al. 2012.

Years lived with disability (YLDs) for 1160 sequelae of 289 diseases and injuries 1990-2010: a systematic analysis for the Global Burden of Disease Study 2010. Lancet. 380(9859):2163-96.

Wang N, Liu W, Tan T, Dong CQ, Lin DY, Zhao J, Yu C, Luo XJ. 2017.Notch signaling negatively regulates BMP9-induced osteogenic differentiation of mesenchymal progenitor cells by inhibiting JunB expression.Oncotarget. 8(65):109661-109674.

Wang Y, Li YP, Paulson C, Shao JZ, Zhang X, Wu M, Chen W. 2014. Wnt and the Wnt signaling pathway in bone development and disease. Frontiers in Bioscience (Landmark Edition). 19:379-407.

Wang C, Gonzales S, Levene H, Gu W, Huang CY. 2013. Energy metabolism of intervertebral disc under mechanical loading. J Orthop Res. 31:1733–1738.

Waxenbaum JA, Futterman B. 2018. Anatomy, Back, Intervertebral Discs.In: StatPearls [Internet]. Treasure Island (FL): StatPearls Publishing.

White N, Burnstock G. 2006. P2 receptors and cancer. Trends Pharmacol Sci. 27(4):211-7.

Wuertz K, Vo N, Kletsas D, Boos N. 2012. Inflammatory and catabolic signalling in intervertebral discs: The roles of NF-κB and MAP kinases. Eur Cell Mater. 23:103–119.

Zeng D, Yao P, Zhao H. 2019. P2X7, a critical regulator and potential target for bone and joint diseases. J Cell Physiol. 234(3):2095-2103.

Zeng Y, Hoque J, Varghese S. 2019. Biomaterial-assisted local and systemic delivery of bioactive agents for bone repair. Acta Biomater. 93:152–168.

Zhou L, Luo L, Qi X, Li X, Gorodeski GI. 2009. Regulation of $P2X_7$ gene transcription. Purinergic Signal. 5(3):409-426.

Zimmermann H, Zebisch M, Sträter N. 2012. Cellular function and molecular structure of ecto-nucleotidases. Purinergic Signal. 8(3):437-502.

# 6. LIST OF PUBLICATIONS

**List of peer-reviewed publications**

1. Penolazzi L, Lambertini E, **Bergamin LS,** Roncada T, De Bonis P, Cavallo M, Piva R. MicroRNA-221 silencing attenuates the degenerated phenotype of intervertebral disc cells. Aging (Albany NY). 2018, 10(8):2001-2015. doi: 10.18632/aging.101525.

2. Lambertini E, Penolazzi L, Angelozzi M, **Bergamin LS,** Manferdini C, Vieceli Dalla Sega F, Paolella F, Lisignoli G, Piva R. Hypoxia Preconditioning of Human MSCs: a Direct Evidence of HIF-1α and Collagen Type XV Correlation. Cell Physiol Biochem. 2018, 51(5):2237-2249. doi: 10.1159/000495869.

3. **Bergamin LS,** Capece M, Salaro E, Sarti AC, Falzoni S, Pereira MSL, De Bastiani MA, Scholl JN, Battastini AMO, Di Virgilio F. Role of the P2X7 receptor in *in vitro* and *in vivo* glioma tumor growth. Oncotarget. 2019, 10(47):4840-4856. doi: 10.18632/oncotarget.27106.

4. Penolazzi L, Lambertini E, **Scussel Bergamin L,** Gandini C, Musio A, De Bonis P, Cavallo M, Piva R. Reciprocal Regulation of TRPS1 and miR-221 in Intervertebral Disc Cells. 2019, 8(10). pii: E1170. doi: 10.3390/cells8101170.

5. Penolazzi L, Pozzobon M, **Bergamin LS**, D'Agostino S, Francescato R, Bonaccorsi G, De Bonis P, Cavallo M, Lambertini E, Piva R. Extracellular Matrix From Decellularized Wharton's Jelly Improves the Behavior of Cells From Degenerated Intervertebral Disc. Front Bioeng Biotechnol. 2020, 8:262. doi: 10.3389/fbioe.2020.00262.

6. **Bergamin LS,** Penolazzi L, Lambertini E, Falzoni S, Sarti AC, Molle CM, Gendron FP, De Bonis P, Di Virgilio F, Piva R. Expression and function of the P2X7 receptor in human osteoblasts: The role of NFATc1 transcription factor. J Cell Physiol. 2021. 236(1):641-652. doi: 10.1002/jcp.29891. Epub 2020 Jun 24. PMID: 32583512

**7. Bergamin LS.** P2X7 receptors and glioma cells. Purinergic Signal. 2020, 16(3):253-254.

8. Gubert C, Andrejew R, Figueiro F, **Bergamin L**, Kapczinski F, Magalhaes PVS, Battastini, AMO. Lithium-induced neuroprotective activity in neuronal and microglial cells: A purinergic perspective. 2021. Psychiatry Research. 2021. 295:113562.